INTER-AMERICAN TROPICAL TUNA COMMISSION

SCIENTIFIC ADVISORY COMMITTEE

NINTH MEETING

La Jolla, California (USA)
14-18 May 2018

DOCUMENT SAC-09-08

EXPLORATORY SPATIALLY-STRUCTURED ASSESSMENT MODEL FOR BIGEYE TUNA IN THE EASTERN PACIFIC OCEAN

Juan L. Valero, Alexandre Aires-da-Silva, Mark. N. Maunder and Cleridy Lennert-Cody

CONTENTS

SUMMARY

The current stock assessment of bigeye tuna in the eastern Pacific Ocean (EPO) assumes a single stock, and is structured as a single area, but accounts for spatial structure to some extent by using a fleet-as-areas approach. The underlying assumption of this approach is that the bigeye stock is randomly mixed within the EPO, with no localized spatial dynamics. However, tagging studies indicate restricted movements and regional fidelity of bigeye in some areas of the EPO, in particular in the equatorial area from around the Galapagos Islands to 120°W. Such restricted movements, combined with the spatial heterogeneity of the fishing effort and the catch, suggest that localized depletion patterns of bigeye sub-stocks may exist in the EPO. A recurrent feature of the assessments of bigeye in the EPO since 2003 is an increase in estimated recruitment, starting in the mid-1990s, resulting in an apparent two-regime pattern of recruitment, with estimates after the mid-1990s about double those of the prior period. Several hypotheses have been proposed regarding the cause of this pattern, including ecological, biological, and fishery processes, and modeling artifacts. In this study we evaluate a "spatial mismatch" hypothesis, which postulates that the pattern results from spatial misspecification in the stock assessment model. The most striking characteristic of the pattern is that the increase in purse seine-catch in a wide equatorial area is not subsequently reflected in a reduction in the longline catch per unit of effort (CPUE), used as the main index of relative abundance in the bigeye stock assessment. This may be due to relatively restricted movements of bigeye, leading to local depletion, and to the fact that the longline CPUE index measures abundance over a wider, or different, area than that where the increased purse-seine catch occurred.

Two approaches are used to investigate the impact of alternative spatial configurations on the bigeye assessment and to determine which configurations may remove the two-regime recruitment pattern. The first evaluates the consistency between catch and the index of abundance for different spatial areas, using

an age-structured production model (ASPM). The second evaluates the performance of a more complete integrated statistical stock assessment model, applied only to the area where the majority of the increase in purse-seine catch occurred. Preliminary results show that the apparent regime shift in recruitment occurs in several areas, even when using the ASPM, indicating that the pattern is independent of the length composition of the catches. Models that include localized catch dynamics and the associated local longline CPUE indices remove the two-regime pattern and indicate more depleted stocks in those areas. These results suggest that finer spatial scales than that currently used in the base case assessment should be considered. The impacts on estimated trends and stock status of using this alternative spatial structure in the assessment suggest that spatial measures should be considered for managing bigeye in the EPO. A spatially-structured assessment should be developed to mitigate existing modelling issues, such as the two-regime recruitment pattern, and to allow the evaluation of alternative management measures.

1. INTRODUCTION

1.1. Background

Bigeye tuna (*Thunnus obesus*) are distributed across tropical to temperate oceanic waters of the Pacific Ocean, although the largest catches are taken towards the eastern and western ends of the ocean basin (Figure 1). Bigeye has been a primary target of Japanese longline fisheries since the 1950s (Miyabe and Bayliff 1998; Miyake *et al*. 2004), and prior to 1994 the longline fishery took about 90% of the total catch. However, with the development of the purse-seine fishery on fish-aggregating devices (FADs) in the mid-1990s, directed mainly at skipjack tuna (*Katsuwonus pelamis*), purse-seine catches rose dramatically, from 10% or less to 60% or more of the total in a two-year period (Figure 2; Fonteneau *et al*. 2013). There are important differences between the two fisheries in the length composition of their catches (Figure 3) and in their areas of operation. Purse seines catch mostly small bigeye, primarily between 5°N and 5°S, whereas longline catches, which consist of large fish, are distributed more continuously geographically, but are relatively low between 160°W and 180° (Schaefer *et al*. 2015). In the eastern Pacific Ocean (EPO), bigeye are rarely caught by purse seiners north of 10°N, but a portion of the longline catches of bigeye is taken north of that parallel (Aires-da-Silva *et al*. 2017).

The current stock assessment of bigeye in the EPO (Aires-da-Silva *et al*. 2017) assumes a single stock. Although this single-unit stock model is not spatially structured, it accounts for spatial structure to some extent by using a “fleet-as-areas” approach (see, for example, Cope and Punt 2011; Hurtado-Ferro *et al*. 2014), which assumes several fisheries that are defined by partitioning the data in space and act on the stock with different catchabilities and selectivities. The underlying assumption of this approach is that the bigeye stock is randomly mixed within the EPO, with no localized spatial dynamics, except possible spatial partitioning by age.

Bigeye movements and potential stock structure in the EPO have been discussed by Schaefer (2009), Schaefer and Fuller (2009), and Schaefer *et al*. (2015). Analyses of conventional and archival tag data indicate constrained dispersion in latitude, some regional fidelity, and extensive eastward longitudinal dispersion (Schaefer *et al*. 2015). One of the areas of higher site fidelity and "viscosity" (the tendency of fish to stay in a particular area, as opposed to dispersion; see Schaefer *et al*. 2015) in movements is the equatorial EPO between approximately 90°W and 115°W (Schaefer and Fuller 2009; Schaefer *et al*. 2015) (Figure 4).

A recurrent feature of bigeye assessments in the EPO since 2003 (Harley *et al*. 2005; Fonteneau and Ariz 2008; Aires-da-Silva 2017) is a sudden increase in the estimated recruitment starting in the mid-1990s, and resulting in an apparent “two-regime” pattern in recruitment, with estimates after 1995 about double those before that year (Figure 5). Although this pattern mostly disappeared in the 2014 assessment (Aires-

da-Silva and Maunder 2014), it resurfaced in subsequent assessments. Several hypotheses have been proposed to explain this pattern (Aires-da-Silva *et al*. 2010), including an environmental regime shift (Fonteneau and Ariz 2008), underestimated floating-object catches for the period prior to 1994 (Fonteneau and Ariz 2008), higher natural mortality rates than those assumed in the assessment models (Fonteneau and Ariz 2008), density-dependent growth (S. Hoyle, pers. comm.), changes in migratory patterns (S. Harley, pers. comm.), and a modeling artifact caused by the large catches of small individuals by the purse-seine fishery (Maunder *et al*. 2010). Although any of these hypotheses might account for the two-regime recruitment pattern, only some of them have been evaluated, and their plausibility remains in question. To date, two analyses have corrected the pattern: first, allowing what were previously considered unrealistically high natural mortalities for medium and large bigeye (Maunder *et al*. 2010), and second, a "spatial mismatch" hypothesis (Aires-da-Silva *et al*. 2010), which postulates that the pattern could be explained by a spatial mis-specification in the assessment model that ignores local depletion. This hypothesis is described in the next section.

1.2. The "spatial mismatch" hypothesis

Under this hypothesis, the two-regime pattern is the result of a spatial mis-specification in the stock assessment model; in other words, it is an artifact of the model, caused by the assumption that bigeye in the EPO form a single homogeneous stock. This hypothesis seems to be consistent with major historic events in the bigeye fishery in the EPO. In particular, the estimated recruitment shift coincided with the very rapid expansion of the purse-seine fishery on FADs in the equatorial EPO in the mid-1990s. This resulted in competition with the longline fishery, which had operated along the equatorial grounds for several decades. Decreased longline catch rates (see Aires-da-Silva and Maunder 2010) and apparent gear conflicts between longline and purse-seine fisheries (see, for example, Skillman *et al*. 1993) resulted in a gradual exodus of longliners from the central equatorial fishing areas towards the west, south, and north. Longliners may also have shifted their fishing effort to less-exploited fishing grounds or to distinct substocks of bigeye in the EPO after the mid-1990s. Preliminary spatial analyses of historical changes in the distribution of longline and purse-seine effort, and some anecdotal information, support this series of historic events. Also, the evidence of restricted movements and limited mixing of bigeye in the equatorial EPO from tagging data (Figure 4) (Schaefer and Fuller 2009; Schaefer *et al*. 2015) suggests that juvenile bigeye exploited by the FAD fishery may not become vulnerable later in life to longliners in those newly-occupied fishing grounds. This would also account for the fact that the increase in purse-seine catch does not appear to reduce the longline CPUE, and hence the index of relative abundance, since the longline CPUE index measures abundance over a wider, or different (Figures 1 and 6), area than where the increased purse-seine catch occurred.

If the spatial mismatch hypothesis is correct, a spatially-structured bigeye assessment should minimize, or even eliminate, the two-regime recruitment pattern. Aires-da-Silva and Maunder (2010) tested the impact of this hypothesis on the results of the bigeye assessment by fitting spatially disaggregated and independent models for four areas of the EPO (Figure 6), resulting in different trends and depletion levels among areas and a partial correction of the two-regime pattern, which is desirable to remove model misspecification and potential model biases.

1.3. Objectives

Identifying the source of the two-regime pattern in the bigeye assessment, particularly if it is due to model misspecification, is important not only for purposes of the stock assessment but also for the ongoing management strategy evaluation (MSE) work at the IATTC (Maunder *et al*. 2016), since the operating model for MSE work is based on the stock assessment model. Realistic operating models are of paramount importance for conducting MSE work, and it is desirable to eliminate potential model misspecification, and the resulting potential bias, in stock assessments to improve the accuracy of the management advice

based on such assessments

This report presents the results of applying exploratory spatially-structured stock assessment models to bigeye tuna in the EPO with alternative model complexities, uses of data, and spatial configurations. The main objective is to evaluate the impact of alternative spatial configurations on the bigeye assessment, and to determine which configurations remove the two-regime recruitment pattern.

2. METHODS

The Stock Synthesis model platform (SS - Version 3.3; Methot and Wetzel 2013) was used to model the population dynamics of bigeye tuna in the EPO under different model complexities and spatial configurations. The current stock assessment of bigeye (Aires-da-Silva et al. 2017) is conducted with an earlier SS version (2.23b), but comparisons between the two versions for the base case model yielded very similar results. Two approaches were used to investigate the impact of alternative spatial configurations on the bigeye assessment and to determine which configurations may remove the two-regime recruitment pattern. The first evaluates the consistency between catch and the index of abundance for different spatial areas, using an age-structured production model (ASPM) (see Minte-Vera *et al*. (2017) for details and application to bigeye tuna); the second evaluates the performance of a more complete integrated statistical stock assessment model, applied only to the area where the increased purse-seine catch occurred.

2.1. Age-structured production model (ASPM)

To systematically explore the effect of alternative spatial configurations on model results, three latitudinal bands (5°N-5°S, 10°N-5°S and 10°N-10°S) and four longitudes (95°W, 100°W, 110°W, and 120°W) were used to divide the EPO into 12 six-area grids (Figure 7), for a total of 72 individual areas. An independent (*i.e*. no movement among areas nor sharing of estimated parameters) age-structured production model (ASPM) was fitted for each area, using area-specific total catches aggregated by fleet (purse-seine and longline) and nominal (unstandardized) longline CPUE. The ASPM estimated recruitment deviates, biomass, and fishing mortality, by quarter, for each of the 72 areas during 1975-2015 (Appendix 1).

2.2. Integrated model

An integrated statistical stock assessment model, using data from 1975-2016 and a quarterly time step, was applied to the area between 5°N and 5°S from 110°W to 85°W, denominated the Central area (Figure 6), which was also used by Aires-da-Silva and Maunder (2010). The fisheries defined in the base case assessment (Aires-da-Silva *et al*. 2017) were re-defined based on their spatial overlap with the Central area (Figure 8). The data included, for the longline fisheries, catches, standardized CPUE, and length compositions for 1975-2016. For the purse-seine fisheries, only post-1993 catch and length-composition data were used, corresponding to the expansion of the FAD fisheries in the equatorial EPO; prior to 1993 there was little to no spatial overlap with the Central area (Waters 1999).

The integrated model runs used the same assumptions as the 2017 base case assessment with regard to growth, reproduction, selectivity, natural mortality, and the steepness of the Beverton-Holt stock-recruitment relationship. Three alternative weightings of the composition data ($\lambda = 0.05$, $\lambda = 1$, and iterative weighting) were used, following the Francis (2011) method. In the current base case assessment (Aires-da-Silva et al. 2017), the length-composition data for all fisheries are down-weighted ($\lambda = 0.05$). Up-weighting the length-composition data ($\lambda = 1$) worsens the two-regime pattern and has a large impact on the assessment results, leading to a more pessimistic stock status.

2.3. Comparison of integrated model and ASPM

The results of the integrated statistical stock assessment for the Central area were compared with those of the ASPM with the closest spatial configuration, the area east of 110°W between 5°N and 5°S (Figure

7, Grid C), which differs spatially only in including the area between 85°W and the coast. Another difference is that the integrated model uses standardized longline CPUE, while the ASPM uses nominal CPUE. To account for this difference, the ASPM was also run with the standardized CPUE for the Central area.

3. RESULTS AND DISCUSSION

3.1. Age-structured production model (ASPM)

Initial ASPM runs without estimating recruitment deviates did not produce good fits to the longline CPUE (Figure 9), and the results are not presented in this report. Subsequent ASPM runs that did estimate recruitment deviates produced reasonable fits to the longline CPUE (see, for example, Figure 10 and Appendix Figures A1-A12). This suggests that recruitment is driving abundance trends more than catch is, which is problematic when relying on the effect of catch on indices of relative abundance to inform absolute abundance (Minte-Vera *et al*. 2017). For most of the twelve possible six-area combinations (Figure 7), some of the areas have too few or too sparse data for meaningful results, especially the inshore areas north and south of the equatorial areas, and to a lesser extent the areas north and west of the equatorial areas (Figure 7 and Appendix). This suggests that, in a systematic division of the EPO at least, six areas are too many, and that fewer areas, or defining spatial areas by other criteria (such as level of overlap between purse-seine and longline fisheries, see Future Directions section) may perhaps be a better approach to delineate spatial areas. For area combinations with enough data, there is general consistency in the results, with larger biomass declines in the equatorial areas (Appendix Figures A13-A24), while the other areas showed either flat biomass trajectories or smaller declines. Overall results indicate that the two-regime recruitment pattern appears in several of the area combinations (see Appendix Figures A25-A36) if the ASPM is used, indicating that the recruitment pattern is independent of length compositions, which are not used in the ASPM.

3.2. Integrated model

The integrated model results show a steeper declining trend in the spawning biomass ratio (the ratio of the spawning biomass of the current stock to that of the unfished stock; SBR), and a more depleted stock status (Figure 11) in the Central area than is estimated by the base case stock assessment for the whole EPO (Figure 12). Recruitment estimates for the Central area (Figure 11) do not show the two-regime pattern typical of previous models (Figure 12). These results are consistent with those of Aires-da-Silva and Maunder (2010).

Alternative data-weighting does not influence the overall results. In the current base case assessment, the length-composition data are down-weighted for all fisheries ($\lambda = 0.05$), since up-weighting them ($\lambda = 1$) worsens the two-regime pattern and has a large impact on the assessment results, leading to a more pessimistic stock status than with $\lambda = 0.05$. In contrast, in the Central area alternative weighting of the length-composition data did not result in meaningful changes in recruitment trends or the SBR (Figure 13). Data weighting following the Francis (2011) method resulted in increased values of λ for all fisheries, to around 0.5 for purse-seine fisheries and to between 0.8 and 2.5 for longline fisheries.

Considering the apparent high degree of viscosity and low mixing rates of bigeye within the equatorial EPO, as shown from tagging data, and the Central area being the area with the largest potential spatial mismatch between the increase in purse-seine catches and the reduction in longline effort, using the Central area to evaluate the spatial structure of bigeye in the EPO seems a reasonable approach.

Other spatial structure assumptions could be evaluated in the future, such as those defined from multivariate regression tree analyses on bigeye length-frequency distributions and CPUE data (Lennert-Cody *et al*. 2010) or other criteria such as level of overlap between purse-seine and longline fisheries (see Future Directions section).

3.3. Comparison of integrated model and ASPM

The declining trends in spawning biomass estimated by the integrated model and the ASPM are similar, although the biomass scale is larger for the ASPM (Figure 14). Using the ASPM with the standardized longline CPUE yields intermediate estimates between the two model approaches (Figure 14). A similar pattern occurs when comparing SBRs, with a more depleted stock status for the Central area and the ASPM using standardized CPUE (Figure 15). Both ASPM models estimated higher average recruitment than the integrated model (Figure 16, top panel). Although the two-regime pattern is not evident in the integrated model, it is evident in the ASPM, whether standardized or nominal CPUE is used (Figure 16, bottom panel). The integrated model estimates area-specific selectivities and recruitment informed by several sources, such as CPUE, catch, and length compositions, whereas the ASPM uses fixed aggregated purse-seine and longline selectivities (based on the 2017 base case assessment, Aires-da-Silva *et al*. 2017) and estimates recruitment based on the longline index and catch alone. This suggests that using smaller areas to resolve the spatial mismatch between purse-seine catches and the longline CPUE index may be only partially successful unless length-composition data are included; however, they are not used in the ASPM.

4. CONCLUSIONS

Although several hypotheses have been proposed as explanations of the source of the apparent two-regime recruitment pattern in bigeye assessments, the spatial mismatch hypothesis is the most plausible to date. The results of this work are consistent with those of Aires-da-Silva and Maunder (2010), showing that spatially disaggregating the assessment of bigeye removes the two-regime pattern, which seems to be an artifact of treating the EPO as a single homogeneous area in the assessment. Not disaggregating the assessment in space causes a mismatch between the substantial increase in purse-seine catches in the mid-1990s in the equatorial region (which leads to localized depletions) and the lack of change in the longline CPUE indices when aggregated to the level of the whole EPO. The base case model detects an increase in catches in the 1990s, but longline CPUE, the main driver of the assessment, remains relatively flat at the level of the whole EPO, forcing the model to increase recruitment to explain the increase in catch with no reduction in the index of abundance. Models that reflect the localized dynamics of the catches and the associated local longline CPUE indices eliminate the two-regime recruitment pattern, and result in greater depletion of the stocks in those areas. This is consistent with the results of the ASPM and the integrated models in this study, as well as those of Aires-da-Silva and Maunder (2010). The results suggest that, in addition to the current management measures for bigeye in the EPO, alternative spatial management measures should be evaluated.

5. FUTURE DIRECTIONS

Other stock structure assumptions could be evaluated in the future, such as those recently obtained from multivariate regression tree analyses on bigeye length-frequency distributions and CPUE data (Lennert-Cody *et al*. 2010). Spatial analyses of the mismatch between the spatial distribution of purse-seine and longline fisheries could also be used to define areas.

One possible factor causing the mismatch between the increased purse-seine catch and the indices of abundance based on longline CPUE is the way in which those indices are standardized. The current index is based on a simple generalized linear model that gives equal weight to each data point in the analysis (1°x1°-month-hooks per basket strata) and assumes that the size structure represented by the index is the same as that of the catch. A more appropriate approach might be to use a spatio-temporal model that sums over areas and deals with the composition data appropriately (Maunder *et al*. 2017).

Although this study focused only on the EPO, there are clear benefits to continuing the collaboration with the Secretariat of the Pacific Community (SPC) on a Pacific-wide assessment of bigeye, particularly due to

the extensive movement of juveniles from the central Pacific to the EPO. This could incorporate new tagging data in a spatially-structured population dynamics model, which should help to evaluate potential biases resulting from the current approach of conducting separate assessments for the EPO and the Western and Central Pacific Ocean (WCPO). Tagging data would be useful not only to help define areas, but also to estimate movement between areas.

A better understanding of the spatial structure and dynamics of bigeye in both in the EPO and the entire Pacific will improve not only the scientific advice for management derived from stock assessments, but also the construction and refinement of operating models for MSE work by the IATTC staff. Operating models are generally more complex than assessment models because they need to describe all the possible states of nature to test the robustness of alternative management strategies. Therefore, including spatial structure in the operating model for bigeye tuna is important.

REFERENCES

Aires-da-Silva A. and M. Maunder, 2010. An evaluation of spatial structure in the stock assessment of bigeye tuna in the eastern Pacific Ocean. Inter-Amer. Trop. Tuna Comm. Document BET-01-02b. External review of IATTC bigeye tuna assessment. La Jolla, California, USA. 3-7 May 2010.

Aires-da-Silva A. and M. Maunder. 2014. Status of bigeye tuna in the eastern Pacific Ocean in 2013 and outlook for the future.

Aires-da-Silva, A., M. N. Maunder, and P. K. Tomlinson. 2010. An investigation of the trend in the estimated recruitment for bigeye tuna in the eastern Pacific Ocean. Document BET-01-06. Inter-Amer. Trop. Tuna Comm. Document BET-01-02b. External review of IATTC bigeye tuna assessment. La Jolla, California, USA. 3-7 May 2010.

Aires-da-Silva, A., Minte-Vera, C., and M.N. Maunder. 2017. Status of bigeye tuna in the eastern Pacific Ocean in 2016 and outlook for the future. Inter-Amer. Trop. Tuna Comm. SAC-08-04a.

Aires-da Silva, A. M., Maunder, M. N., Schaefer, K. M., and Fuller, D. W. 2015. Improved growth estimates from integrated analysis of direct aging and tag-recapture data: An illustration with bigeye tuna (*Thunnus obesus*) of the eastern Pacific Ocean with implications for management. Fisheries Research, 163: 119-126.

Cope, J.M., Punt, A.E., 2011. Reconciling stock assessment and management scales under conditions of spatially varying catch histories. Fish. Res. 107, 22–38.

Fonteneau, A., and Ariz, J. 2008. An overview of 10 years of IATTC bigeye stock assessments in the Eastern Pacific Ocean. In 'The 9th Stock assessment review meeting, La Jolla, 12–16 May 2008'. (Inter-American Tropical Tuna Commission: La Jolla, San Diego, CA.)

Fonteneau, A., Chassot, E., Bodin, N., 2013. Global spatio-temporal patterns in tropical tuna purse seine fisheries on drifting fish aggregating devices (DFADs): taking a historical perspective to inform current challenges. Aquat. Living Resour. 26,37–48.

Francis, R. 2011. Data weighting in statistical fisheries stock assessment models. Can J Fish Aquat Sci. 68: 1124-1138.

Hurtado-Ferro, F., Punt, A.E. and Hill, K.T. 2014. Use of multiple selectivity patterns as a proxy for spatial structure. Fisheries Research 158, 102–115.

Lennert-Cody, C., M.N. Maunder, and A. Aires-da-Silva. 2010. Preliminary analysis of spatial-temporal pattern in bigeye tuna length-frequency distributions and catch-per-unit-effort trends. BET-01-02. External review of IATTC bigeye tuna assessment, La Jolla, California, USA, 3-7 May, 2010.

Maunder, M.N., and Piner, K.R. 2015. Contemporary fisheries stock assessment: many issues still remain. ICES Journal of Marine Science (2015), 72(1), 7–18. doi:10.1093/icesjms/fsu015.

Maunder, M.N., Aires-da-Silva, A. and Lennert-Cody, C.E. Summary of issues in the Eastern Pacific Ocean Bigeye Tuna assessment. 2010. Inter-Amer. Trop. Tuna Comm. Document BET-01-01. External review of IATTC bigeye tuna assessment. La Jolla, California, USA. 3-7 May 2010.

Maunder, M. N., Aires-da-Silva, A., Minte-Vera, C and Valero, J. L. 2016. Current and future research on management strategy evaluation (MSE) for tunas and related species in the Eastern Pacific Ocean. Inter-Amer. Trop. Tuna Comm., 7th Scient. Adv. Com. Meeting. SAC-07.

Maunder, M.N., Thorson, J.T., Lee, H.H., Kai, M., Chang, S.K., Kitakado, T., Albertsen, C.M., Lennert-Cody, C.E., Aires-da-Silva, A.M., Piner, K.R. 2017. The need for spatial-temporal modeling of catch-per-unit-effort data when used to derive indices of relative abundance to include in stock assessment models. Inter-Amer. Trop. Tuna Comm., 8th Scient. Adv. Com. Meeting. SAC-08-05d.

Methot, R. D. 2005. Technical description of the Stock Synthesis II assessment program. NOAA Fisheries. http://www.sefsc.noaa.gov/sedar/download/S16_AW_04.pdf

Methot, R.D., and Wetzel, C.R. 2013. Stock Synthesis: A biological and statistical framework for fish stock assessment and fishery management. Fish Res. 142: 86-99.

Minte-Vera, C. V., Maunder, M. N., Aires-da-Silva, A. M., Satoh, K., Uosaki, K. Get the biology right, or use size-composition data at your own risk. 2017. Fisheries research. 192: 114-125.

Miyabe, N., Bayliff, W.H., 1998. A review of information on the biology, fisheries, andstock assessment of bigeye tuna, *Thunnus obesus*, in the Pacific Ocean. Inter-Am. Trop. Tuna Comm. Spec. Rep. 9, 129–170.

Miyake, M.P., Miyabe, N., Nakano, H., 2004. Historical trends of tuna catches in the world. FAO Fish. Tech. Pap. 467, 74 pp.

Schaefer, K. M., D. W. Fuller. 2002. Movements, behavior, and habitat selection of bigeye tuna (*Thunnus obesus*) in the eastern equatorial Pacific, ascertained through archival tags. Fish. Bull. 100: 765-788.

Schaefer, K.M. 2009. Stock structure of bigeye, yellowfin, and skipjack tunas in the eastern Pacific Ocean. Inter-Amer. Trop. Tuna Comm., Stock Assess. Rep. 9. 203-221

Schaefer, K.M. and D.W. Fuller. 2009. Horizontal movements of bigeye tuna (*Thunnus obesus*) in the eastern Pacific Ocean, as determined from conventional and archival tagging experiments initiated during 2000-2005. IATTC Bulletin, Vol. 24(2).

Schaefer, K., Fuller, D., Hampton, J., Caillot, S., Leroy, B., and Itano, D. 2015. Movements, dispersion, and mixing of bigeye tuna (*Thunnus obesus*) tagged and released in the equatorial Central Pacific Ocean, with conventional and archival tags. Fisheries Research, 161:336-355.

Skillman, A., R., Boggs, C. H., and Pooley, S. 1993. Fishery interaction between the tuna longline and other pelagic fisheries in Hawaii. NOAA Technical Memorandum NMFS 189.

Watters, G.M. 1999. Geographical distributions of effort and catches of tunas by purse-seine vessels in the eastern Pacific Ocean during 1965-1998. IATTC Data Report 10.

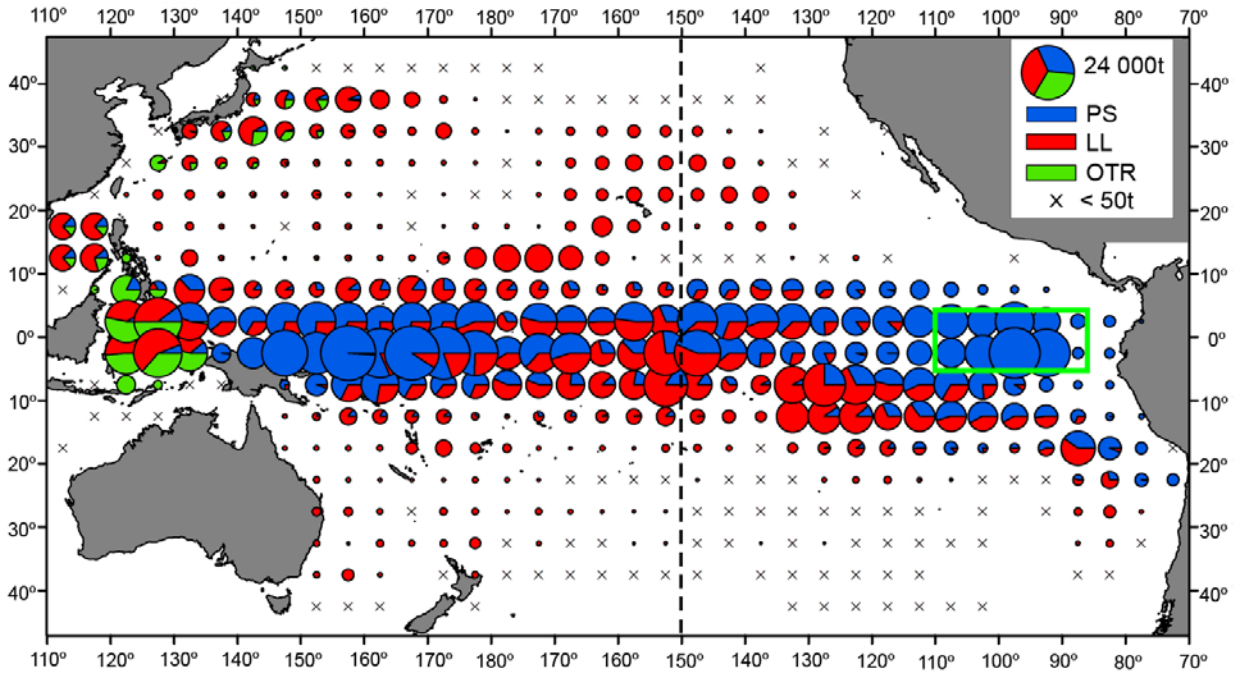

FIGURE 1. Distribution of the catches of bigeye tuna in the Pacific Ocean, by 5° x 5° area and gear type, 2008-2012. The sizes of the circles are proportional to the catch. The vertical dashed line at 150°W marks the western boundary of the eastern Pacific Ocean (EPO). The green rectangle represents the Central area used in this study (modified from Schaefer *et al*. 2015). PS: purse seine; LL: longline; OTR: other gears.
FIGURA 1. Distribución de las capturas de atún patudo en el Océano Pacífico, por área de 5° x 5° y tipo de arte, 2008-2012. El tamaño de los círculos es proporcional a la captura. La línea de trazos vertical en 150°O marca el límite occidental del Océano Pacífico oriental de (OPO). El rectángulo verde representa el área Central usada en el presente estudio (modificado de Schaefer *et al*. 2015). PS: red de cerco; LL: palangre; OTR: otras artes.

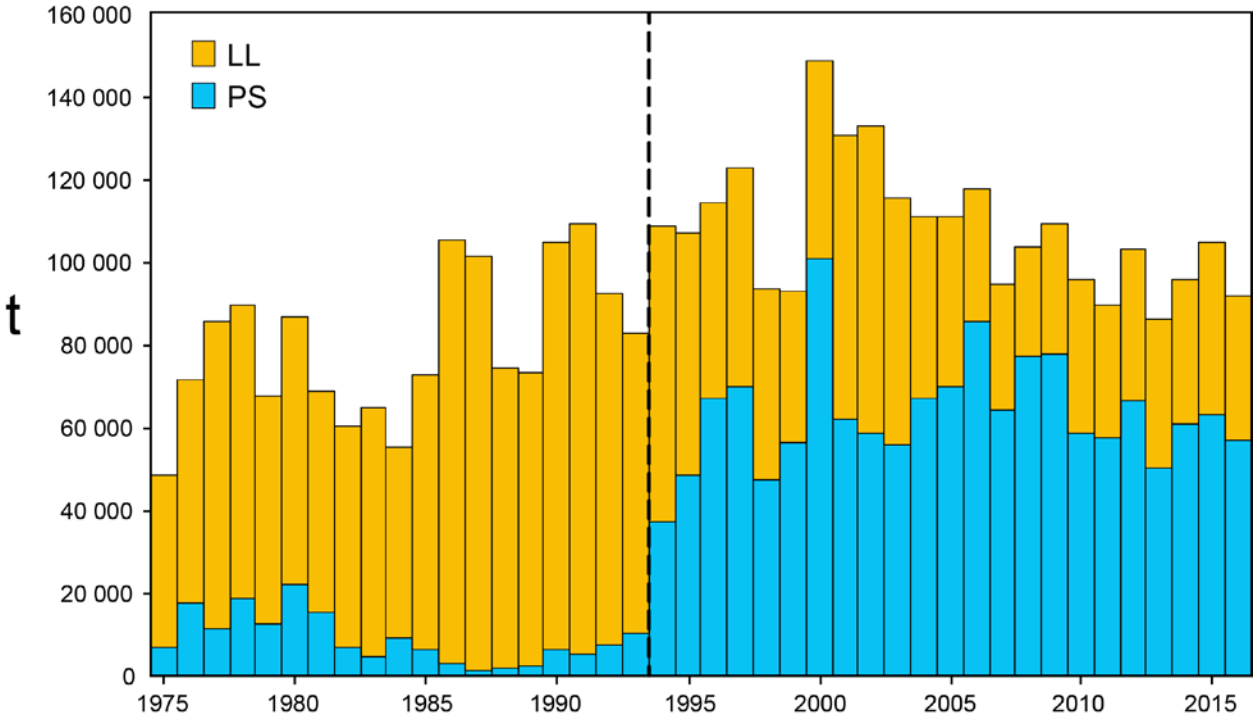

FIGURE 2. Annual catches of bigeye tuna in the eastern Pacific Ocean, by gear, 1975-2016, showing the sudden change (dashed vertical line) resulting from the introduction of fish-aggregating devices (FADs) in the early 1990s. PS: purse seine; LL: longline.

FIGURA 2. Capturas anuales de atún patudo en el Océano Pacífico oriental, por arte, 1975-2016, mostrando el cambio súbito (línea de trazos vertical) que resultó de la introducción de los dispositivos agregadores de peces (plantados) a principios de la década de 1990. PS: red de cerco; LL: palangre.

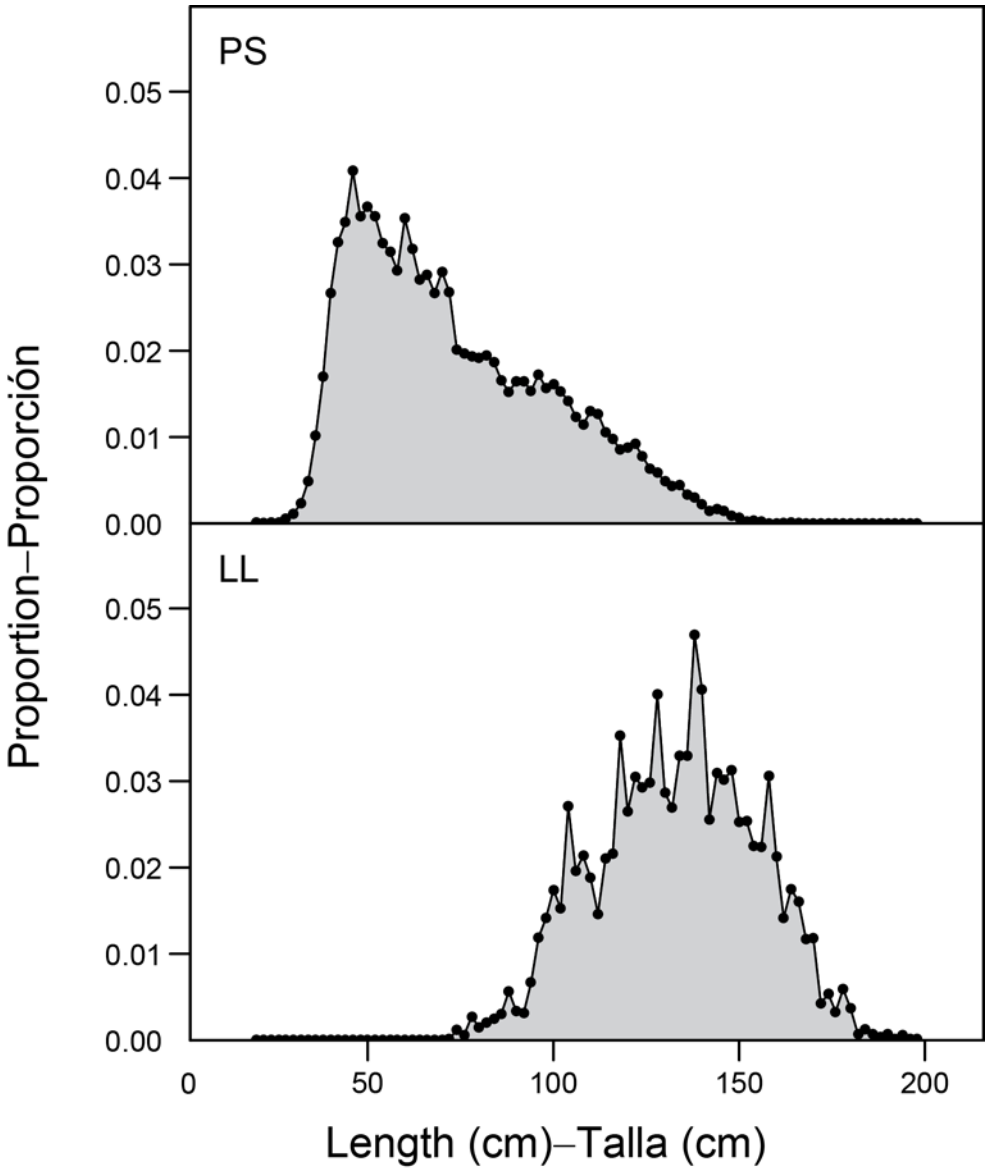

FIGURE 3. Length compositions of bigeye tuna caught in the Central area, by fleet, 1975-2016. PS: purse seine; LL: longline.

FIGURA 3. Composiciones por talla del atún patudo capturado en el área Central, por flota, 1975-2016. PS: red de cerco; LL: palangre.

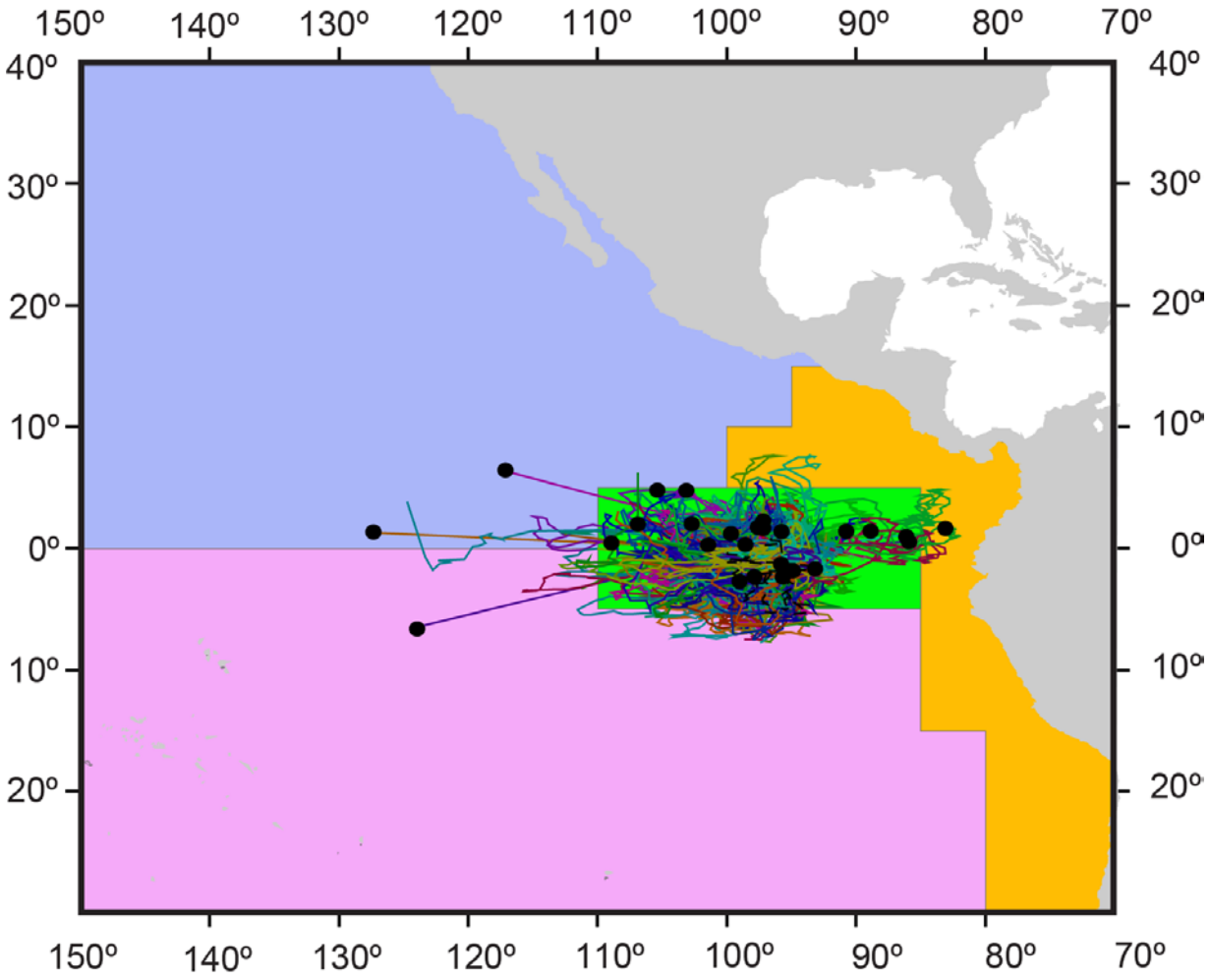

FIGURE 4. Movement paths of bigeye tuna at liberty for 30 days or longer, inferred from archival tagging data from 2000-2006 (Schaefer and Fuller 2009).
FIGURA 4. Rutas de desplazamiento de atunes patudo en libertad durante 30 o más días, inferidas a partir de datos de marcas archivadoras de 2000-2006 (Schaefer y Fuller 2009).

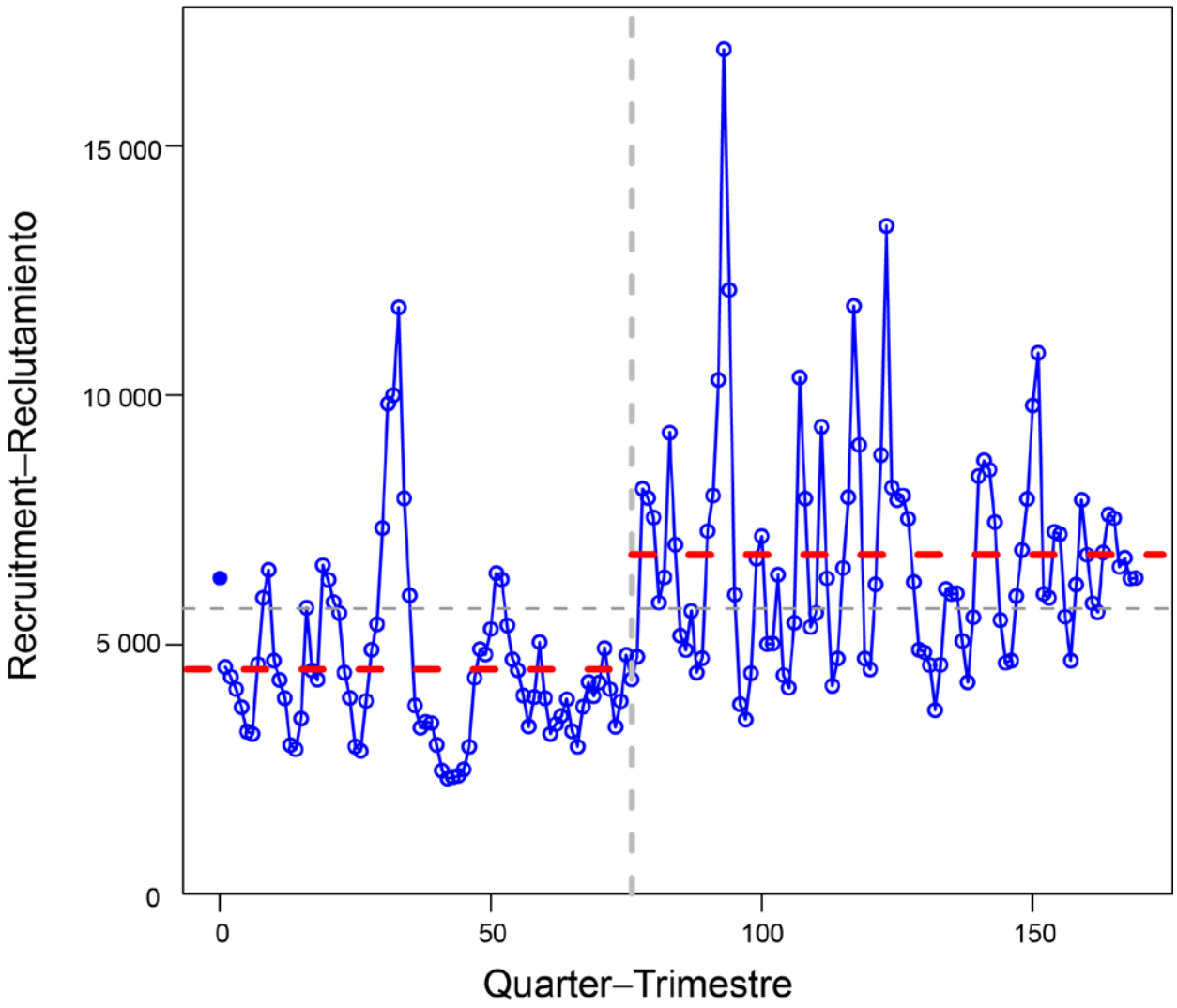

FIGURE 5. Time series of estimated recruitment, in thousands of fish, during 1975-2016, showing apparent two-regime pattern before and after 1995.

FIGURA 5. Serie temporal de reclutamientos, en miles de peces, estimados durante 1975-2016, mostrando el patrón aparente de dos regímenes antes y después de 1995.

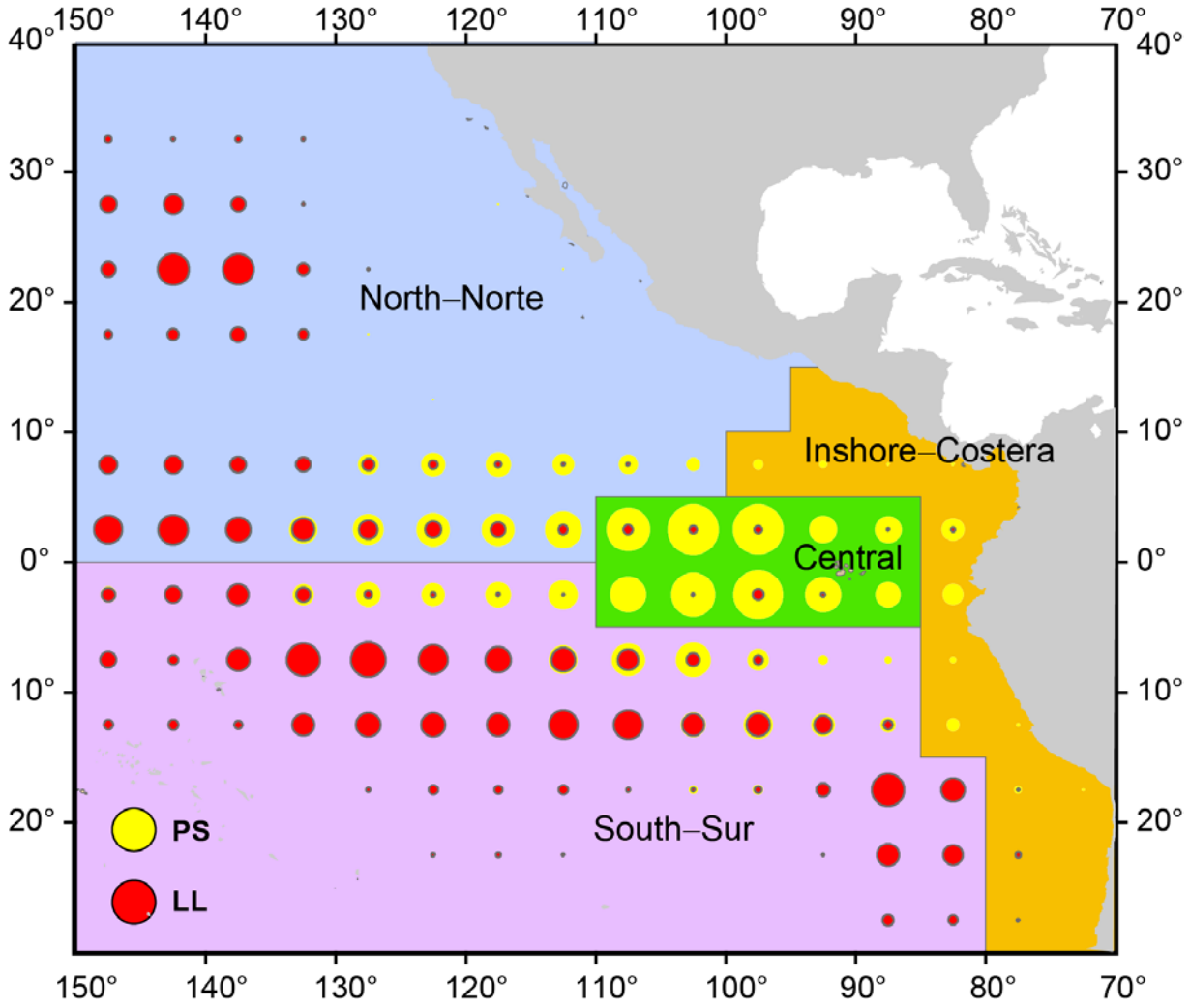

FIGURE 6. Spatial distribution of the catches of bigeye tuna in the eastern Pacific Ocean, 2000-2006, by gear and sub-stock (North, South, Central, and Inshore). The sizes of the circles are proportional to the catch (from Aires-da-Silva and Maunder 2010). PS: purse seine; LL: longline.

FIGURA 6. Distribución espacial de las capturas de atún patudo en el Océano Pacífico oriental, 2000-2006, por arte y sub-población (Norte, Sur, Central, y Costera). El tamaño de los círculos es proporcional a la captura (de Aires-da-Silva y Maunder 2010). PS: red de cerco; LL: palangre.

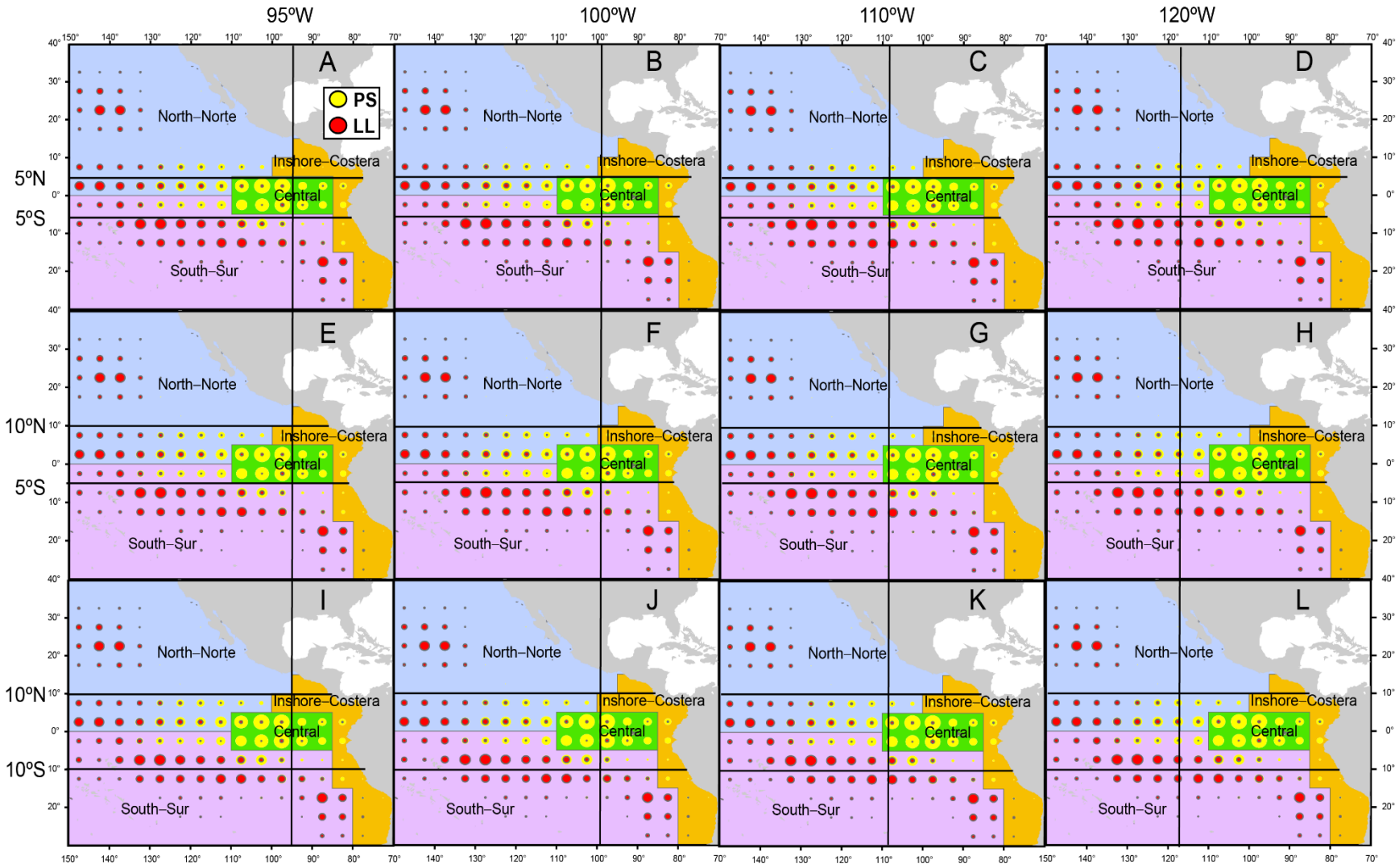

FIGURE 7. The 72 combinations of 12 grids (A-L) and six areas used for the age-structured production models (ASPM). PS: purse seine; LL: longline.
FIGURA 7. Las 72 combinaciones de 12 rejillas (A-L) y 6 áreas usadas para los modelos de producción estructurados por edad (ASPM). PS: red de cerco; LL: palangre.

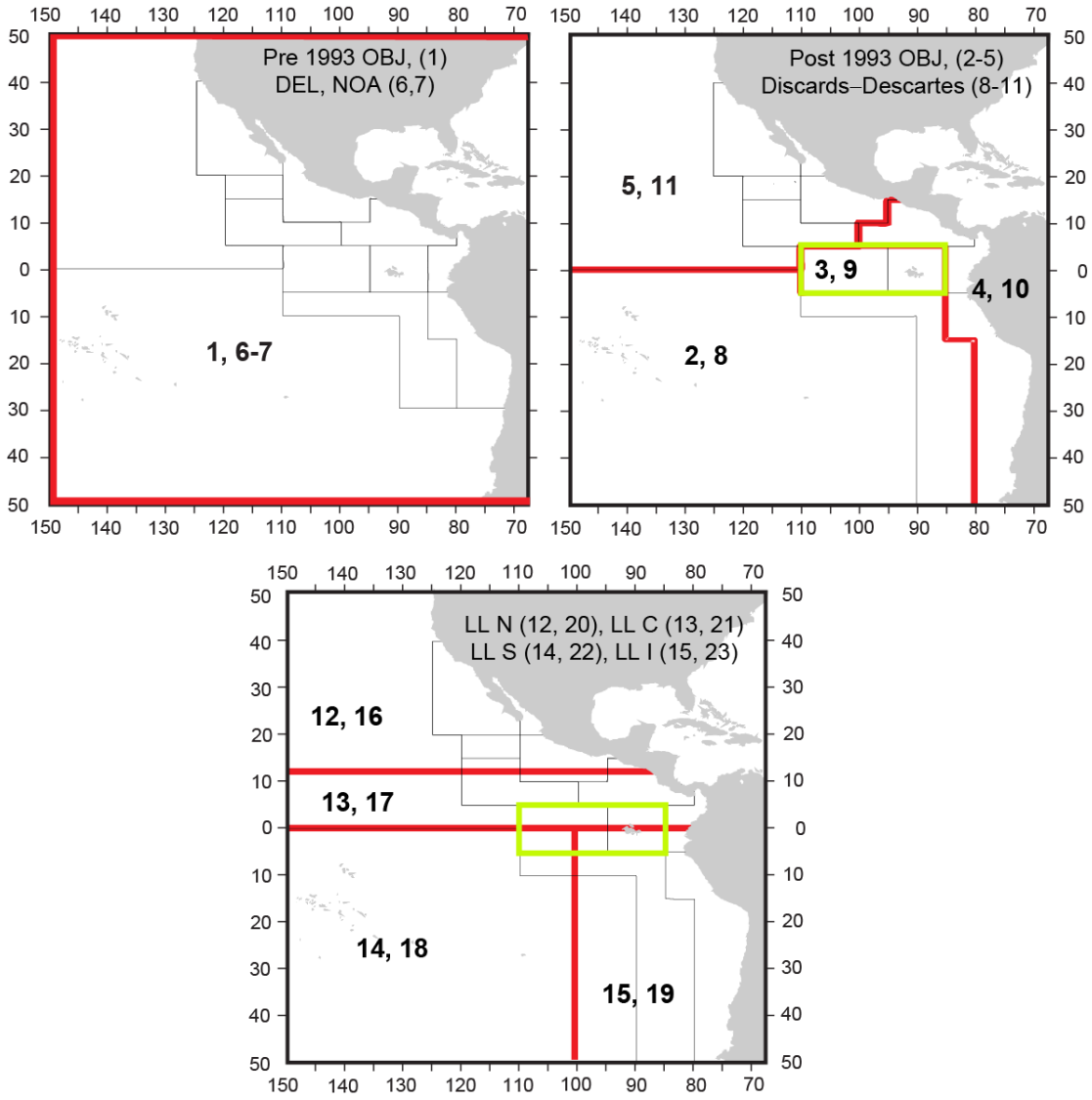

FIGURE 8. Fisheries defined for the Central area (green rectangle) and for the base case stock assessment of bigeye tuna in the EPO (Aires-da-Silva *et al*. 2017). The thin lines indicate the boundaries of 13 length-frequency sampling areas, the bold red lines the boundaries of each fishery defined for the base case stock assessment, and the numbers the fisheries to which the latter boundaries apply. The Central area does not include fisheries 1, 6, 7, 12 and 16. Fisheries: purse-seine (PS) on floating objects (OBJ), unassociated tunas (NOA), dolphins (DEL); LL: longline.

FIGURA 8. Pesquerías definidas para el área Central (rectángulo verde) y para la evaluación de caso base de la población de atún patudo en el OPO (Aires-da-Silva *et al*. 2017). Las líneas delgadas indican los límites de 13 zonas de muestreo de frecuencia de tallas, las líneas gruesas rojas los límites de cada pesquería definida para la evaluación de caso base, y los números las pesquerías correspondientes a esos límites. El área central no incluye las pesquerías 1, 6, 7, 12 y 16. Pesquerías: red de cerco (PS) sobre objetos flotantes (OBJ), atunes no asociados (NOA), delfines (DEL); LL: Palangre.

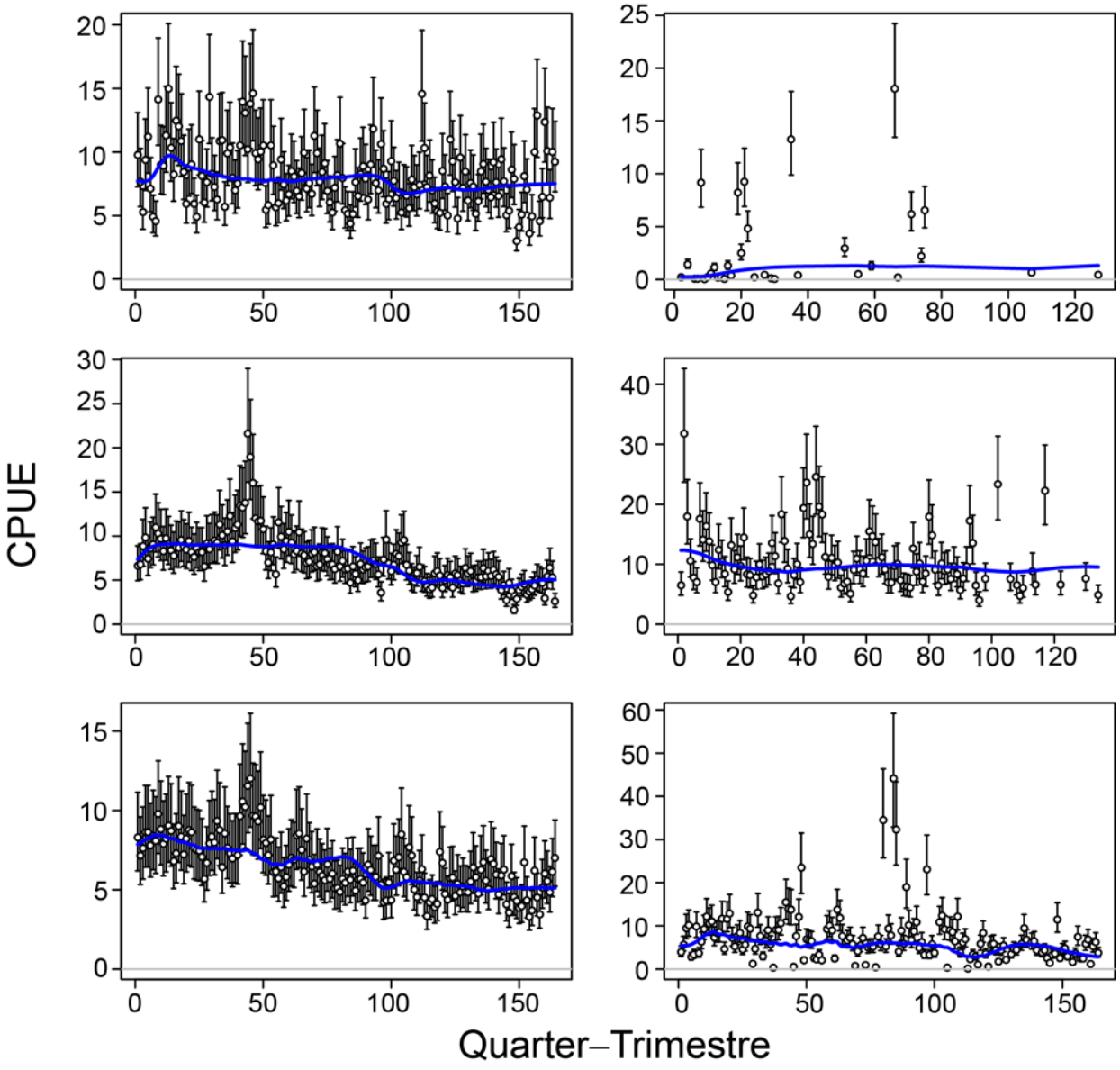

FIGURE 9. ASPM fits to longline CPUE for the six areas in grid A (Figure 7), without estimation of recruitment deviates.

FIGURA 9. Ajustes del ASPM a la CPUE palangrera correspondiente a las seis áreas en la cuadrícula A (Figura 7), sin estimaciones de las desviaciones del reclutamiento.

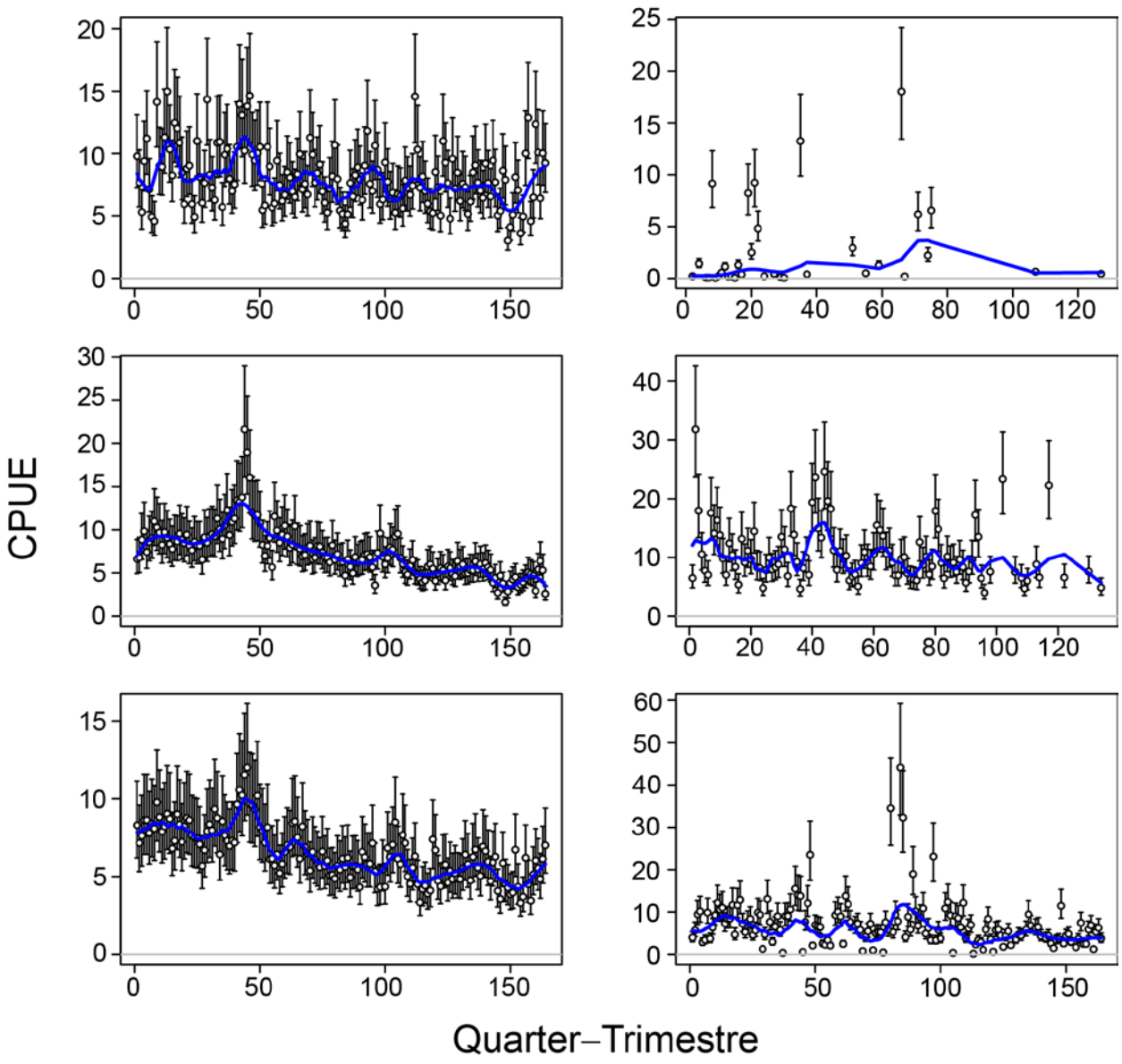

FIGURE 10. ASPM fits to longline CPUE for the six areas in grid A (Figure 7), with estimation of recruitment deviates.

FIGURA 10. Ajustes del ASPM a la CPUE palangrera correspondiente a las seis áreas en la cuadrícula A (Figura 7), con estimaciones de las desviaciones del reclutamiento.

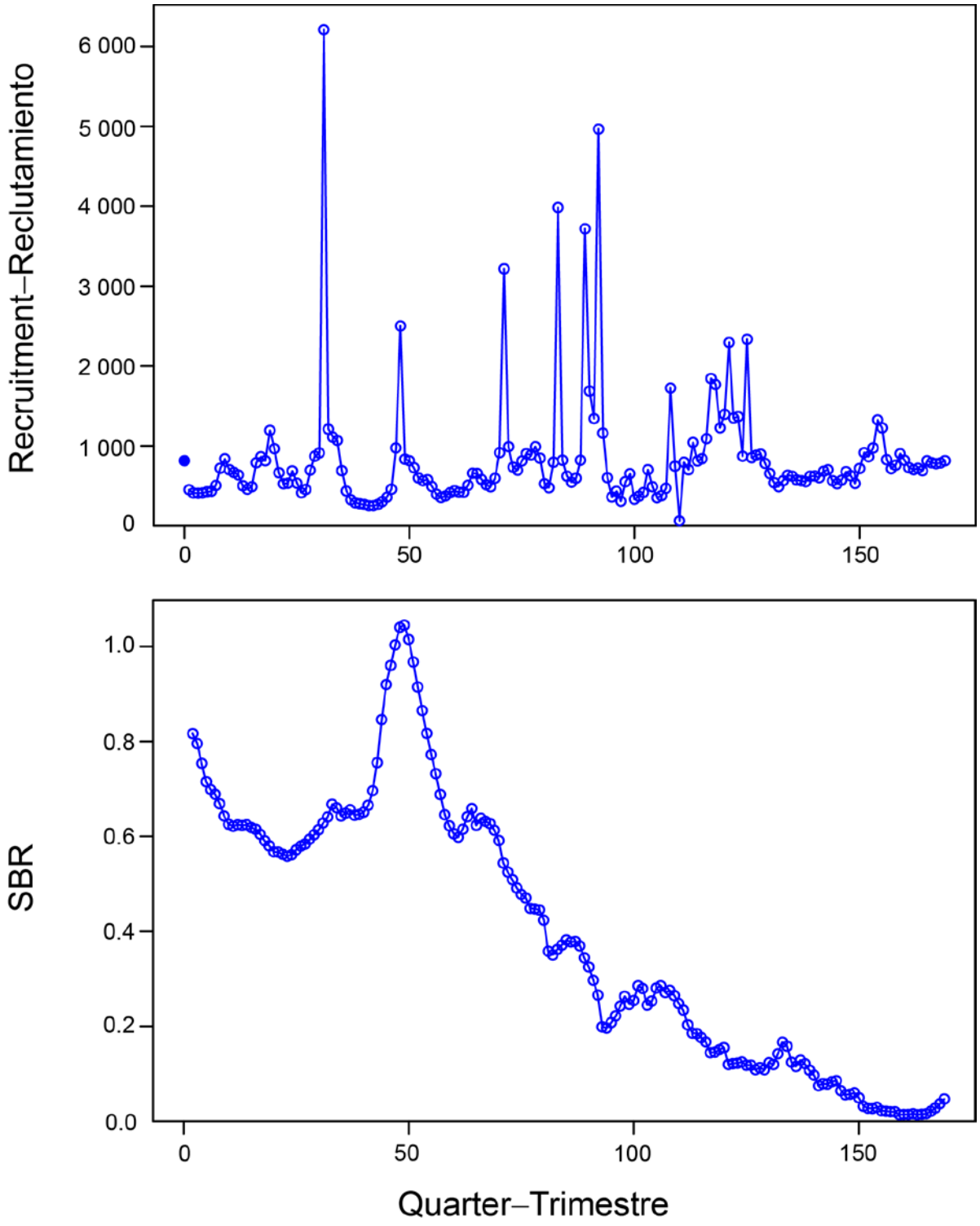

FIGURE 11. Estimates from the integrated model of quarterly recruitment, in thousands of fish (top panel), and spawning biomass ratio (SBR, bottom panel) of bigeye tuna in the Central area, 1975-2016.
FIGURA 11. Estimaciones del modelo integrado del reclutamiento trimestral, en miles de peces, (panel superior) y cociente de biomasa reproductora (SBR, panel inferior) de atún patudo en el área Central, 1975-2016.

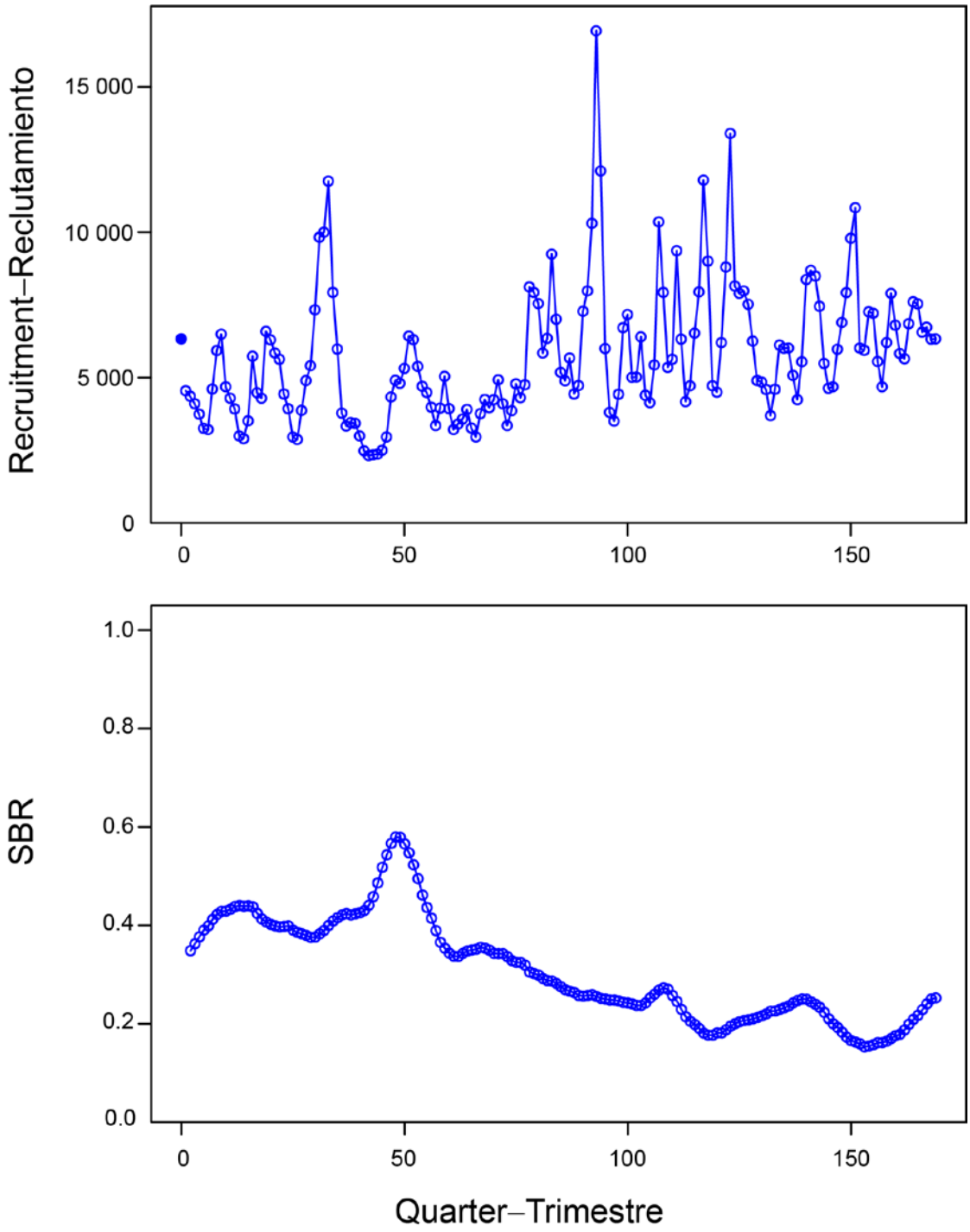

FIGURE 12. Estimates from the base case assessment model of quarterly recruitment, in thousands of fish, (top panel) and spawning biomass ratio (SBR, bottom panel) of bigeye tuna in the EPO, 1975-2016.
FIGURA 12. Estimaciones del modelo de evaluación de caso base del reclutamiento trimestral, en miles de peces, (panel superior) y cociente de biomasa reproductora (SBR, panel inferior) de atún patudo en el OPO entero, 1975-2016.

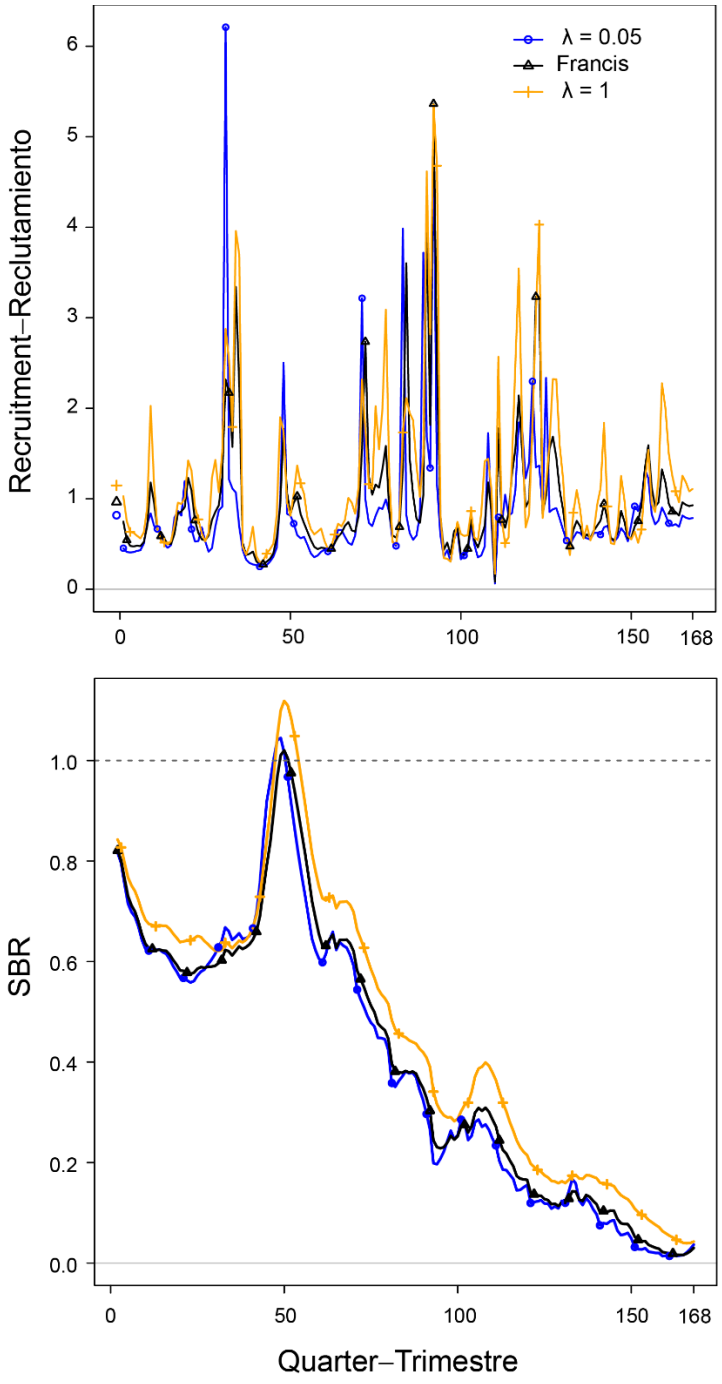

FIGURE 13. Estimates from the integrated model of quarterly recruitment, in millions of fish (top panel), and spawning biomass ratio (SBR, bottom panel) of bigeye tuna in the EPO with different weightings of the length-composition data: λ = 0.05 for all fisheries, as in the 2017 base case model; iterative weighting (Francis method) by fishery; λ = 1 for all fisheries.

FIGURA 13. Estimaciones del modelo integrado del reclutamiento trimestral (panel superior) y cociente de biomasa reproductora (SBR, panel inferior) del atún patudo en el OPO con distintas ponderaciones de los datos de composición por talla: λ = 0.05 para todas las pesquerías, al igual que en el modelo de caso base de 2017; ponderación iterativa (método de Francis) por pesquería; λ = 1 para todas las pesquerías.

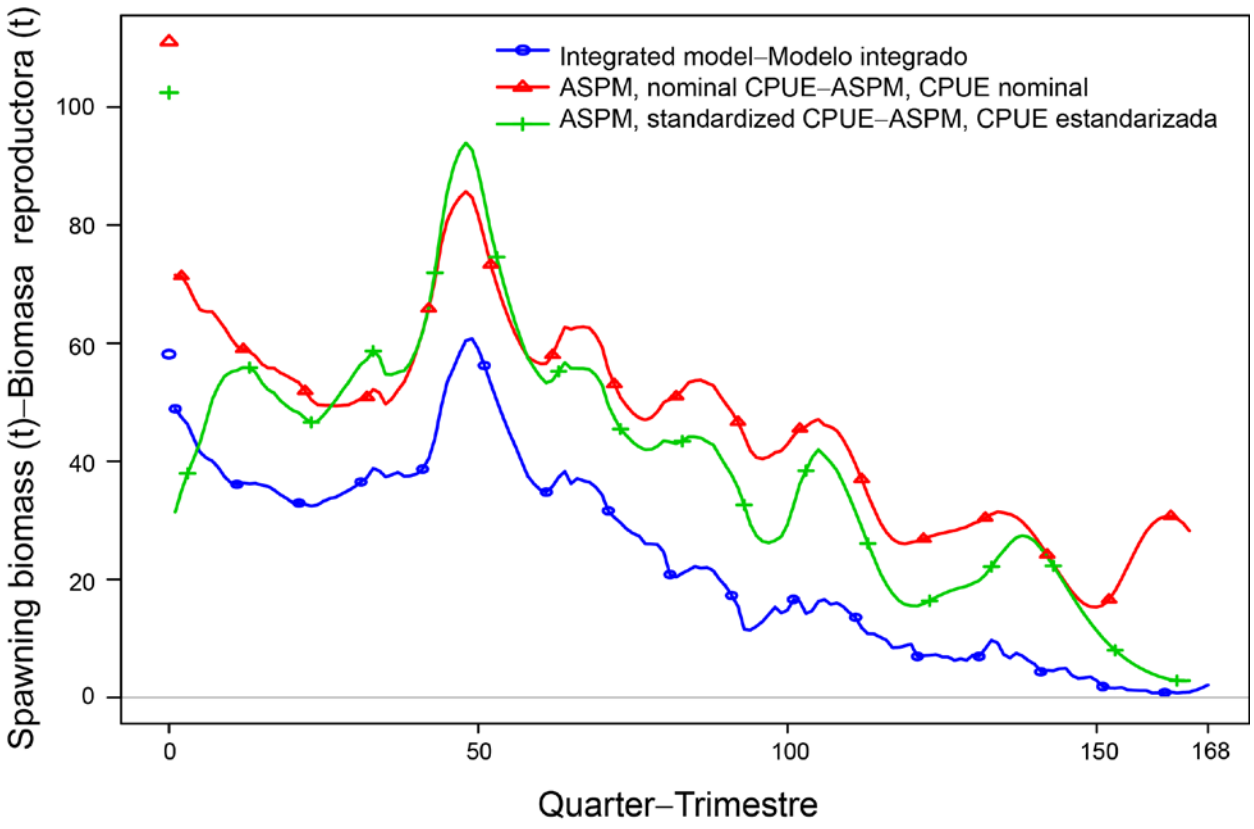

FIGURE 14. Estimated spawning biomass, in tons, of bigeye tuna in the Central area from the integrated model (blue line), and in the closest matching spatial area from the ASPM using nominal (red line) and standardized (green line) CPUE.

FIGURA 14. Biomasa reproductora estimada, en toneladas, de atún patudo en el área Central del modelo integrado (línea azul), y del área más parecida del modelo ASPM usando CPUE nominal (línea roja) y estandarizada (línea verde).

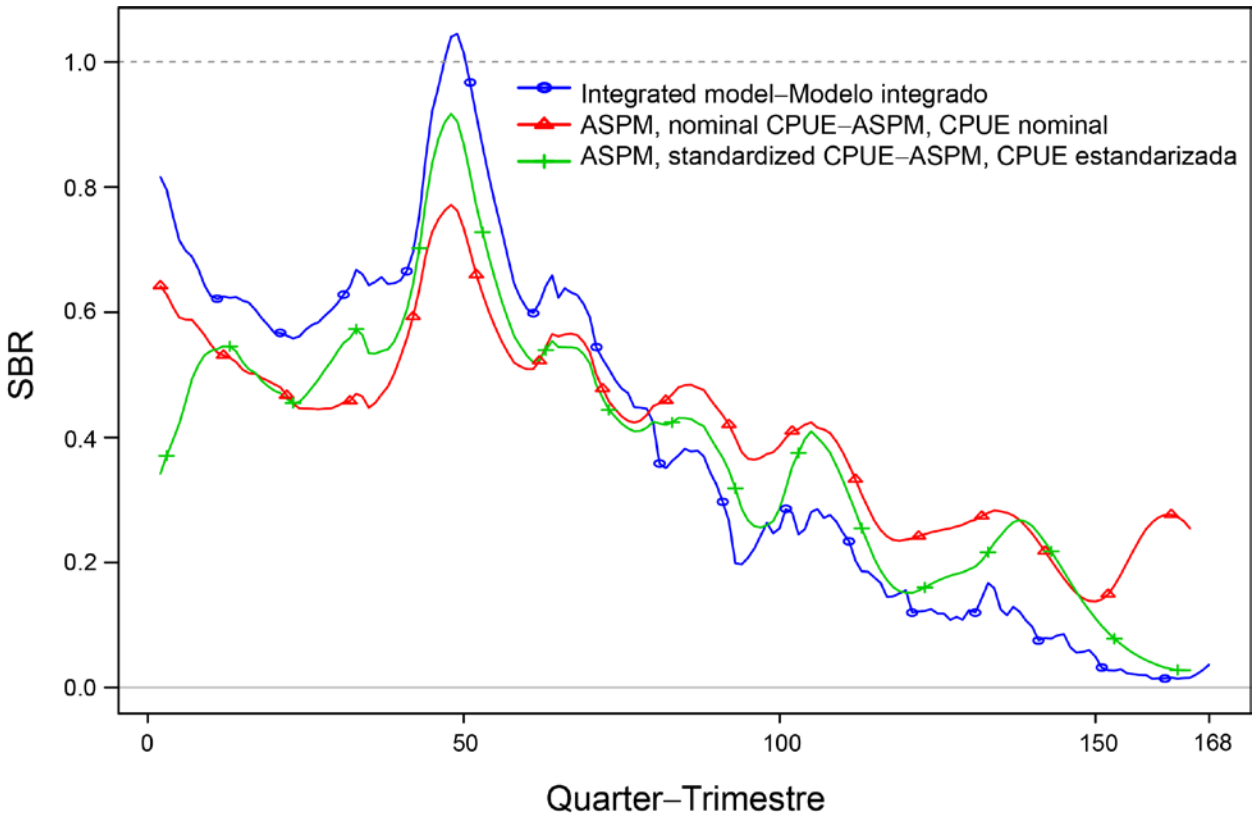

FIGURE 15. Spawning biomass ratio (SBR) of bigeye tuna in the EPO from the integrated model (blue line) and from the ASPM using nominal (red line) and standardized (green line) CPUE.
FIGURA 15. Cociente de biomasa reproductora (SBR) de atún patudo en el EPO del modelo integrado (línea azul), y del modelo ASPM usando CPUE nominal (línea roja) y estandarizada (línea verde).

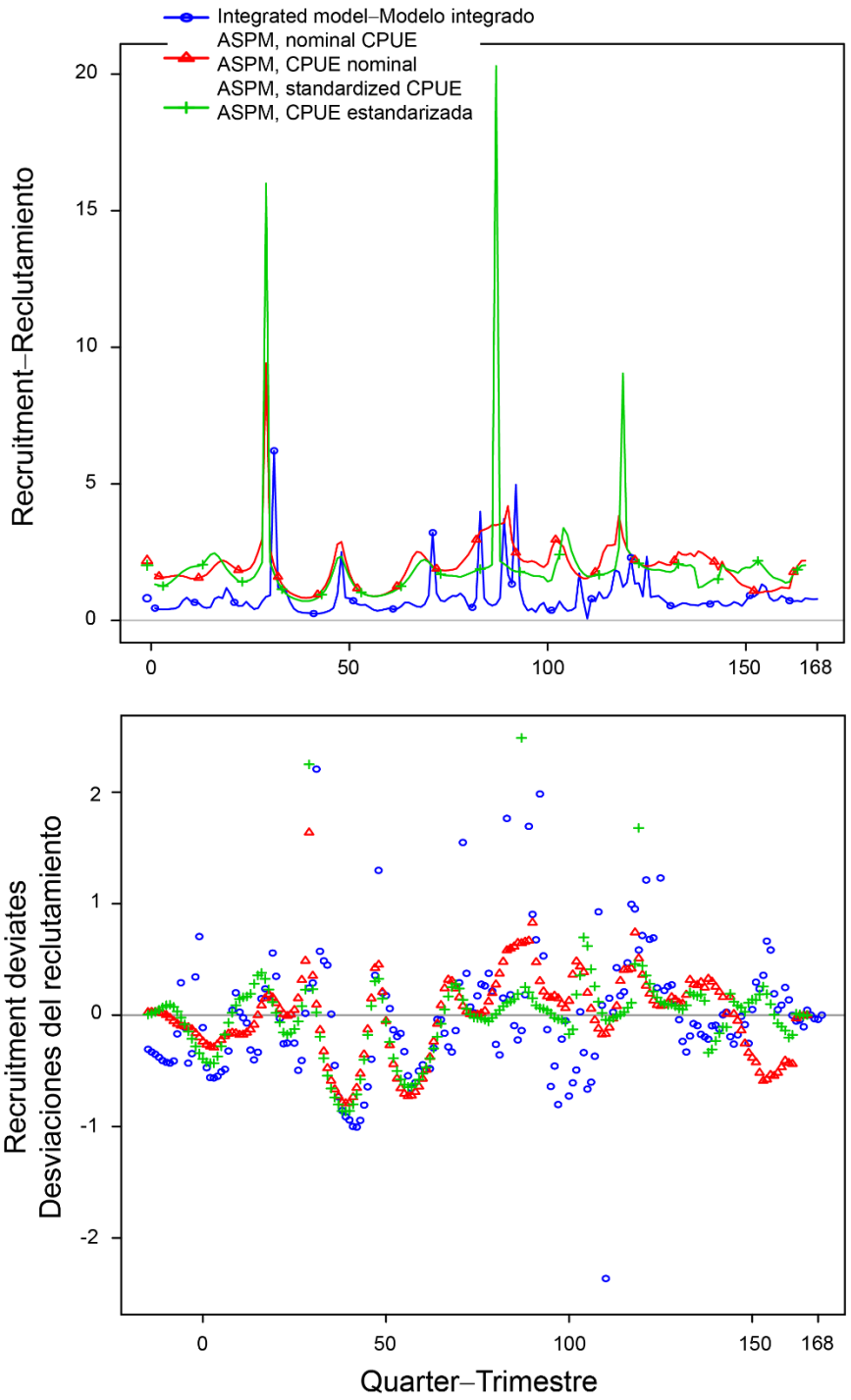

FIGURE 16. Quarterly recruitment (top panel) and recruitment deviates (bottom panel) of bigeye tuna in the EPO, from the integrated model (blue circles) and from the ASPM using nominal (red triangles) and standardized (green crosses) CPUE.

FIGURA 16. Reclutamiento trimestral (panel superior) y desviaciones del reclutamiento (panel inferior) del atún patudo en el OPO, del modelo integrado (círculos azules) y del modelo ASPM usando CPUE nominal (triángulos rojos) y estandarizada (cruces verdes).

APPENDIX – ANEXO

Results of the Age-Structured Production Model (ASPM)
Resultados del Modelo de producción con estructura por edad (ASPM)

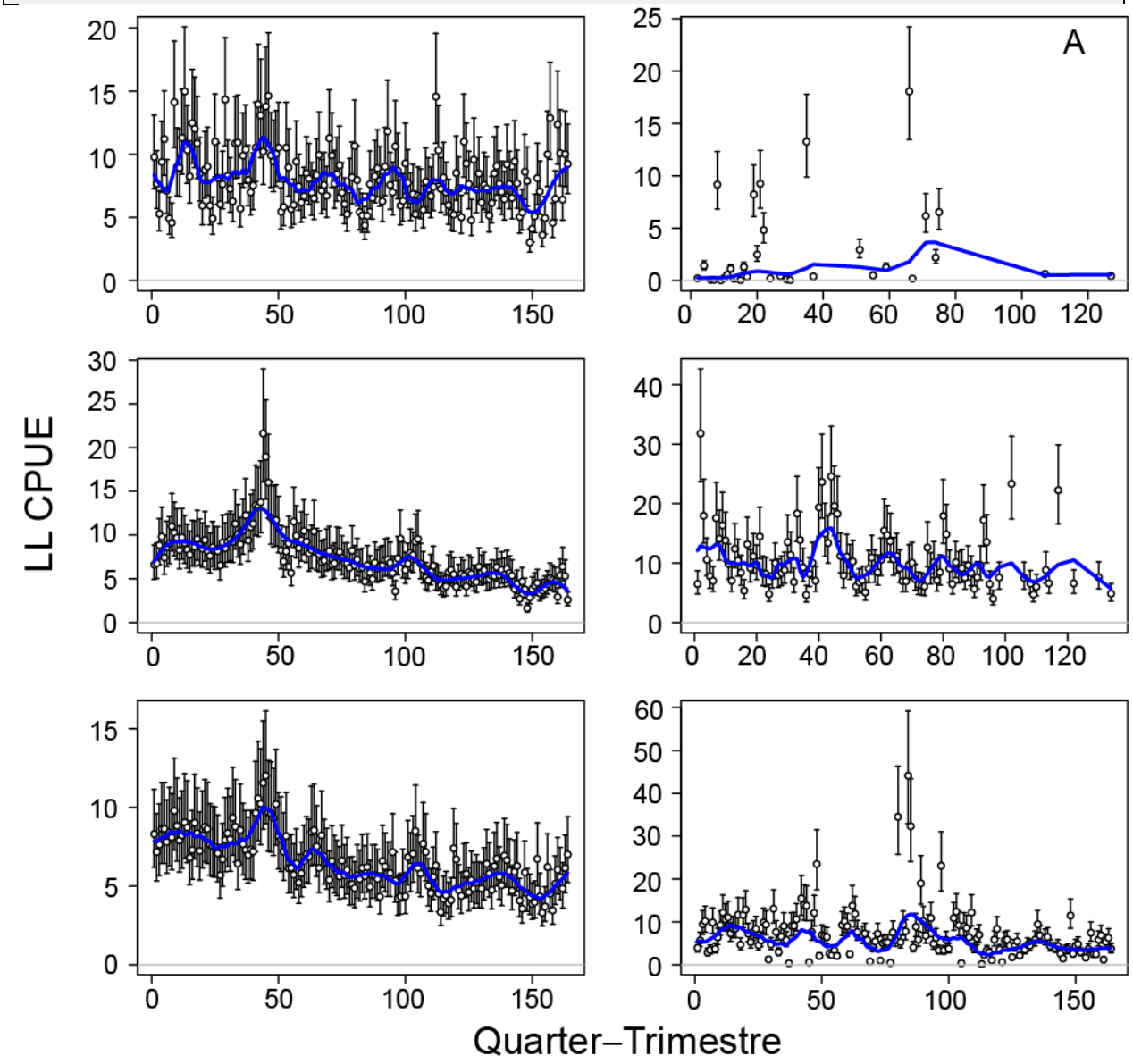

FIGURE A1. ASPM fits to longline CPUE for the six areas in grid A (Figure 7), with estimates of recruitment deviates.

FIGURA A1. Ajustes del ASPM a la CPUE palangrera correspondiente a las seis áreas en la cuadrícula A (Figura 7), con estimaciones de las desviaciones del reclutamiento.

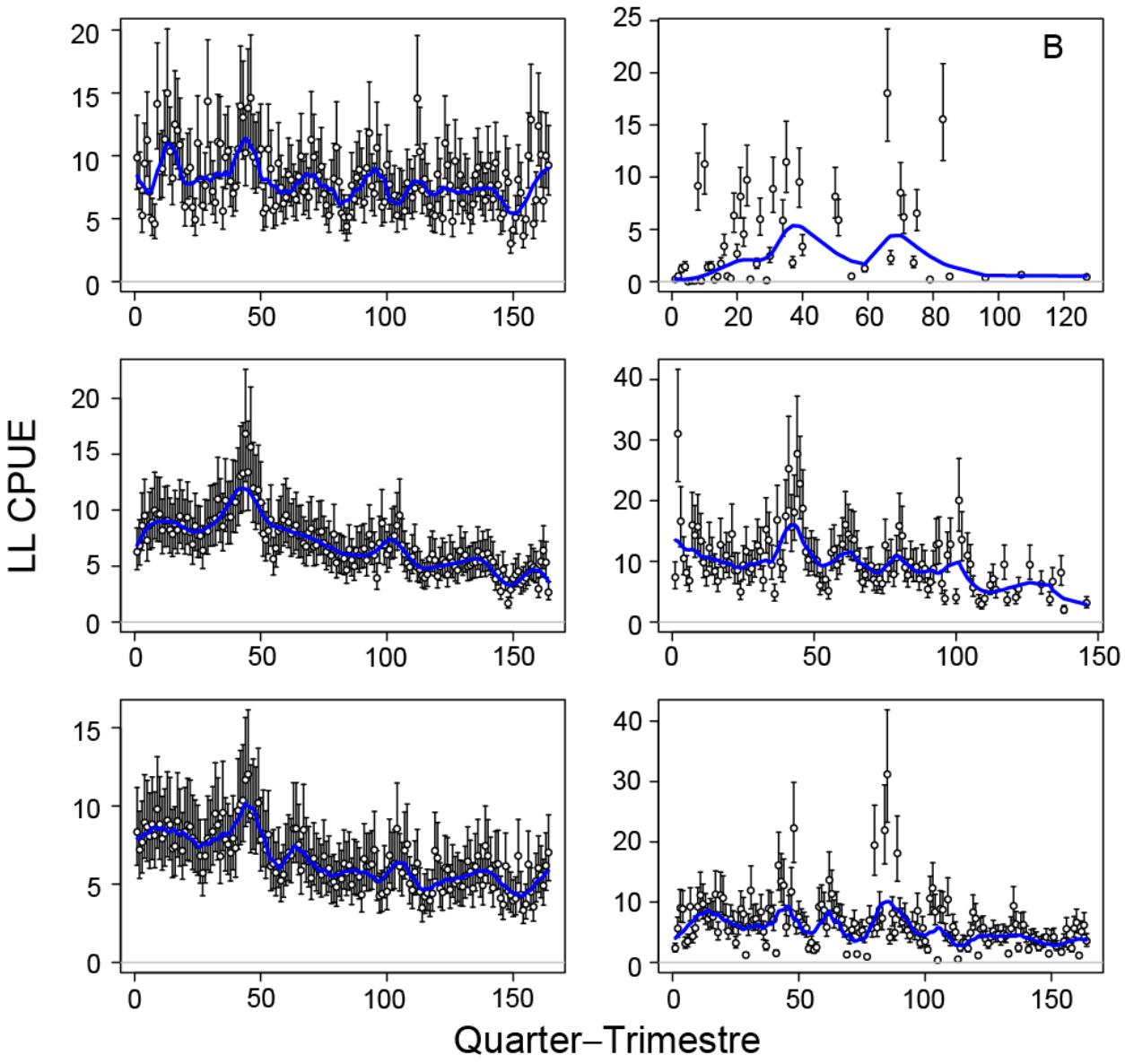

FIGURE A2. ASPM fits to longline CPUE for the six areas in grid B (Figure 7), with estimates of recruitment deviates.

FIGURA A2. Ajustes del ASPM a la CPUE palangrera correspondiente a las seis áreas en la cuadrícula B (Figura 7), con estimaciones de las desviaciones del reclutamiento.

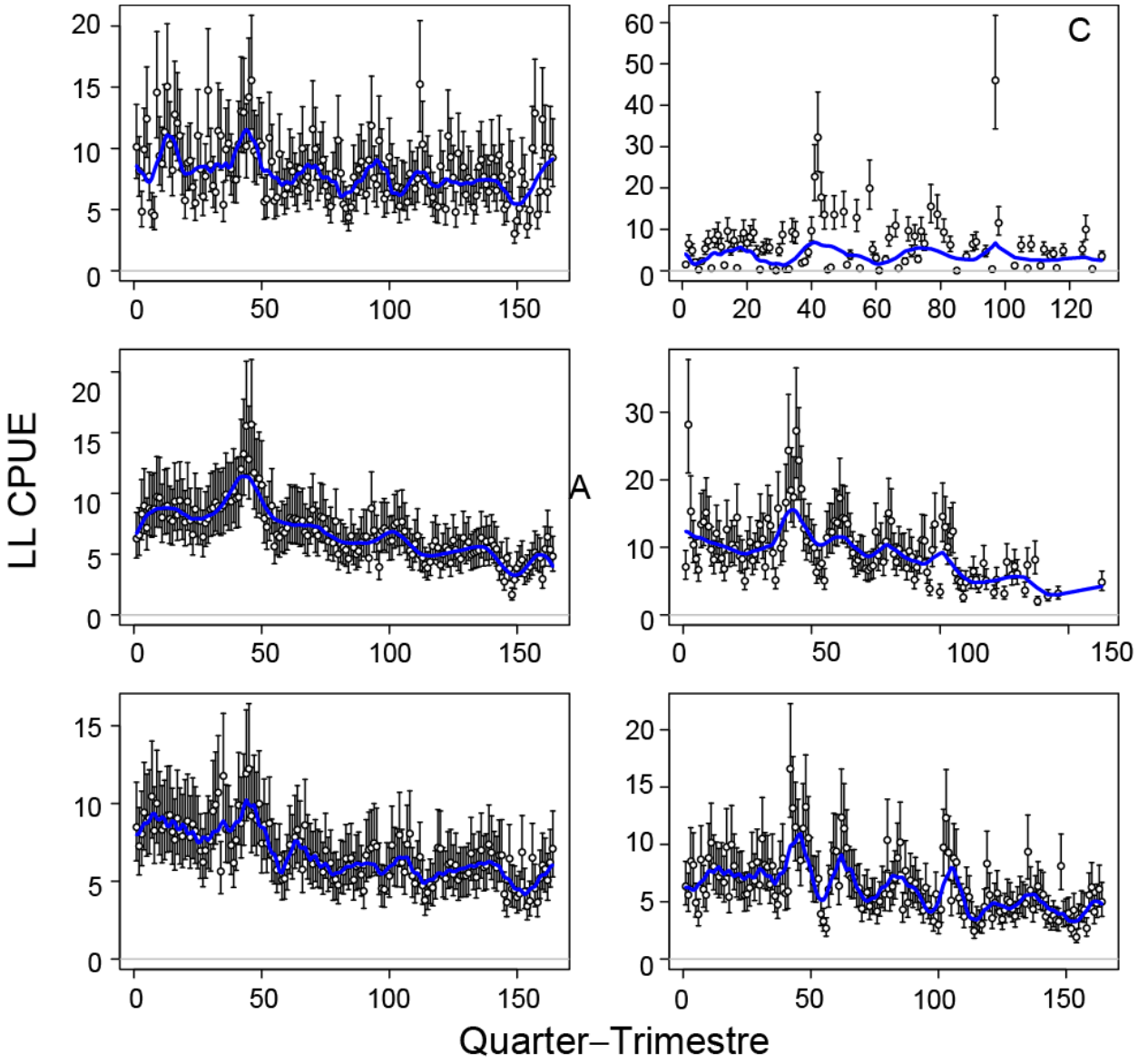

FIGURE A3. ASPM fits to longline CPUE for the six areas in grid C (Figure 7), with estimates of recruitment deviates.

FIGURA A3. Ajustes del ASPM a la CPUE palangrera correspondiente a las seis áreas en la cuadrícula C (Figura 7), con estimaciones de las desviaciones del reclutamiento.

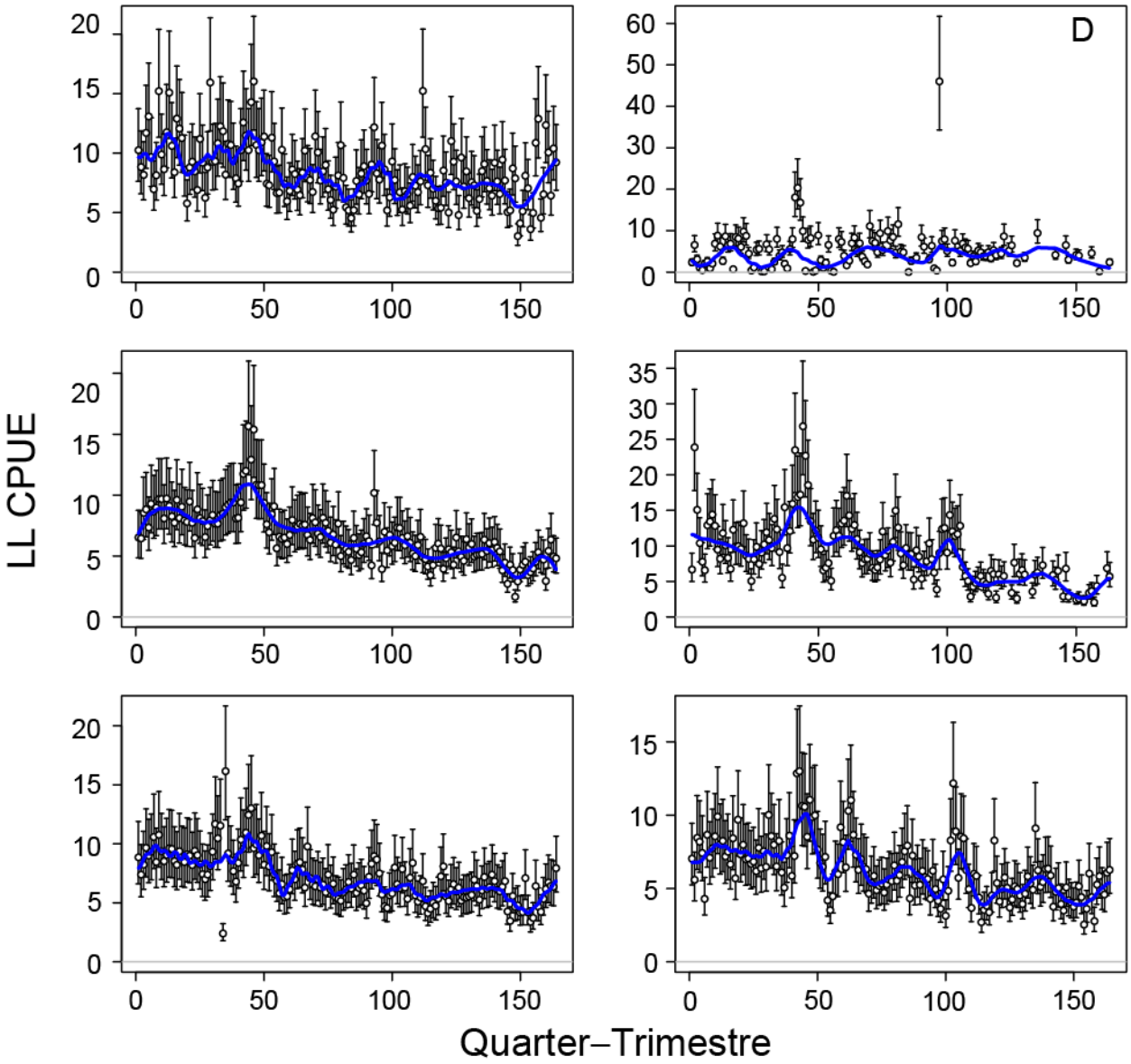

FIGURE A4. ASPM fits to longline CPUE for the six areas in grid D (Figure 7), with estimates of recruitment deviates.

FIGURA A4. Ajustes del ASPM a la CPUE palangrera correspondiente a las seis áreas en la cuadrícula D (Figura 7), con estimaciones de las desviaciones del reclutamiento.

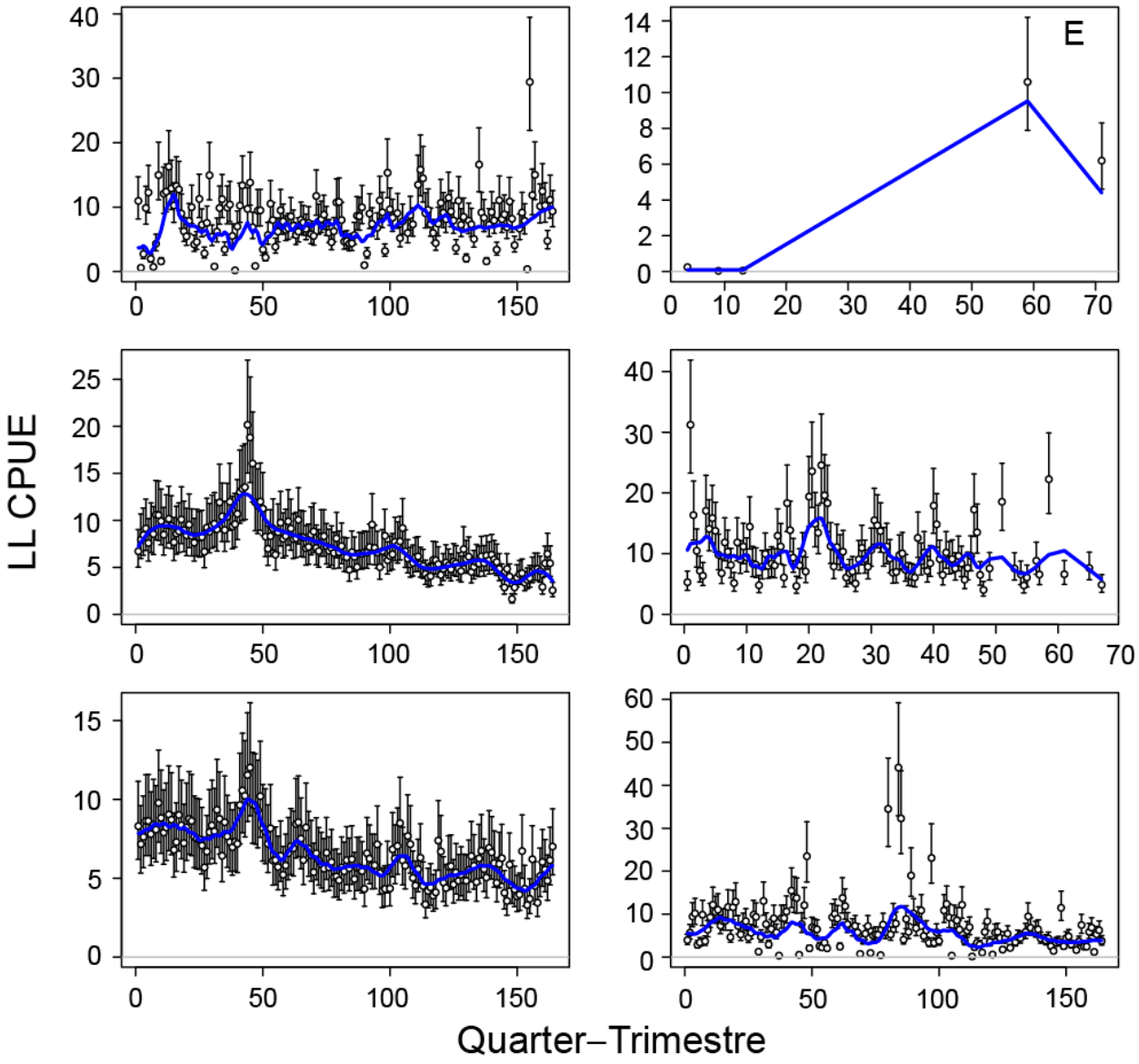

FIGURE A5. ASPM fits to longline CPUE for the six areas in grid E (Figure 7), with estimates of recruitment deviates.

FIGURA A5. Ajustes del ASPM a la CPUE palangrera correspondiente a las seis áreas en la cuadrícula E (Figura 7), con estimaciones de las desviaciones del reclutamiento.

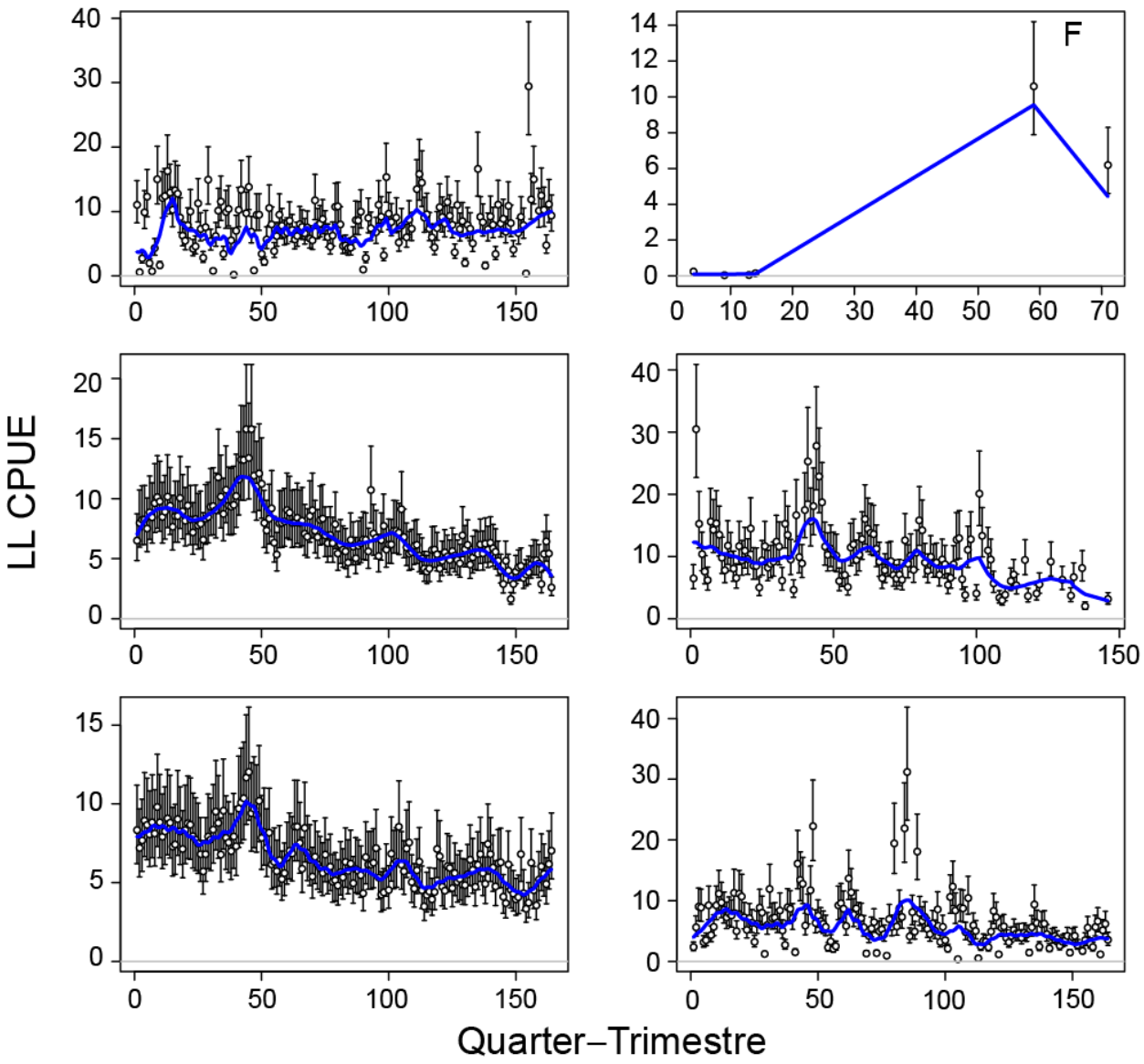

FIGURE A6. ASPM fits to longline CPUE for the six areas in grid F (Figure 7), with estimates of recruitment deviates.

FIGURA A6. Ajustes del ASPM a la CPUE palangrera correspondiente a las seis áreas en la cuadrícula F (Figura 7), con estimaciones de las desviaciones del reclutamiento.

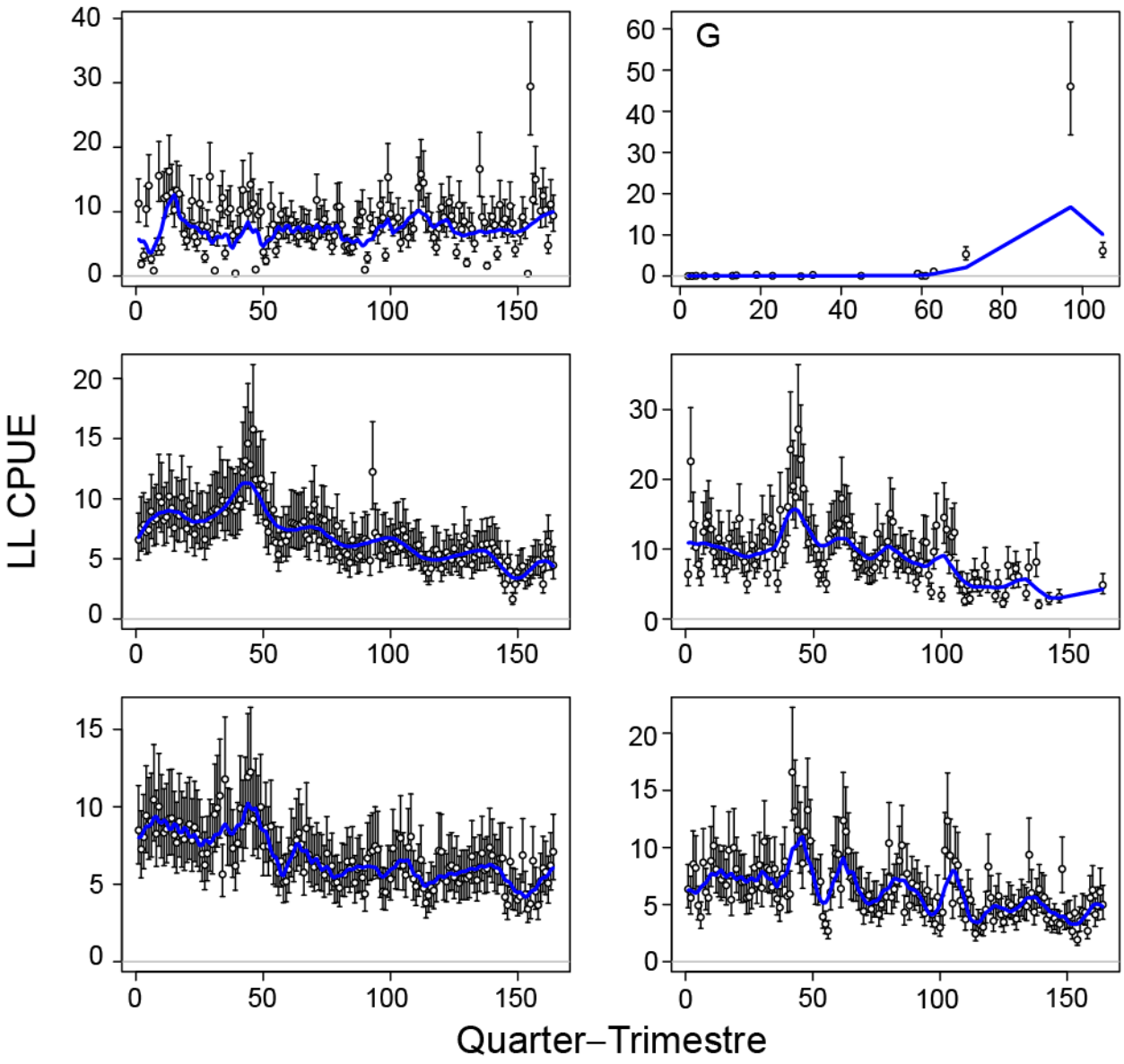

FIGURE A7. ASPM fits to longline CPUE for the six areas in grid G (Figure 7), with estimates of recruitment deviates.

FIGURA A7. Ajustes del ASPM a la CPUE palangrera correspondiente a las seis áreas en la cuadrícula G (Figura 7), con estimaciones de las desviaciones del reclutamiento.

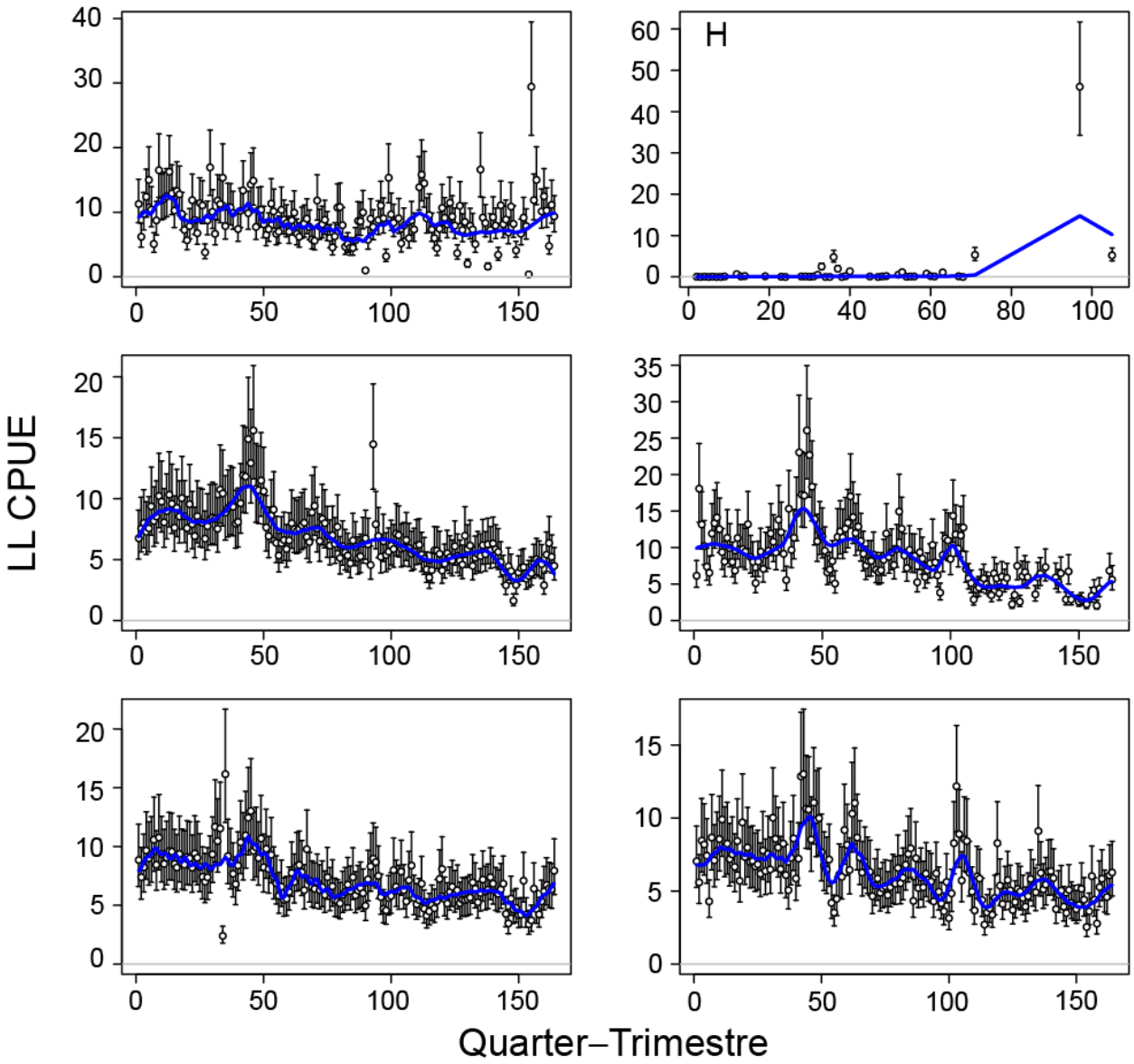

FIGURE A8. ASPM fits to longline CPUE for the six areas in grid H (Figure 7), with estimates of recruitment deviates.

FIGURA A8. Ajustes del ASPM a la CPUE palangrera correspondiente a las seis áreas en la cuadrícula H (Figura 7), con estimaciones de las desviaciones del reclutamiento.

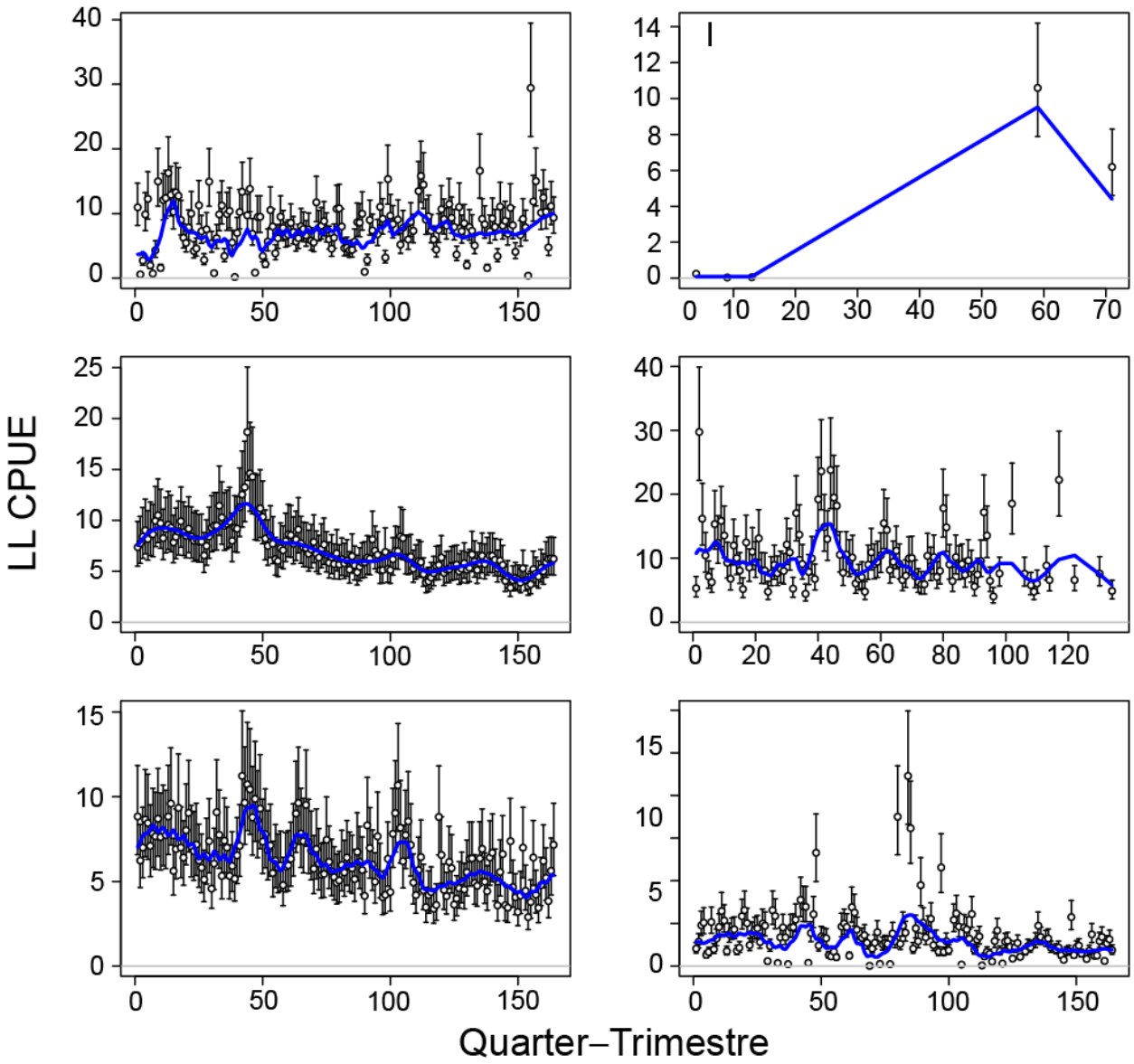

FIGURE A9. ASPM fits to longline CPUE for the six areas in grid I (Figure 7), with estimates of recruitment deviates.

FIGURA A9. Ajustes del ASPM a la CPUE palangrera correspondiente a las seis áreas en la cuadrícula I (Figura 7), con estimaciones de las desviaciones del reclutamiento.

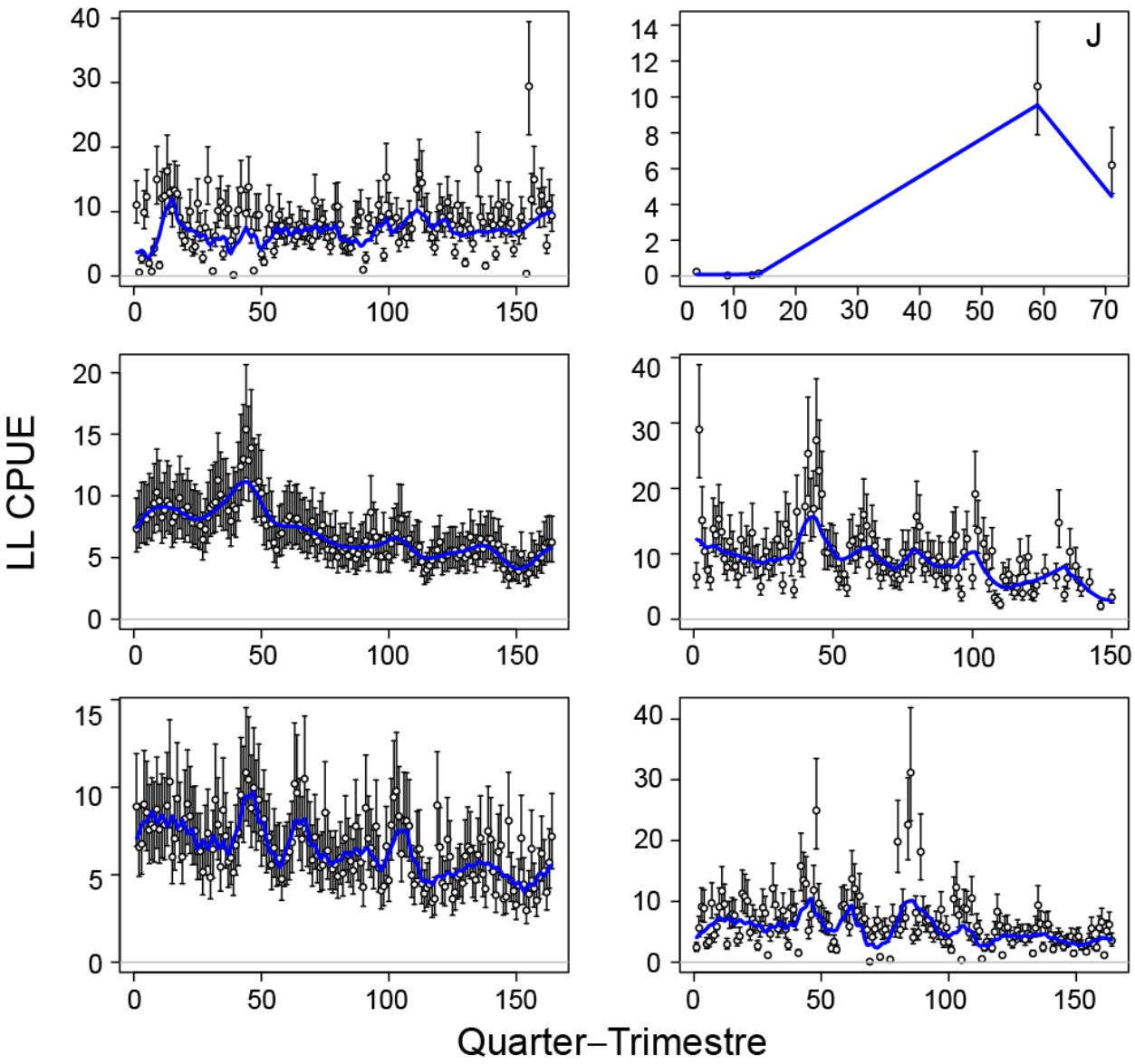

FIGURE A10. ASPM fits to longline CPUE for the six areas in grid J (Figure 7), with estimates of recruitment deviates.

FIGURA A10. Ajustes del ASPM a la CPUE palangrera correspondiente a las seis áreas en la cuadrícula J (Figura 7), con estimaciones de las desviaciones del reclutamiento.

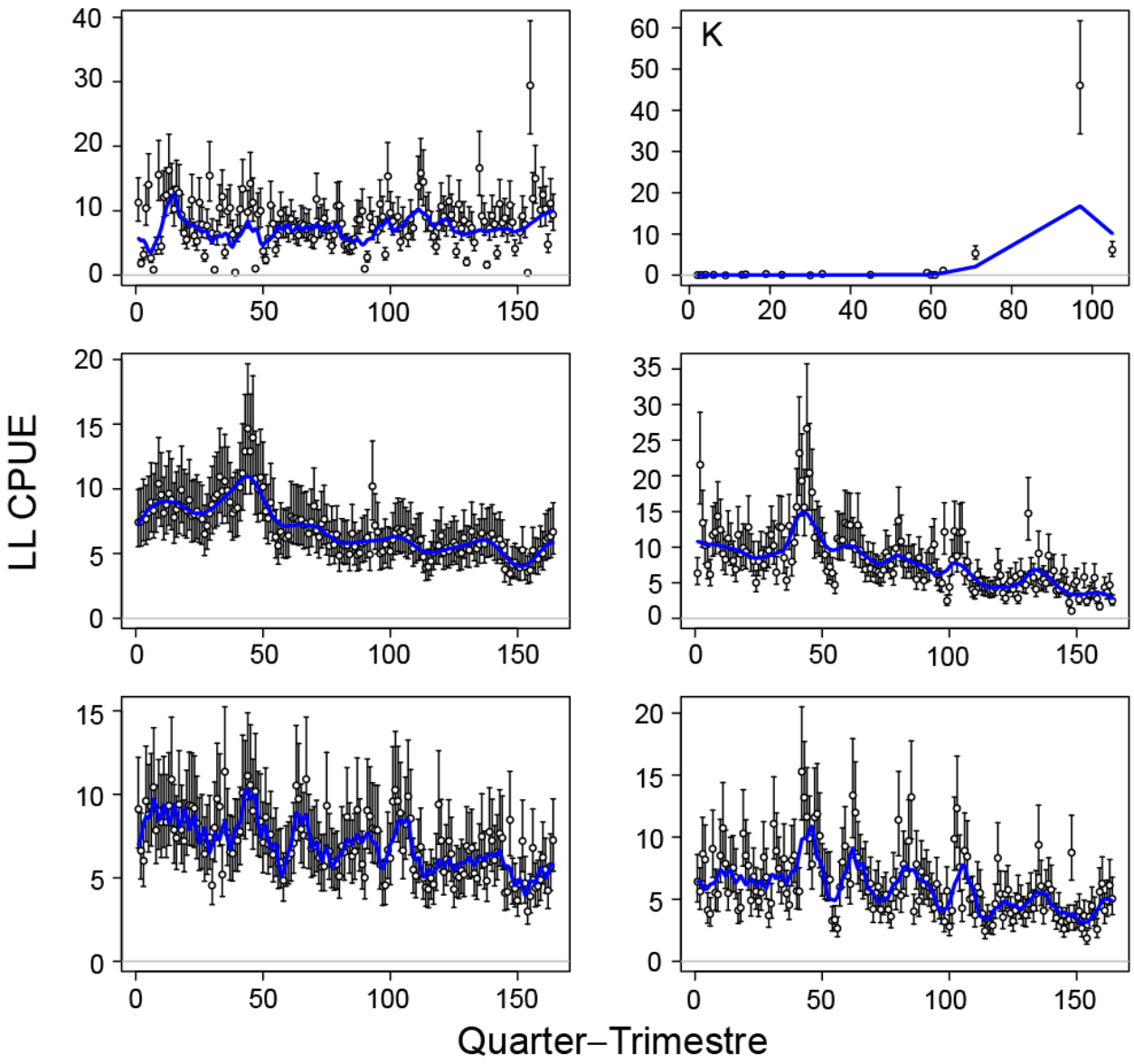

FIGURE A11. ASPM fits to longline CPUE for the six areas in grid K (Figure 7), with estimates of recruitment deviates.

FIGURA A11. Ajustes del ASPM a la CPUE palangrera correspondiente a las seis áreas en la cuadrícula K (Figura 7), con estimaciones de las desviaciones del reclutamiento.

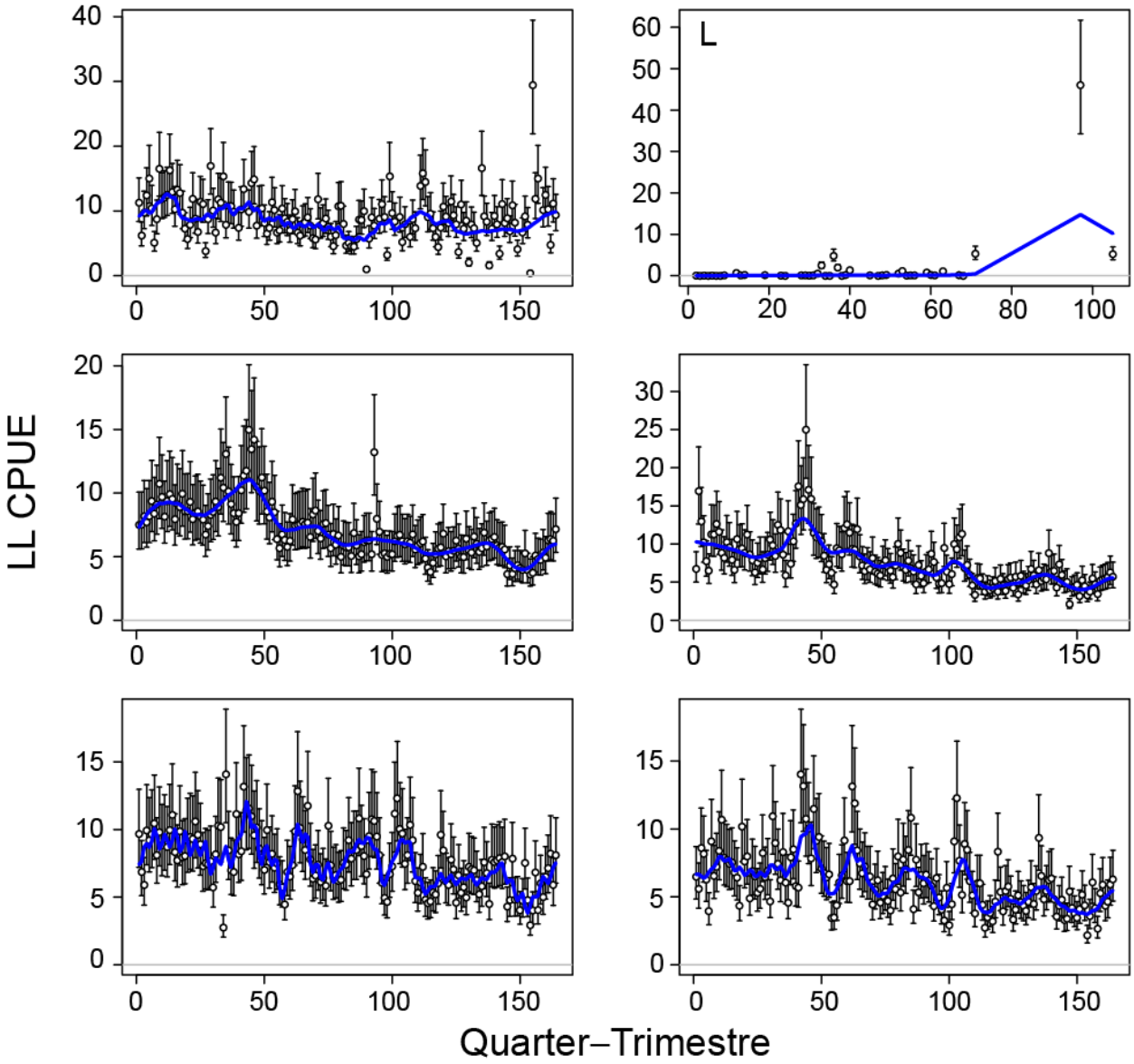

FIGURE A12. ASPM fits to longline CPUE for the six areas in grid L (Figure 7), with estimates of recruitment deviates.

FIGURA A12. Ajustes del ASPM a la CPUE palangrera correspondiente a las seis áreas en la cuadrícula L (Figura 7), con estimaciones de las desviaciones del reclutamiento.

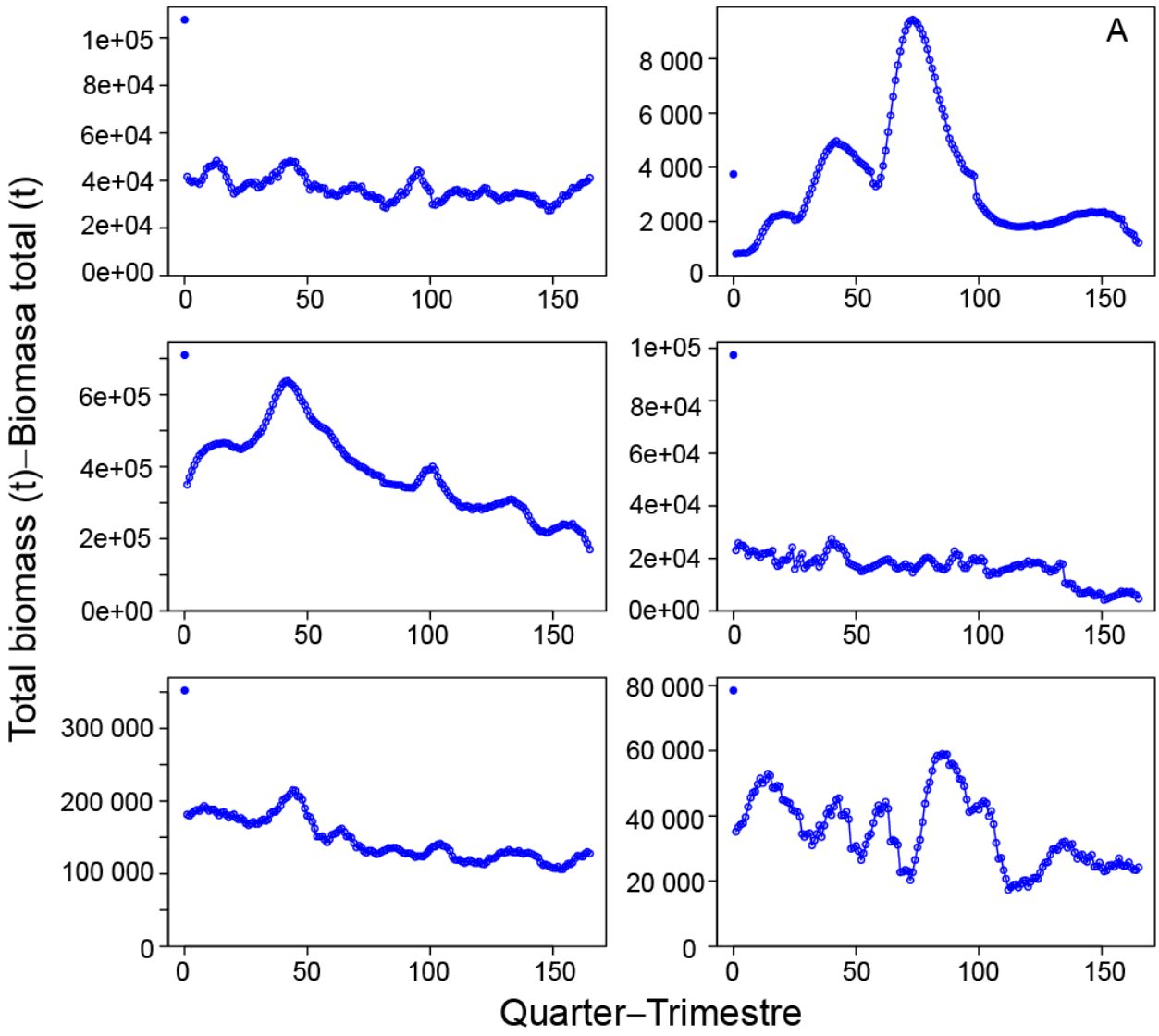

FIGURE A13. ASPM estimates of total biomass for the six areas in grid A (Figure 7), with estimates of recruitment deviates.

FIGURA A13. Estimaciones del ASPM de biomasa total correspondientes a las seis áreas en la cuadrícula A (Figura 7), con estimaciones de las desviaciones del reclutamiento.

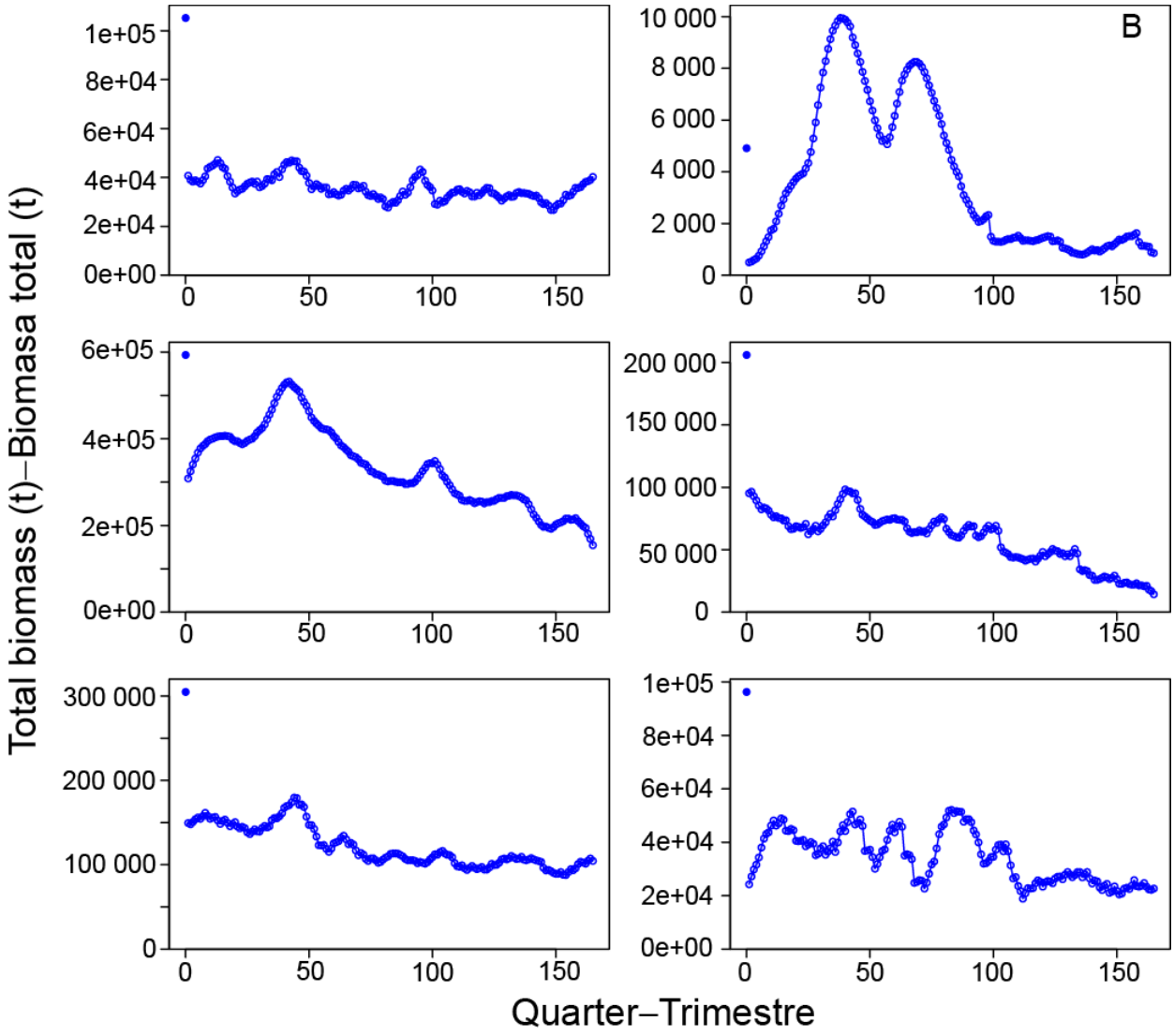

FIGURE A14. ASPM estimates of total biomass for the six areas in grid B (Figure 7), with estimates of recruitment deviates.

FIGURA A14. Estimaciones del ASPM de biomasa total correspondientes a las seis áreas en la cuadrícula B (Figura 7), con estimaciones de las desviaciones del reclutamiento.

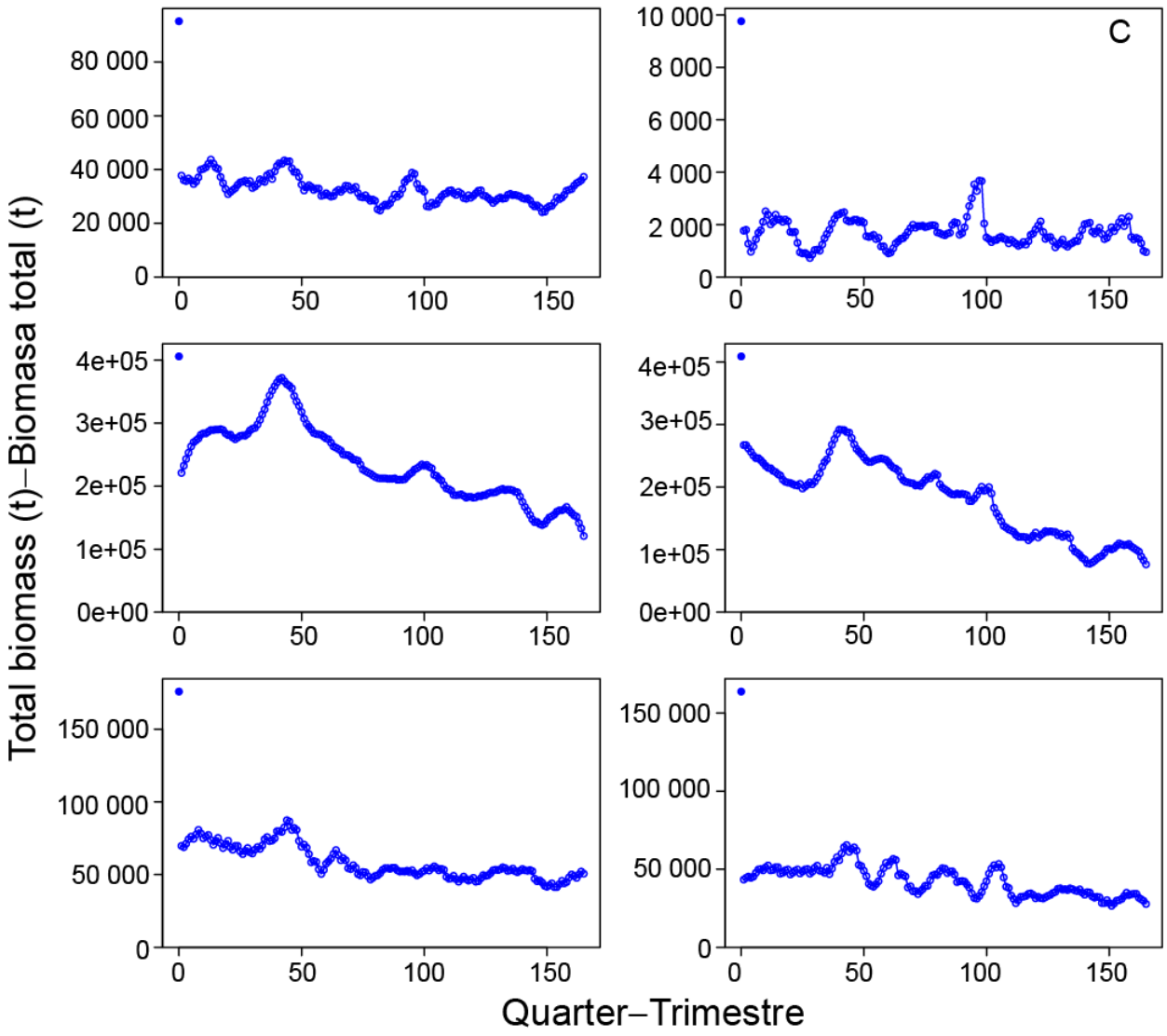

FIGURE A15. ASPM estimates of total biomass for the six areas in grid C (Figure 7), with estimates of recruitment deviates.

FIGURA A15. Estimaciones del ASPM de biomasa total correspondientes a las seis áreas en la cuadrícula C (Figura 7), con estimaciones de las desviaciones del reclutamiento.

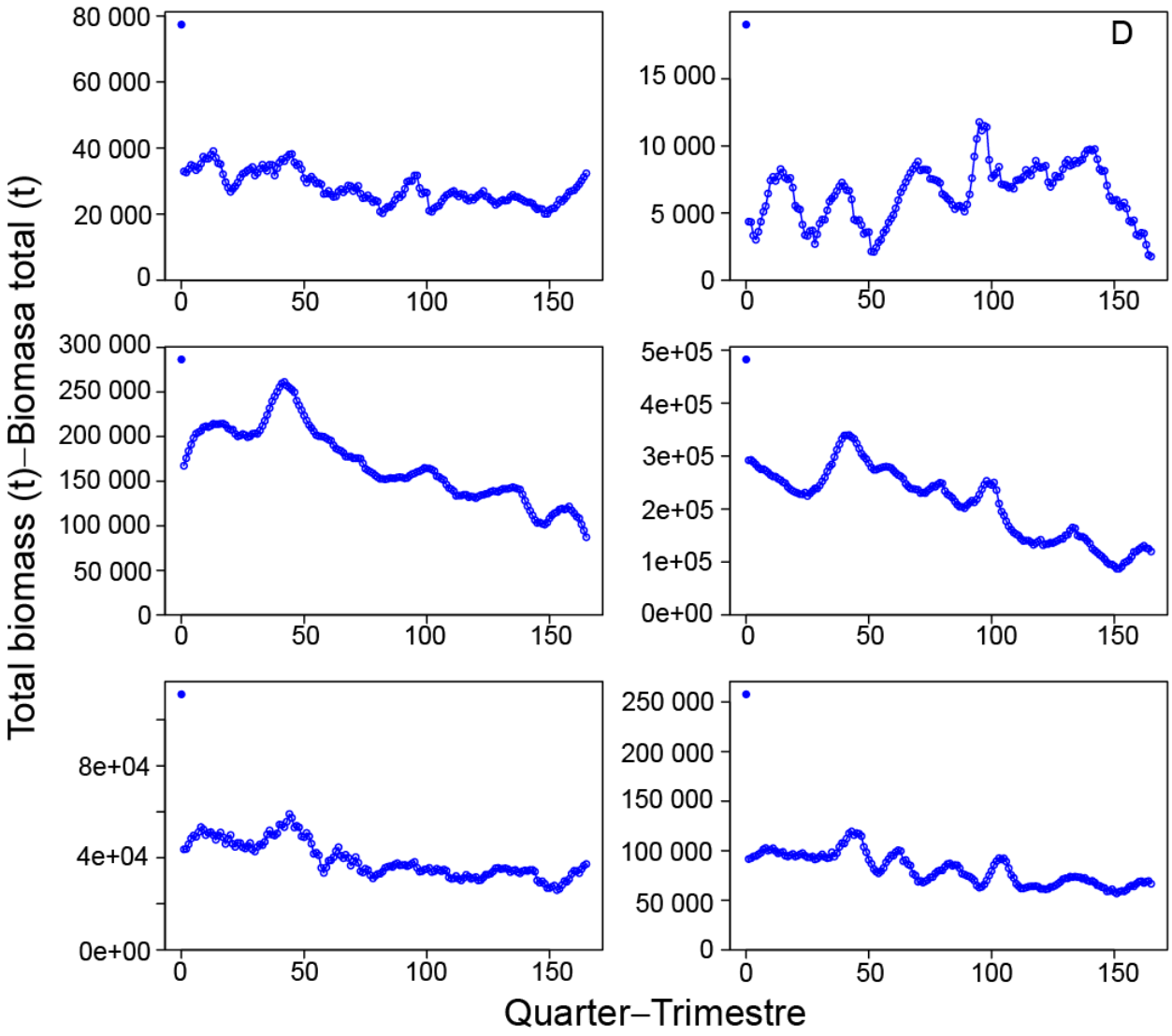

FIGURE A16. ASPM estimates of total biomass for the six areas in grid D (Figure 7), with estimates of recruitment deviates.

FIGURA A16. Estimaciones del ASPM de biomasa total correspondientes a las seis áreas en la cuadrícula D (Figura 7), con estimaciones de las desviaciones del reclutamiento.

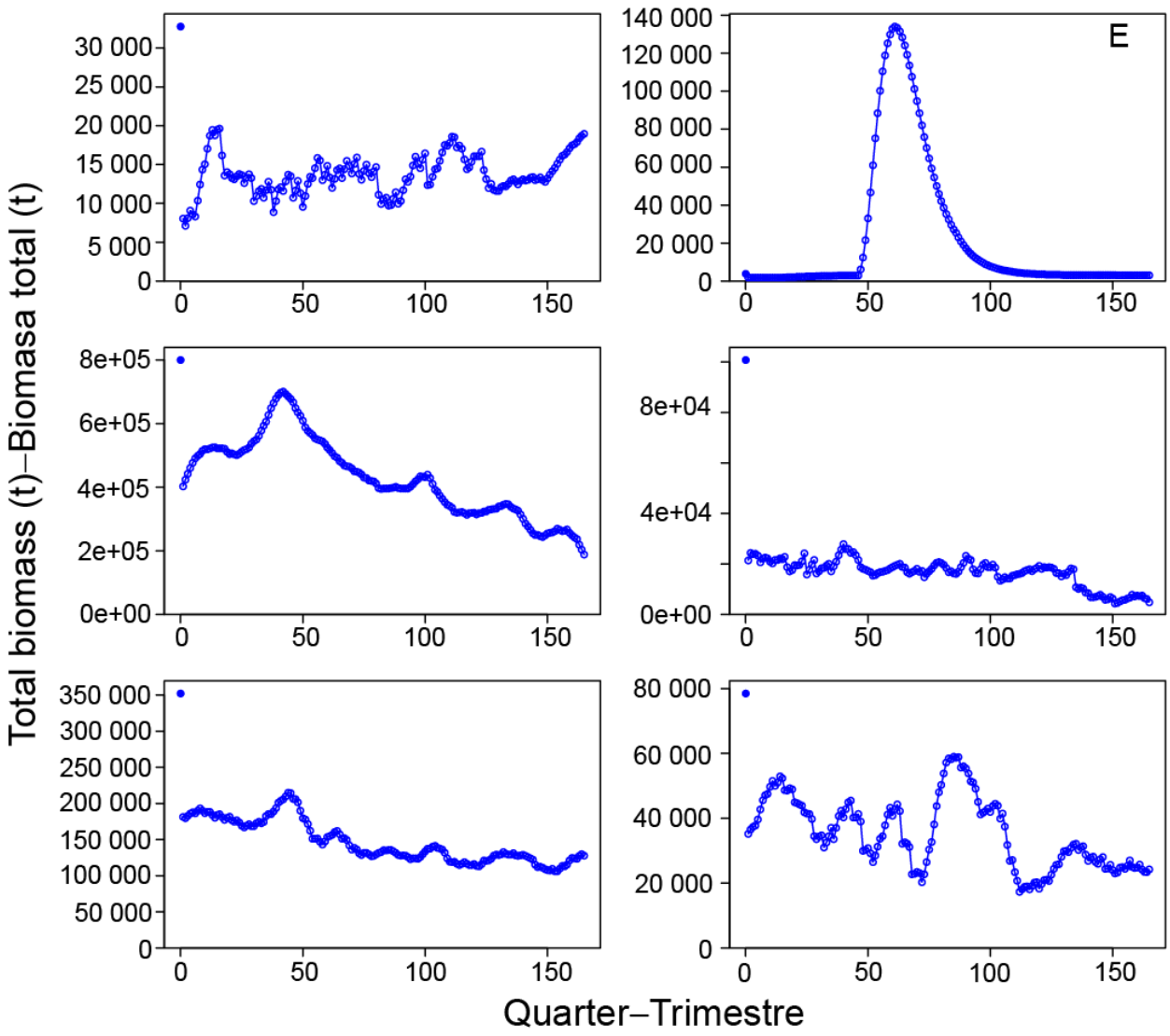

FIGURE A17. ASPM estimates of total biomass for the six areas in grid E (Figure 7), with estimates of recruitment deviates.

FIGURA A17. Estimaciones del ASPM de biomasa total correspondientes a las seis áreas en la cuadrícula E (Figura 7), con estimaciones de las desviaciones del reclutamiento.

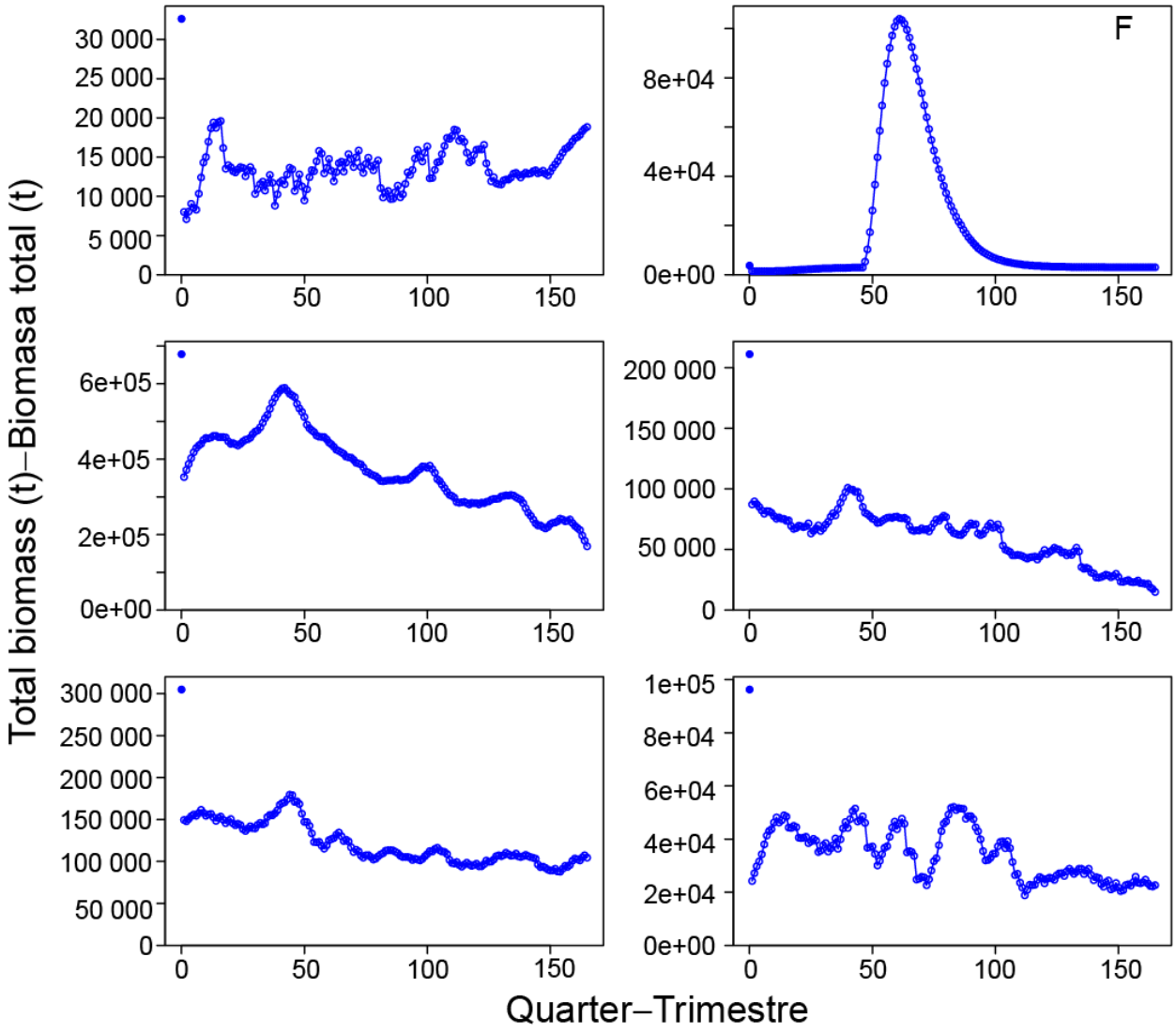

FIGURE A18. ASPM estimates of total biomass for the six areas in grid F (Figure 7), with estimates of recruitment deviates.

FIGURA A18. Estimaciones del ASPM de biomasa total correspondientes a las seis áreas en la cuadrícula F (Figura 7), con estimaciones de las desviaciones del reclutamiento.

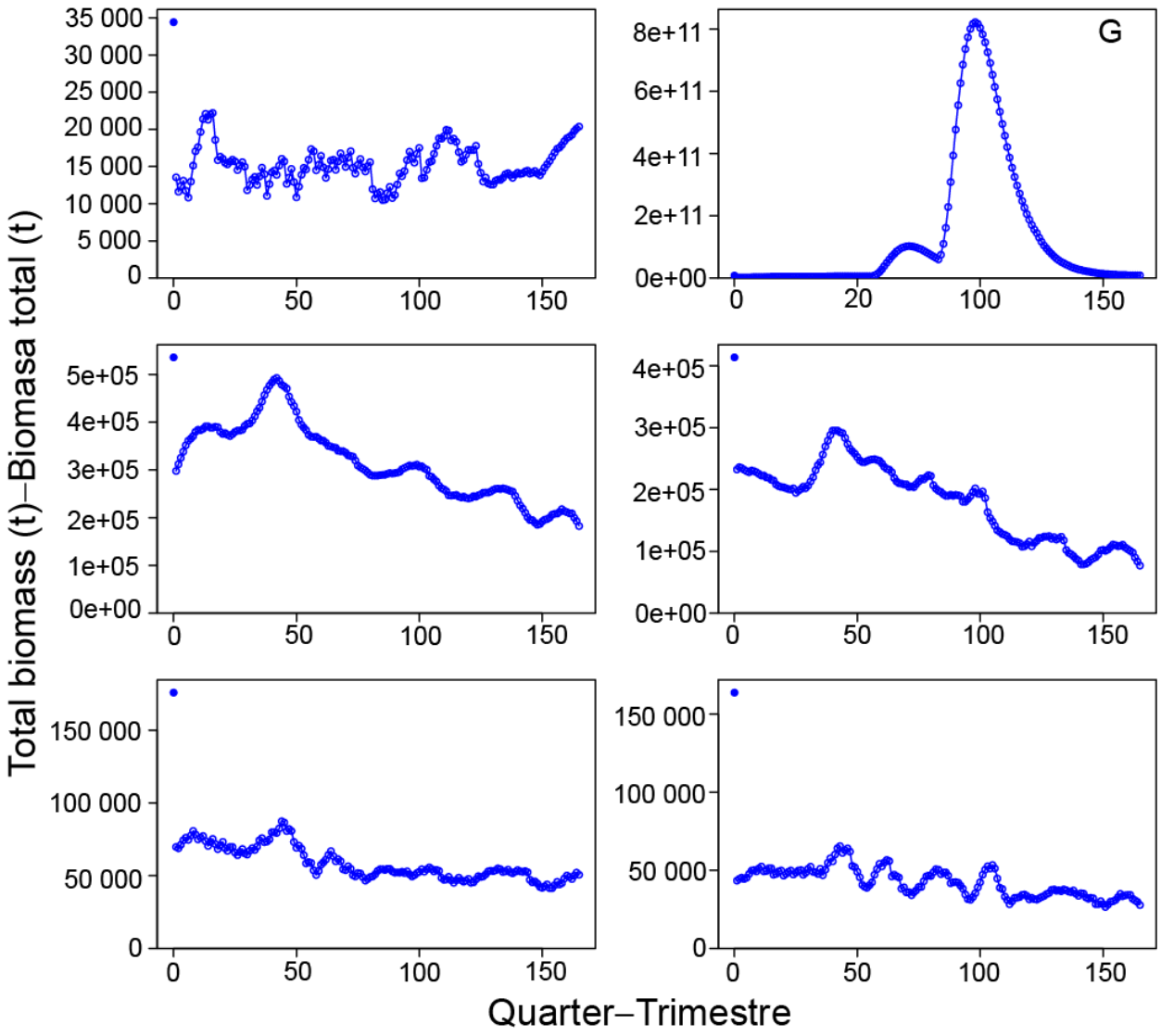

FIGURE A19. ASPM estimates of total biomass for the six areas in grid G (Figure 7), with estimates of recruitment deviates.

FIGURA A19. Estimaciones del ASPM de biomasa total correspondientes a las seis áreas en la cuadrícula G (Figura 7), con estimaciones de las desviaciones del reclutamiento.

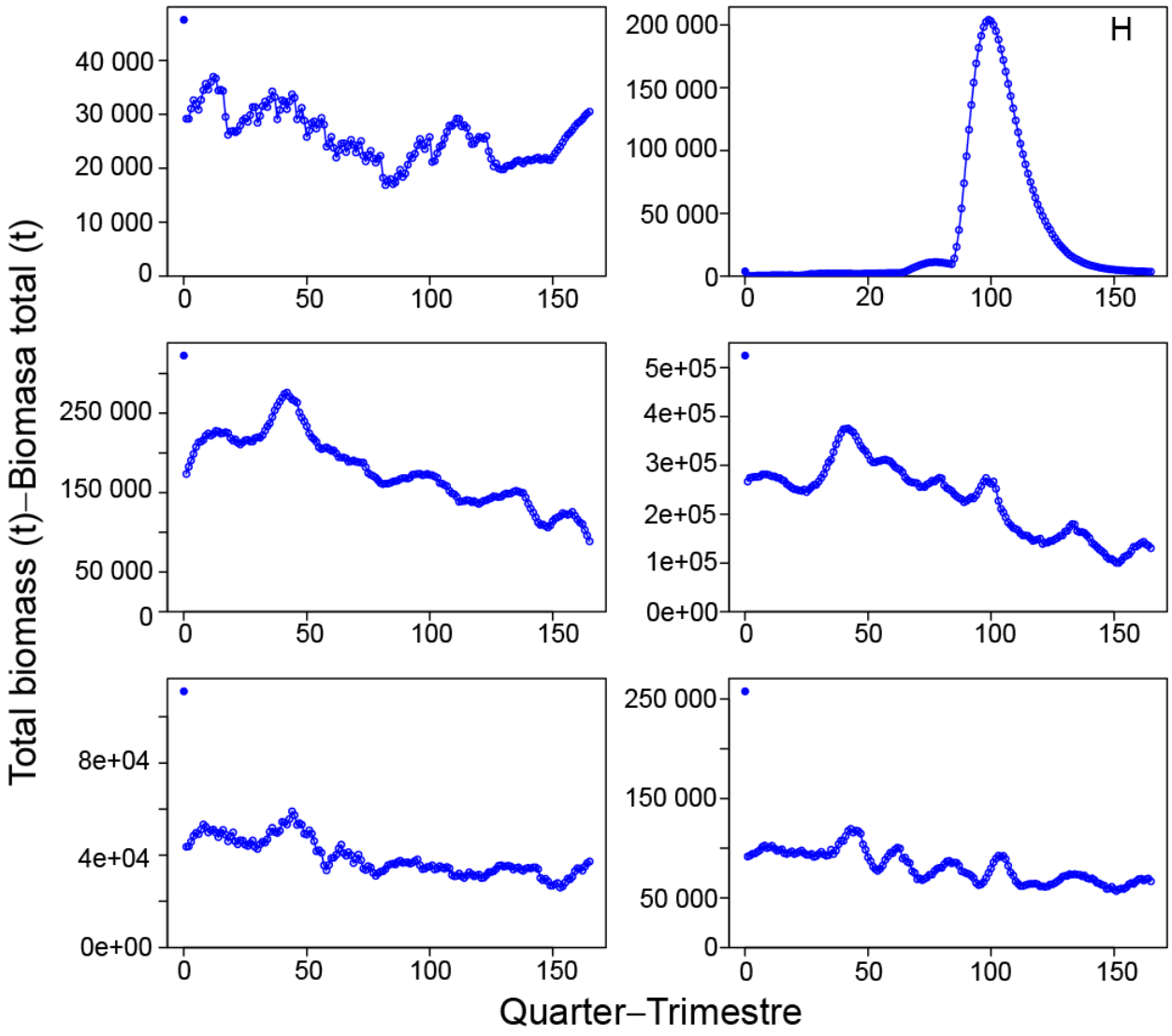

FIGURE A20. ASPM estimates of total biomass for the six areas in grid H (Figure 7), with estimates of recruitment deviates.

FIGURA A20. Estimaciones del ASPM de biomasa total correspondientes a las seis áreas en la cuadrícula H (Figura 7), con estimaciones de las desviaciones del reclutamiento.

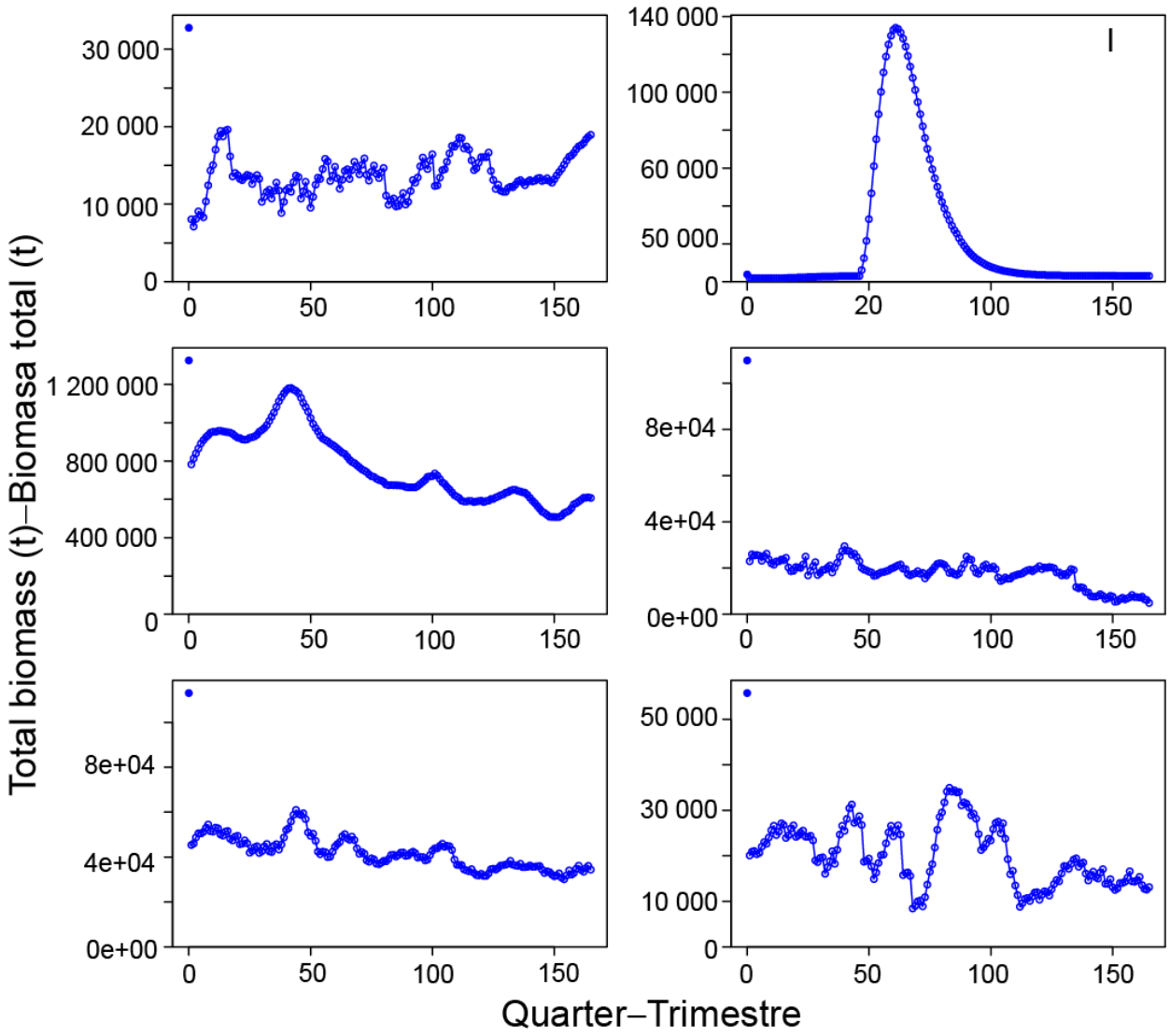

FIGURE A21. ASPM estimates of total biomass for the six areas in grid I (Figure 7), with estimates of recruitment deviates.

FIGURA A21. Estimaciones del ASPM de biomasa total correspondientes a las seis áreas en la cuadrícula I (Figura 7), con estimaciones de las desviaciones del reclutamiento.

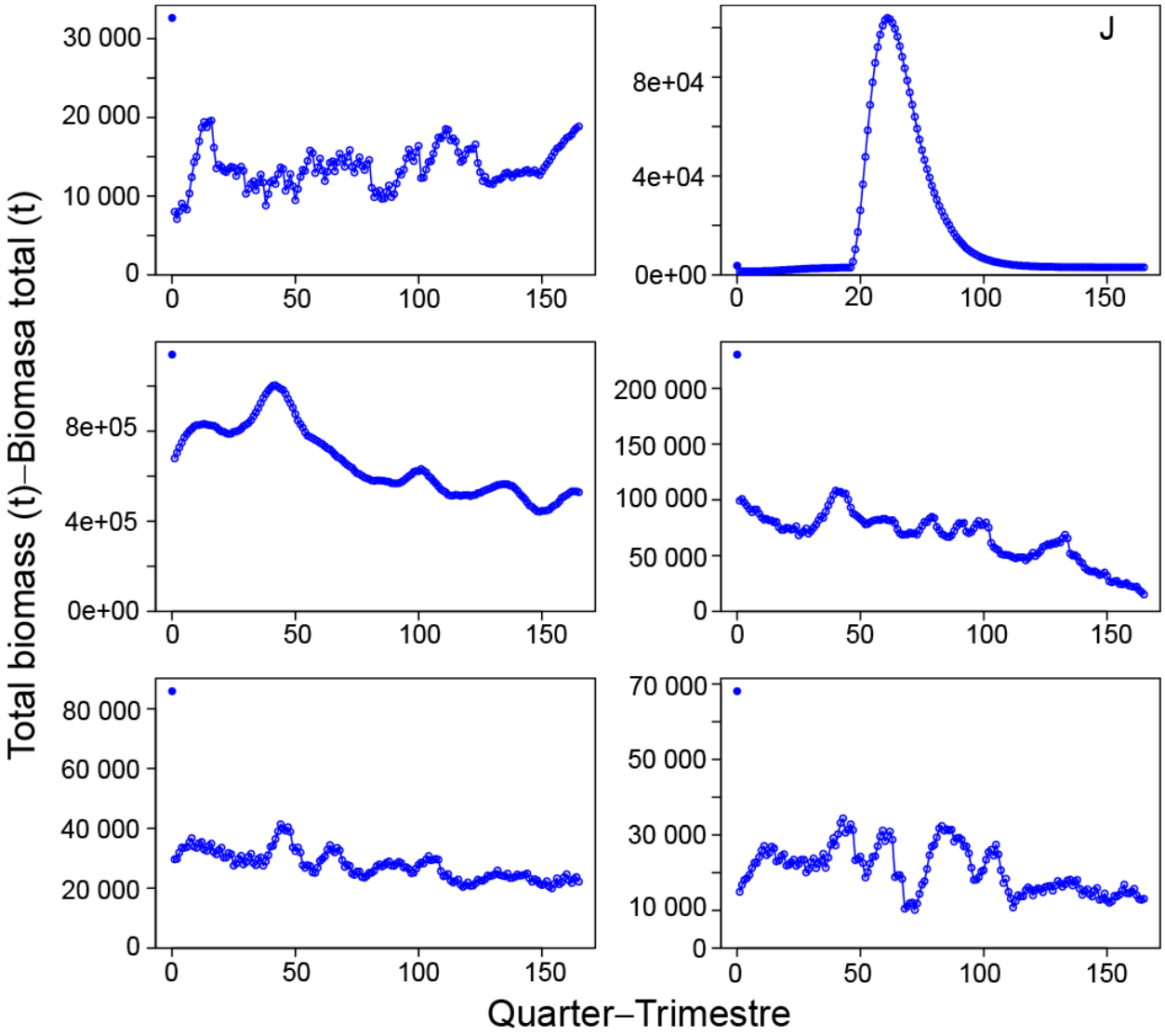

FIGURE A22. ASPM estimates of total biomass for the six areas in grid J (Figure 7), with estimates of recruitment deviates.

FIGURA A22. Estimaciones del ASPM de biomasa total correspondientes a las seis áreas en la cuadrícula J (Figura 7), con estimaciones de las desviaciones del reclutamiento.

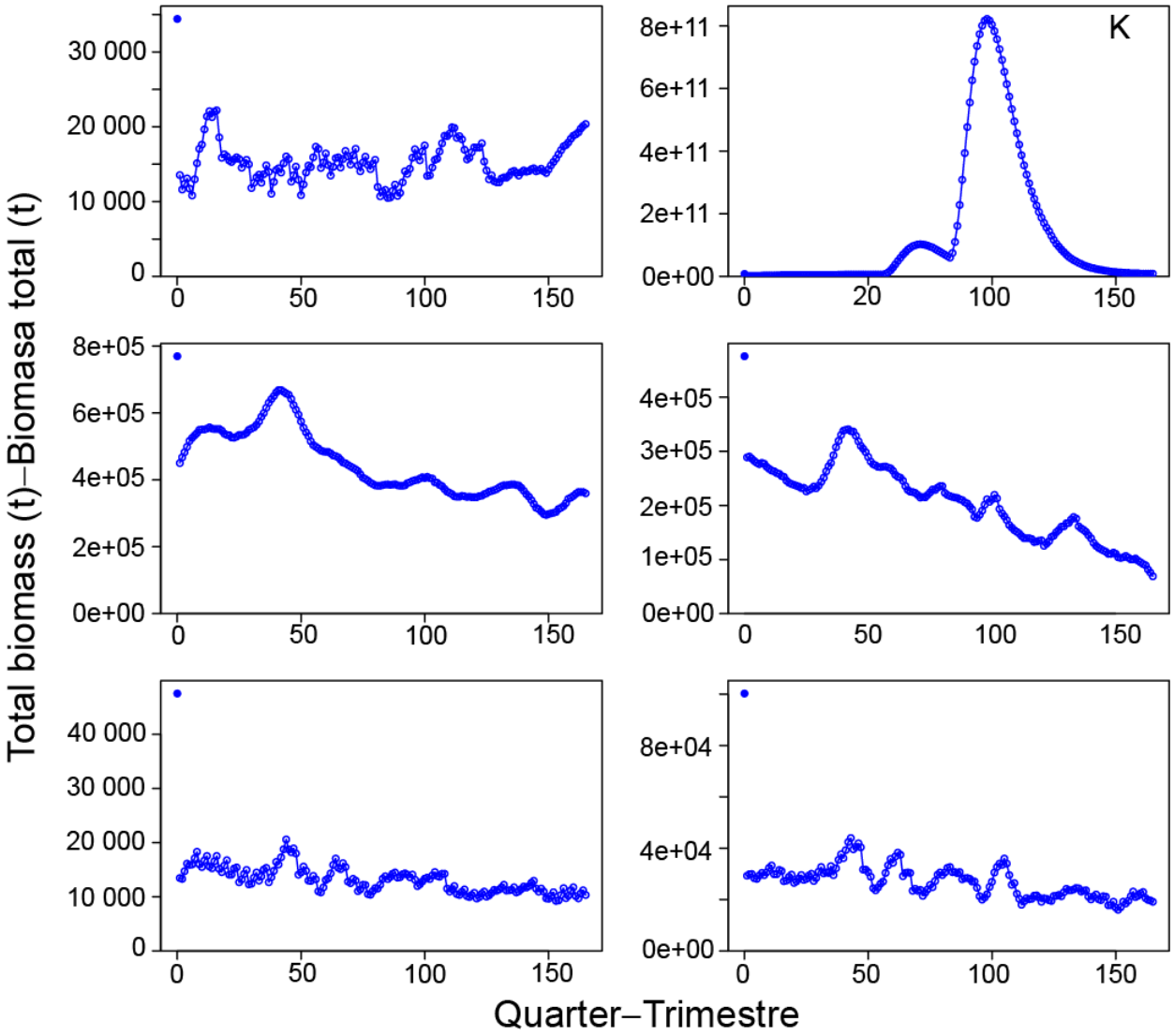

FIGURE A23. ASPM estimates of total biomass for the six areas in grid K (Figure 7), with estimates of recruitment deviates.

FIGURA A23. Estimaciones del ASPM de biomasa total correspondientes a las seis áreas en la cuadrícula K (Figura 7), con estimaciones de las desviaciones del reclutamiento.

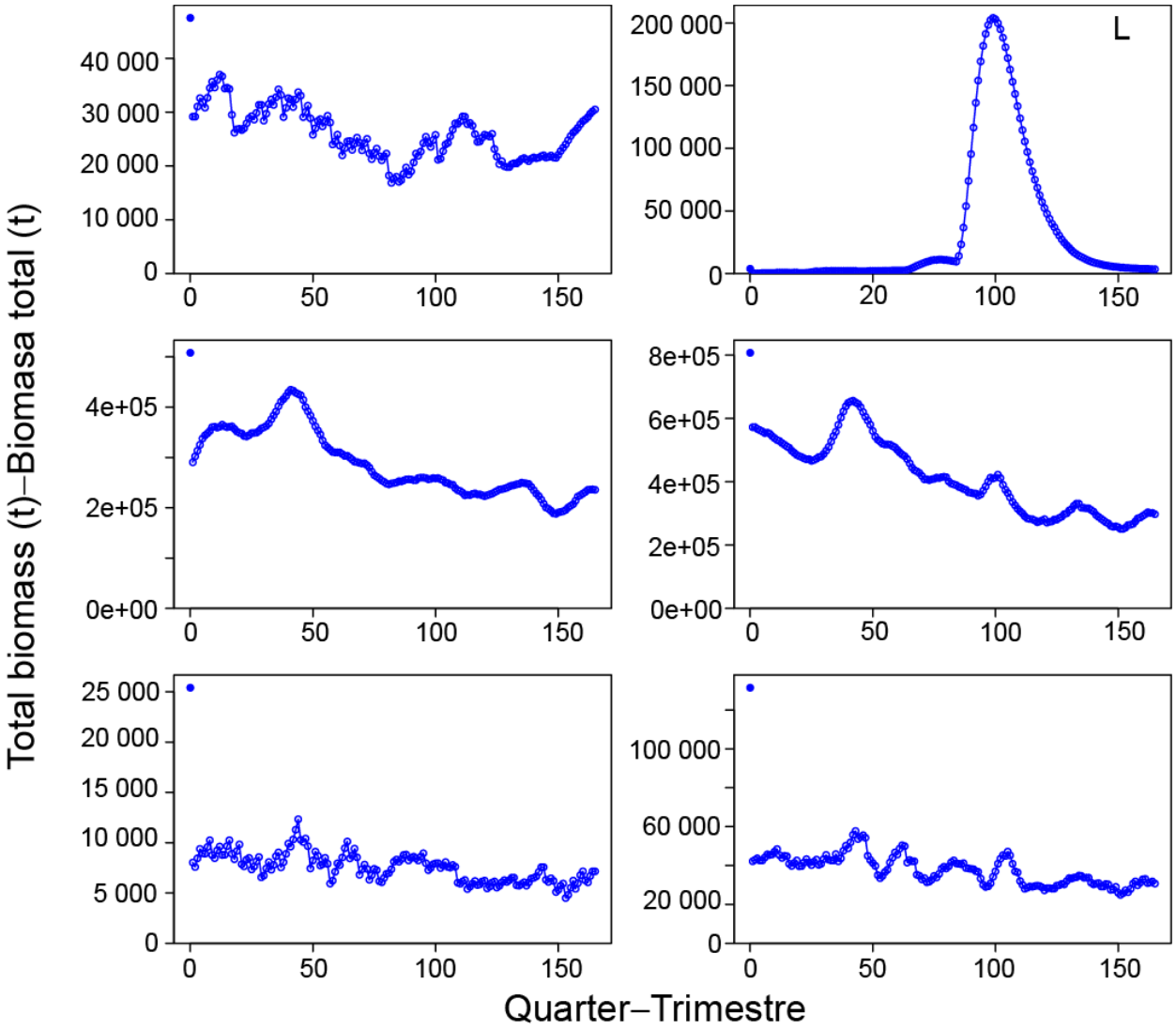

FIGURE A24. ASPM estimates of total biomass for the six areas in grid L (Figure 7), with estimates of recruitment deviates.

FIGURA A24. Estimaciones del ASPM de biomasa total correspondientes a las seis áreas en la cuadrícula L (Figura 7), con estimaciones de las desviaciones del reclutamiento.

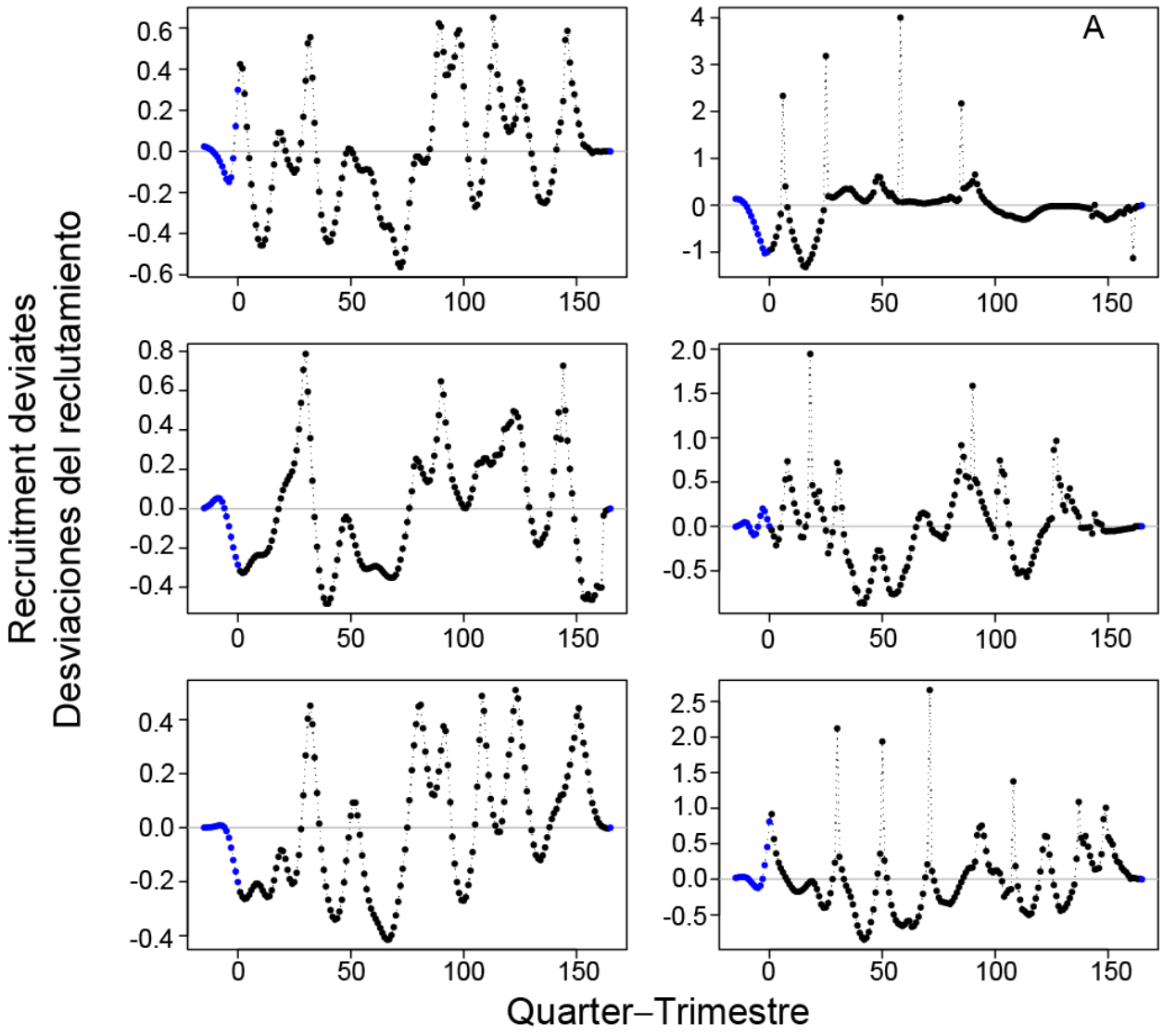

FIGURE A25. Quarterly recruitment deviates estimated by ASPM for the six areas in grid A (Figure 7).
FIGURA A25. Desviaciones trimestrales del reclutamiento estimadas por el ASPM correspondientes a las seis áreas en la cuadrícula A (Figura 7).

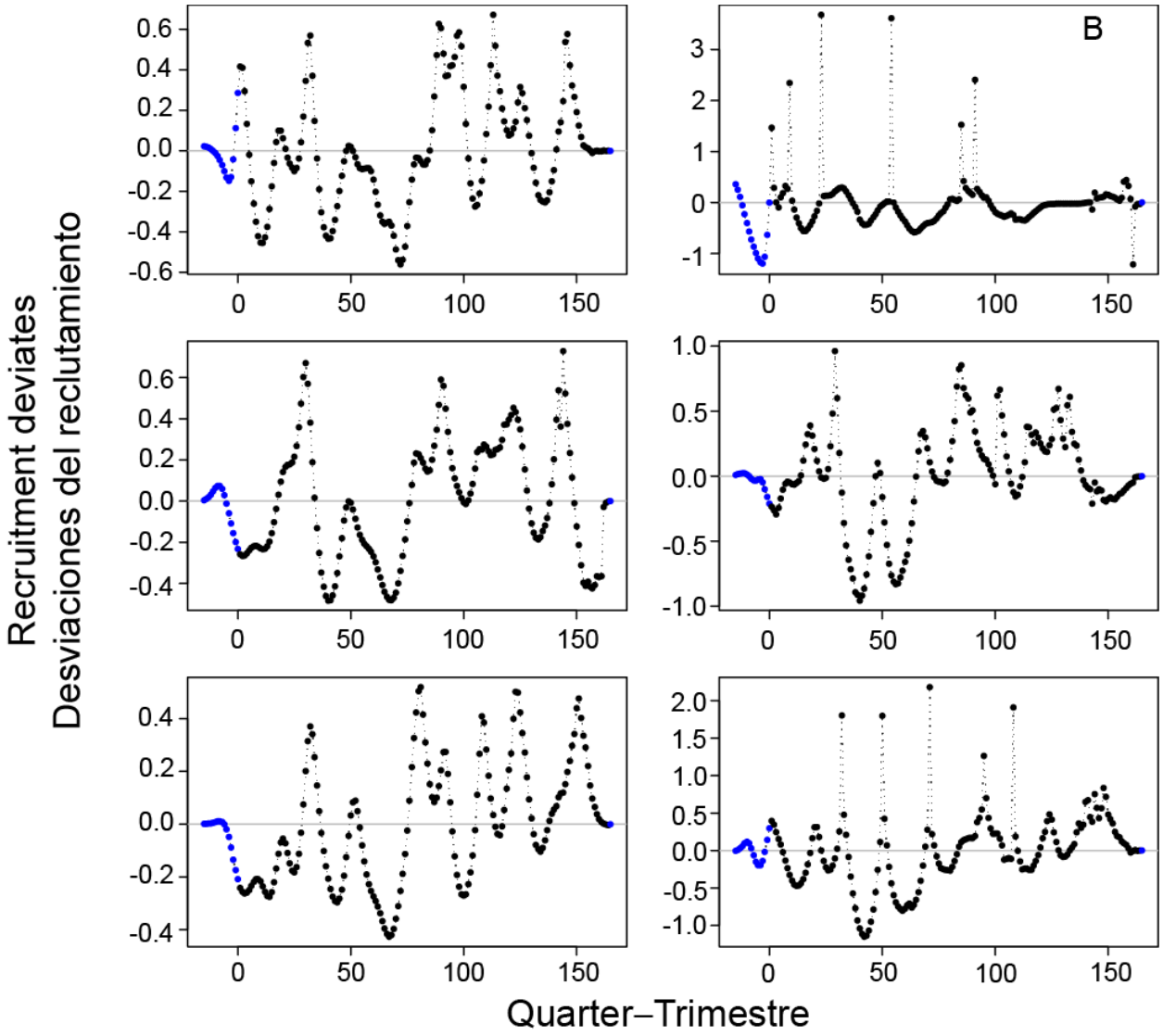

FIGURE A26. Quarterly recruitment deviates estimated by ASPM for the six areas in grid B (Figure 7).
FIGURA A26. Desviaciones trimestrales del reclutamiento estimadas por el ASPM correspondientes a las seis áreas en la cuadrícula B (Figura 7).

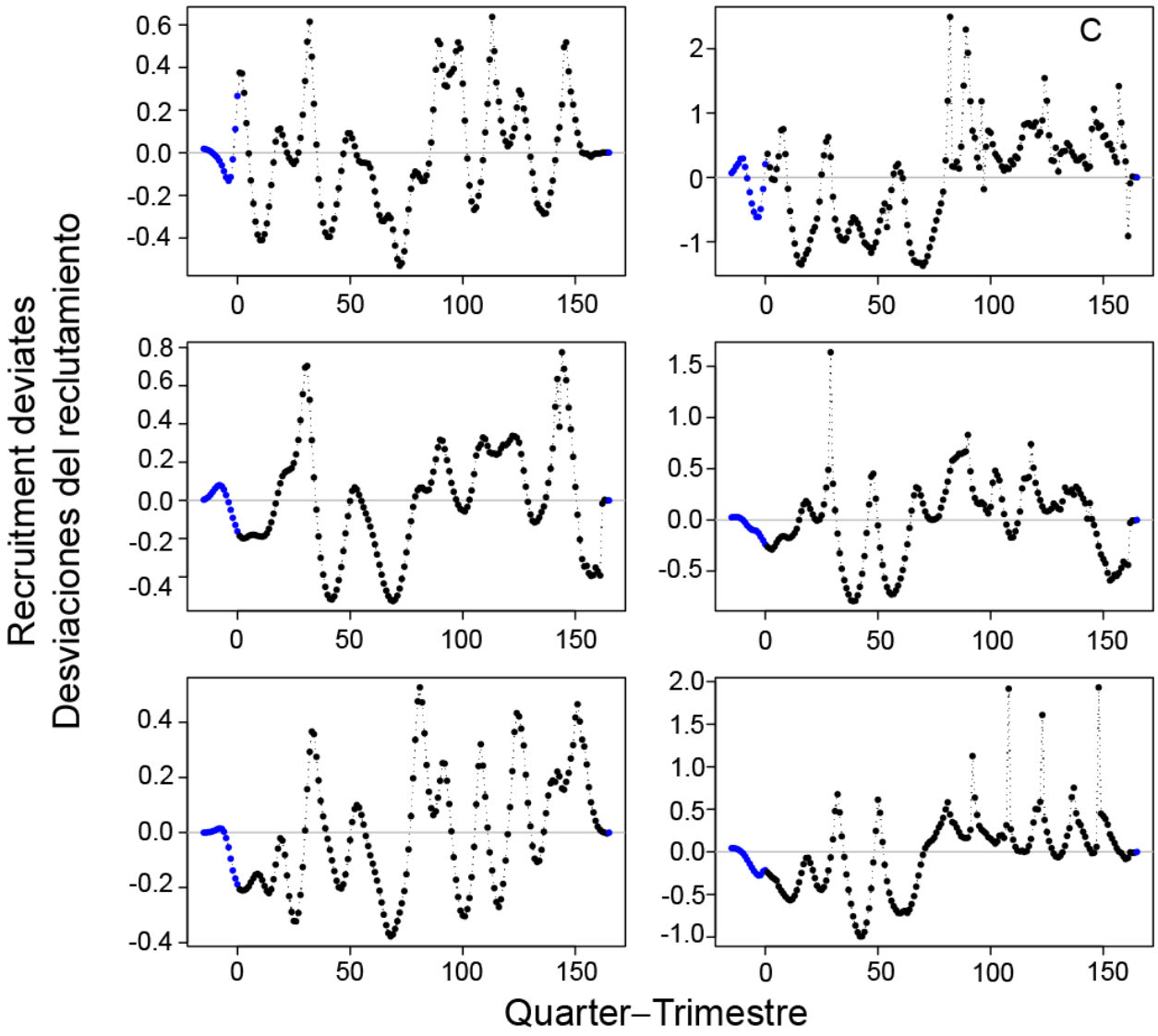

FIGURE A27. Quarterly recruitment deviates estimated by ASPM for the six areas in grid C (Figure 7).
FIGURA A27. Desviaciones trimestrales del reclutamiento estimadas por el ASPM correspondientes a las seis áreas en la cuadrícula C (Figura 7).

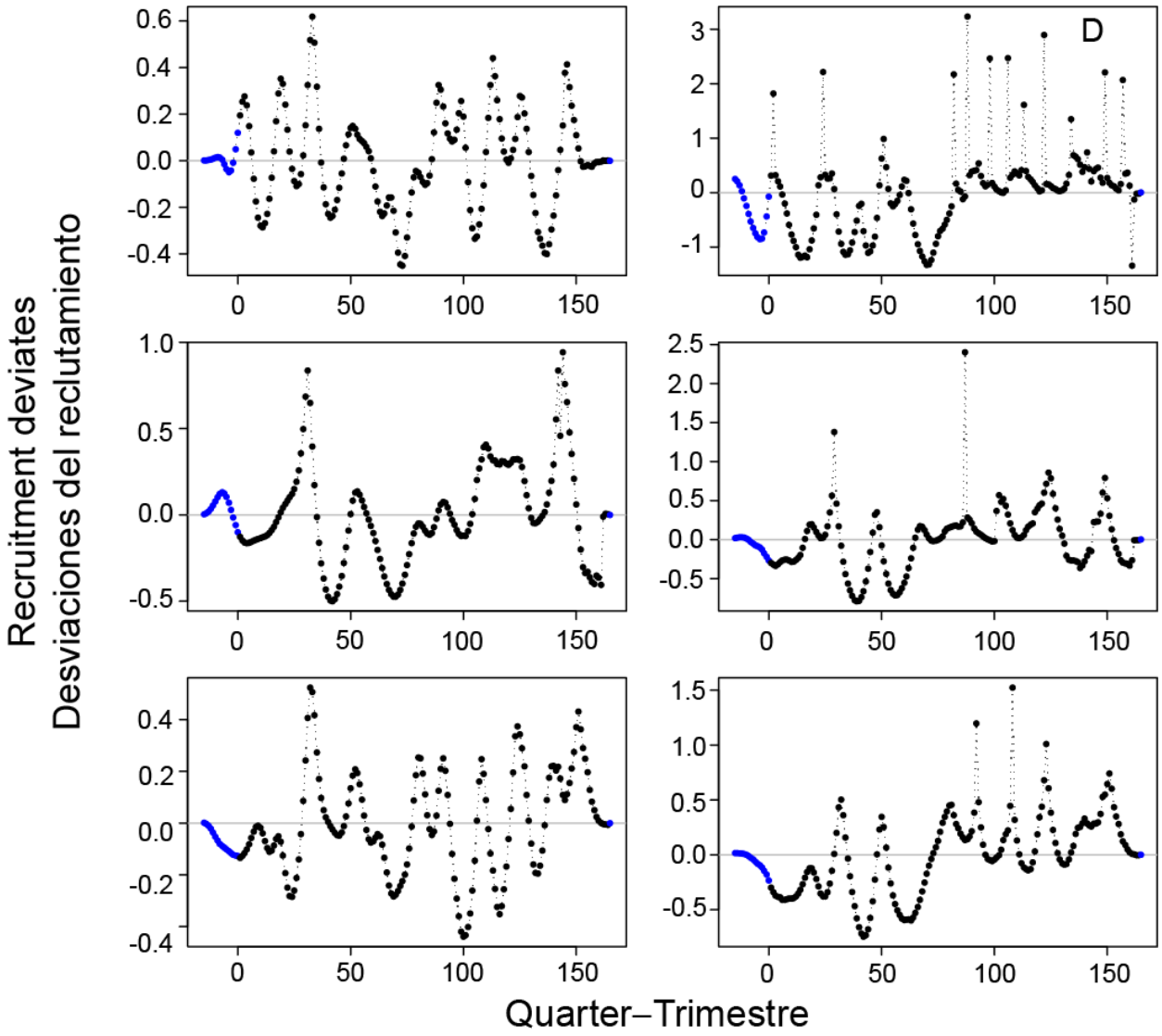

FIGURE A28. Quarterly recruitment deviates estimated by ASPM for the six areas in grid D (Figure 7).
FIGURA A28. Desviaciones trimestrales del reclutamiento estimadas por el ASPM correspondientes a las seis áreas en la cuadrícula D (Figura 7).

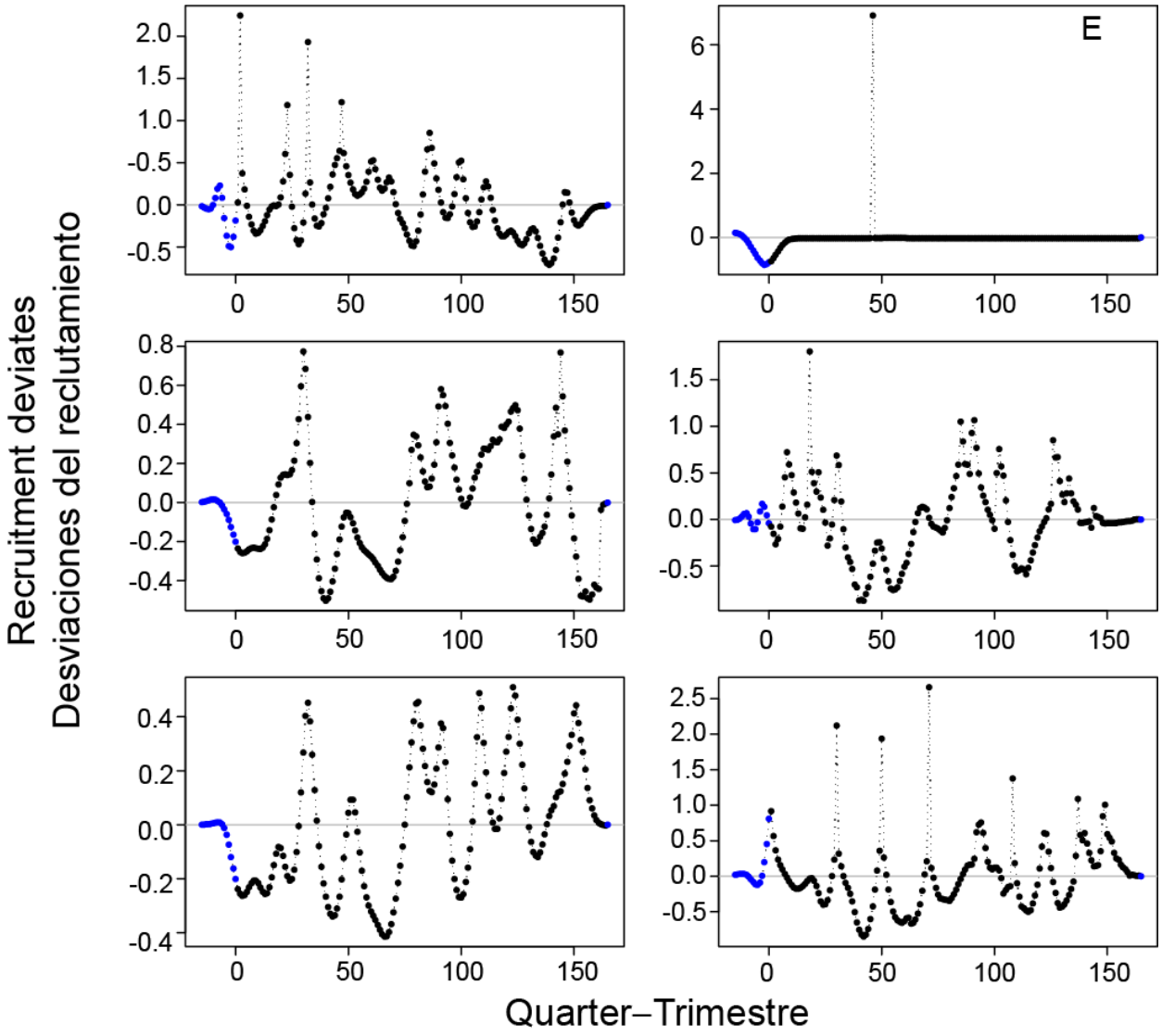

FIGURE A29. Quarterly recruitment deviates estimated by ASPM for the six areas in grid E (Figure 7).
FIGURA A29. Desviaciones trimestrales del reclutamiento estimadas por el ASPM correspondientes a las seis áreas en la cuadrícula E (Figura 7).

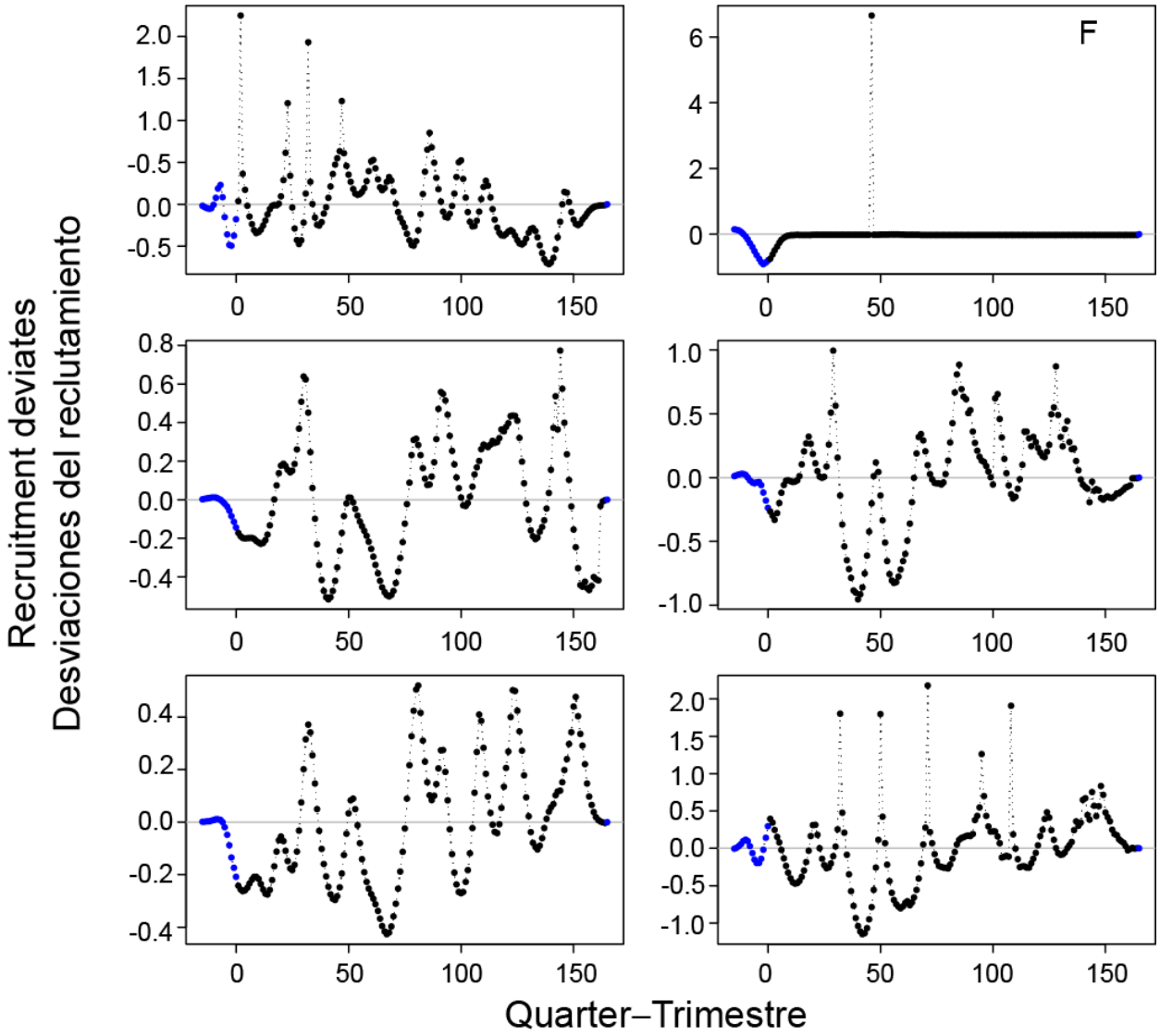

FIGURE A30. Quarterly recruitment deviates estimated by ASPM for the six areas in grid F (Figure 7).
FIGURA A30. Desviaciones trimestrales del reclutamiento estimadas por el ASPM correspondientes a las seis áreas en la cuadrícula F (Figura 7).

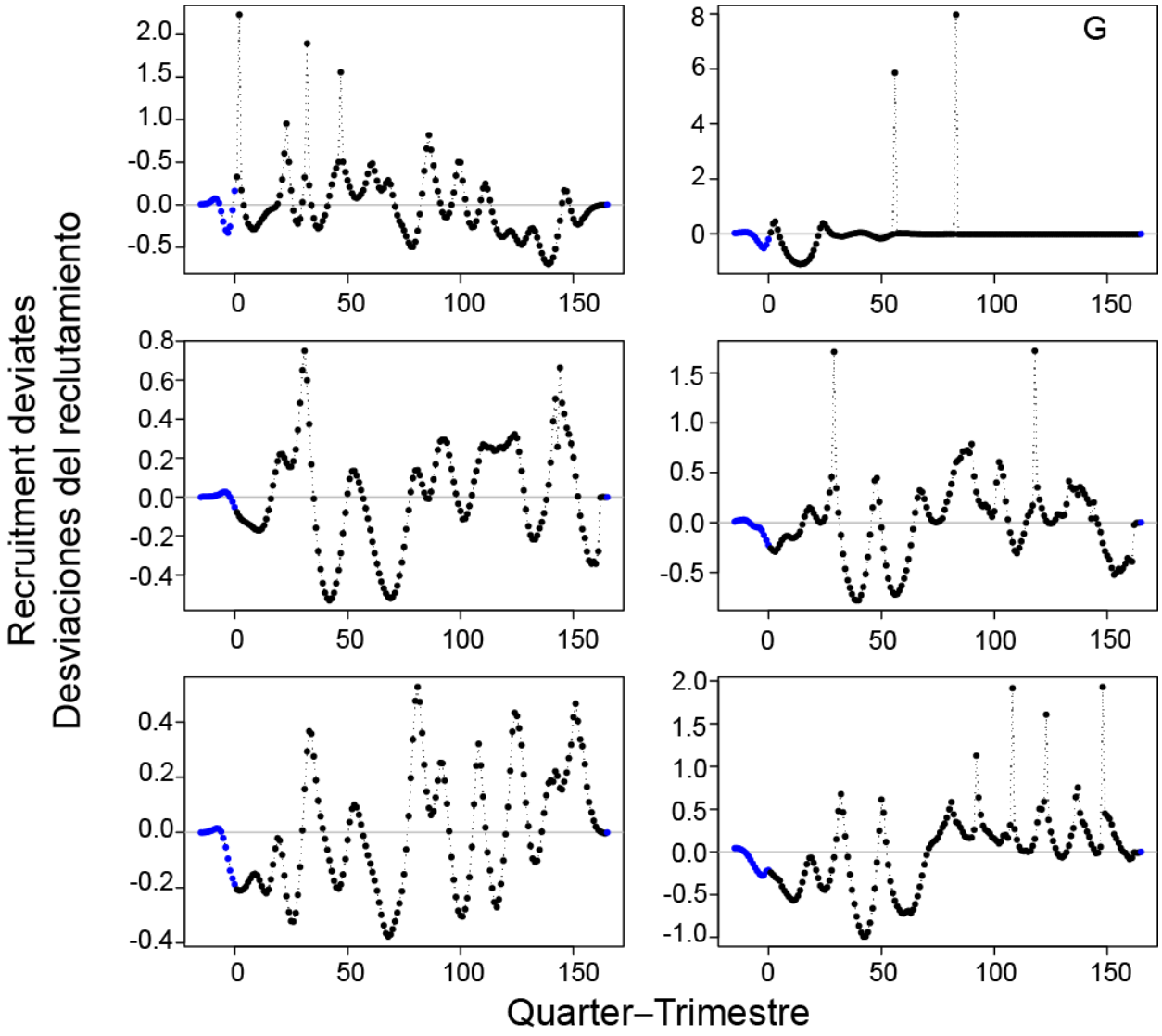

FIGURE A31. Quarterly recruitment deviates estimated by ASPM for the six areas in grid G (Figure 7).
FIGURA A31. Desviaciones trimestrales del reclutamiento estimadas por el ASPM correspondientes a las seis áreas en la cuadrícula G (Figura 7).

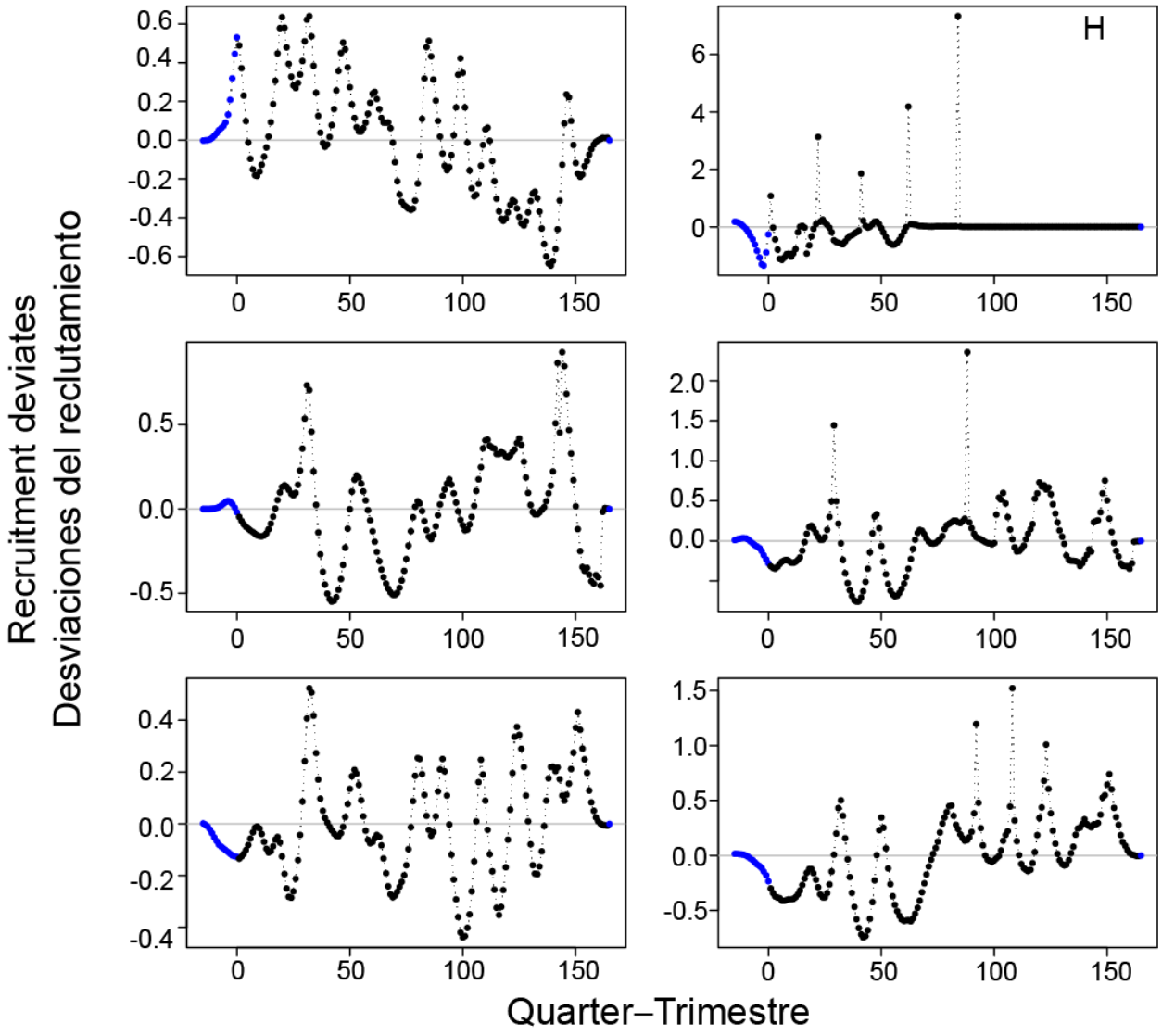

FIGURE A32. Quarterly recruitment deviates estimated by ASPM for the six areas in grid H (Figure 7).
FIGURA A32. Desviaciones trimestrales del reclutamiento estimadas por el ASPM correspondientes a las seis áreas en la cuadrícula H (Figura 7).

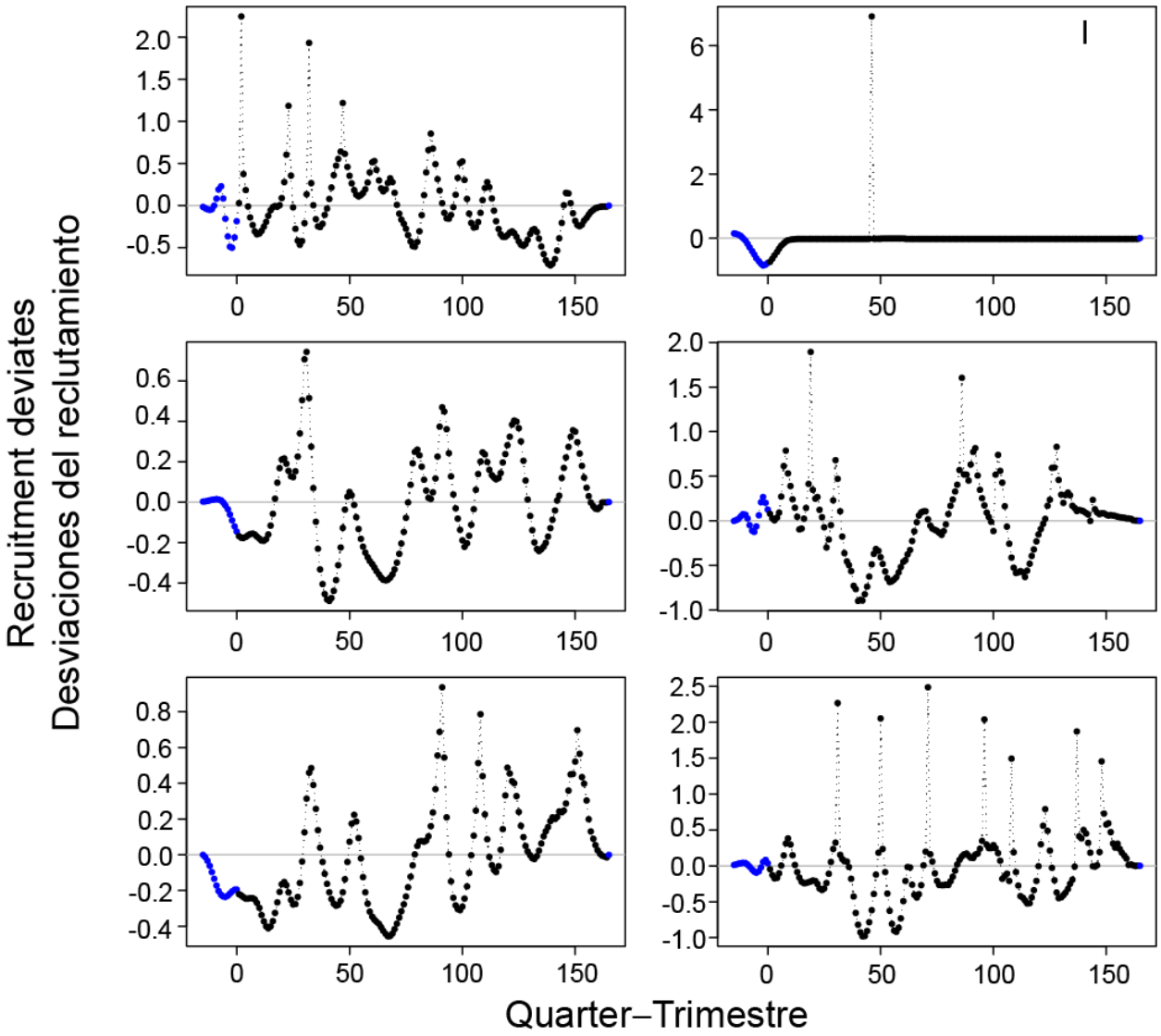

FIGURE A33. Quarterly recruitment deviates estimated by ASPM for the six areas in grid I (Figure 7).
FIGURA A33. Desviaciones trimestrales del reclutamiento estimadas por el ASPM correspondientes a las seis áreas en la cuadrícula I (Figura 7).

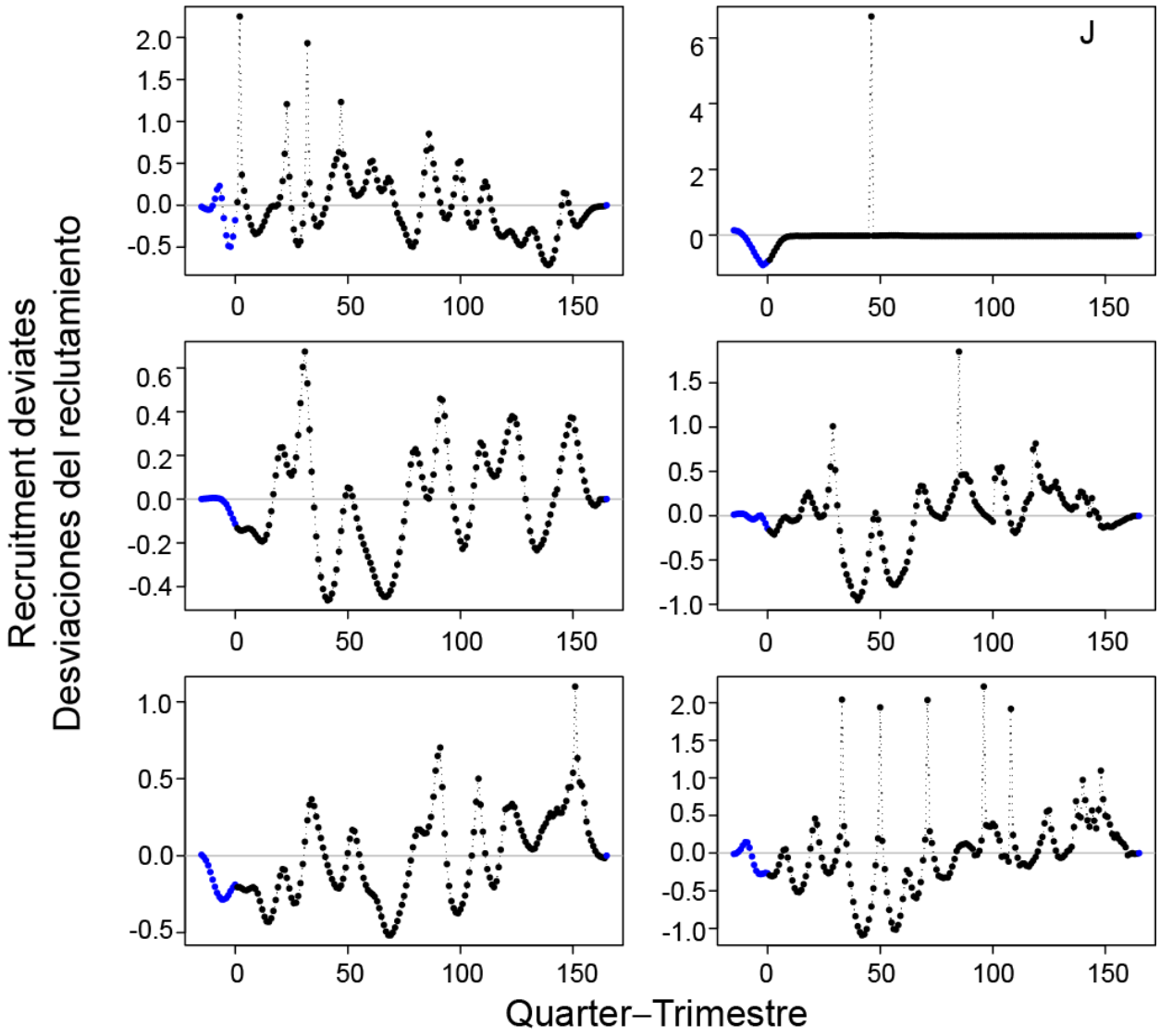

FIGURE A34. Quarterly recruitment deviates estimated by ASPM for the six areas in grid J (Figure 7).
FIGURA A34. Desviaciones trimestrales del reclutamiento estimadas por el ASPM correspondientes a las seis áreas en la cuadrícula J (Figura 7).

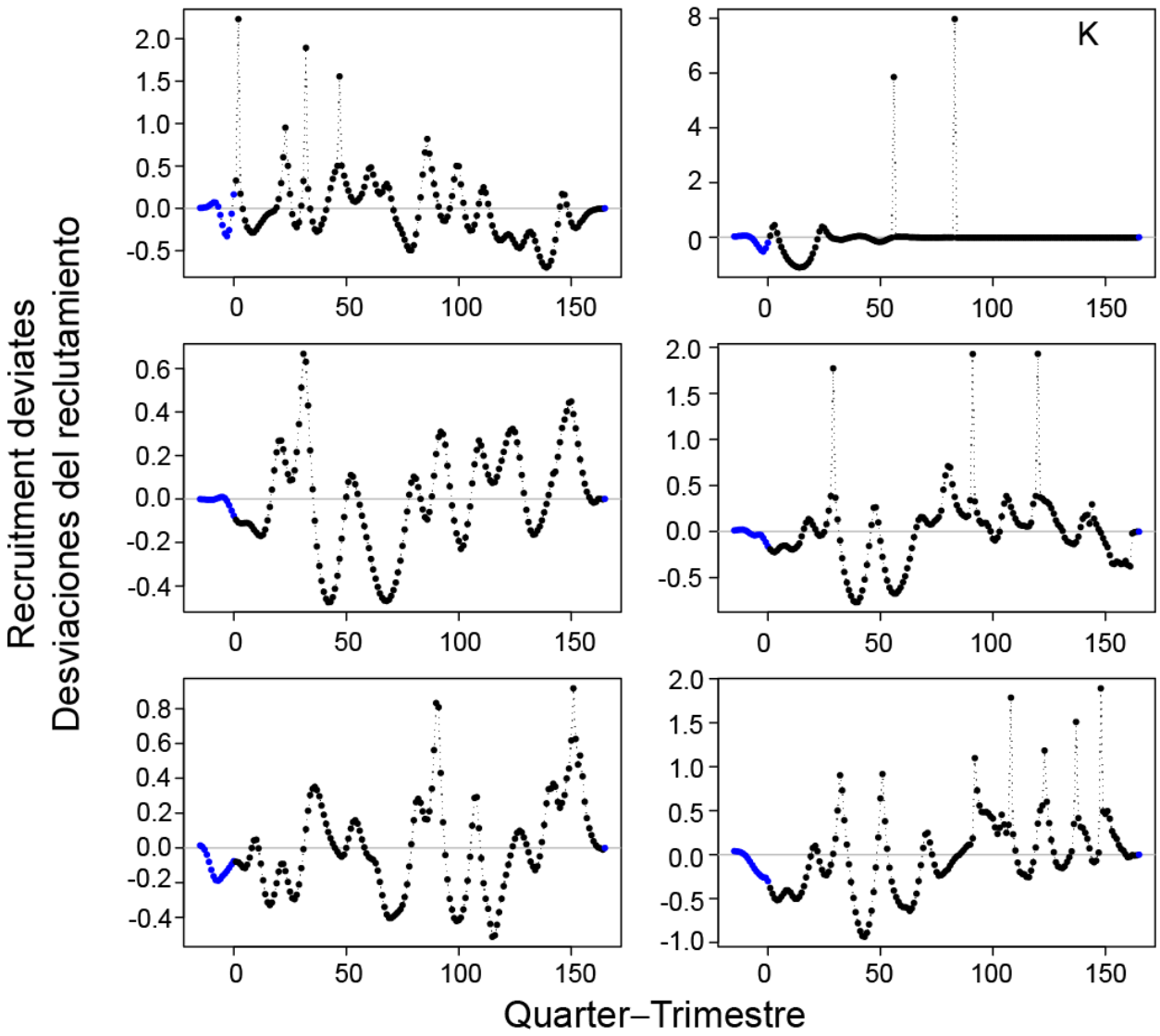

FIGURE A35. Quarterly recruitment deviates estimated by ASPM for the six areas in grid K (Figure 7).
FIGURA A35. Desviaciones trimestrales del reclutamiento estimadas por el ASPM correspondientes a las seis áreas en la cuadrícula K (Figura 7).

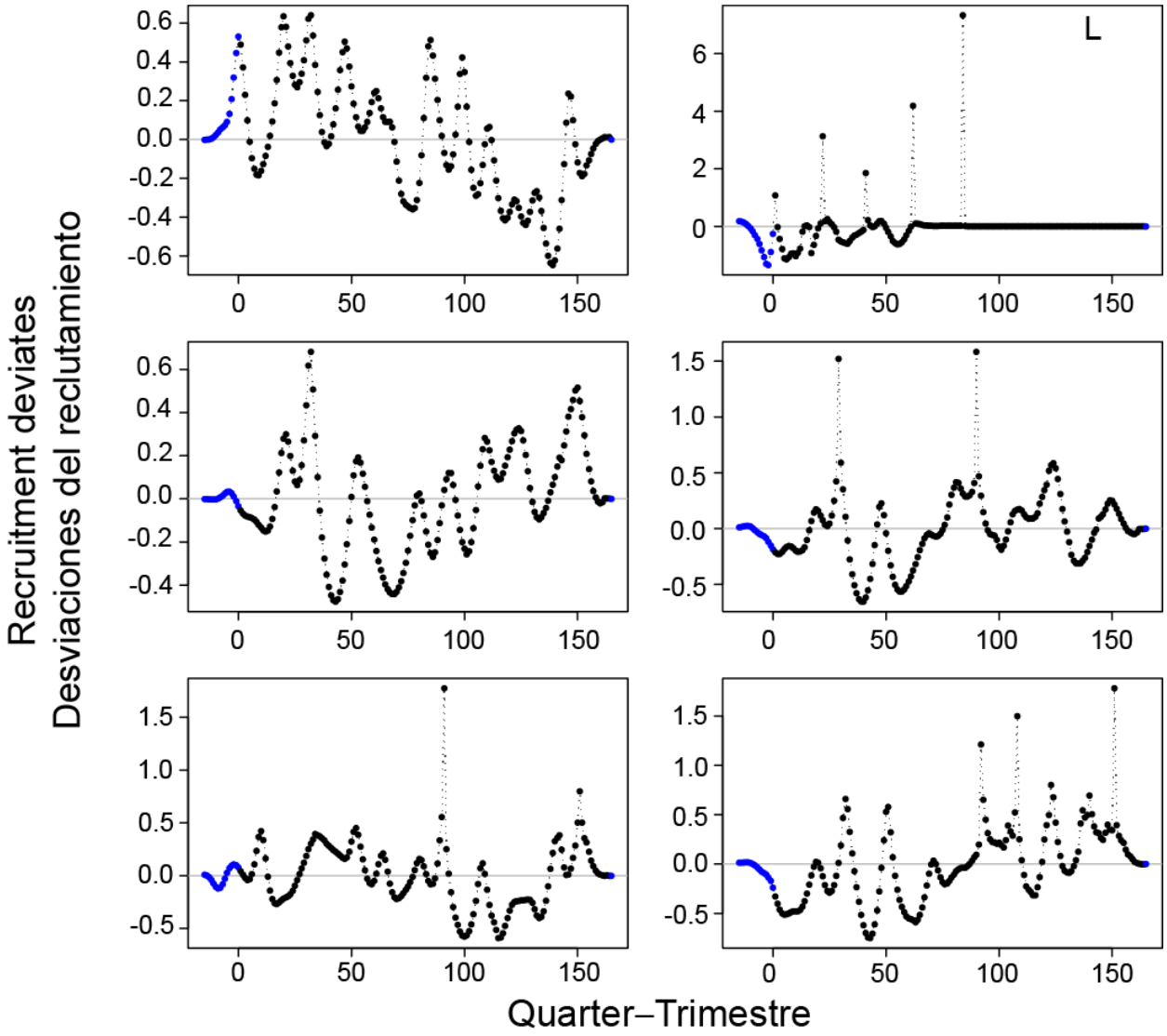

FIGURE A36. Quarterly recruitment deviates estimated by ASPM for the six areas in grid L (Figure 7).
FIGURA A36. Desviaciones trimestrales del reclutamiento estimadas por el ASPM correspondientes a las seis áreas en la cuadrícula L (Figura 7).